2015•2016
FACULTEIT GENEESKUNDE EN LEVENSWETENSCHAPPEN
master in de biomedische wetenschappen

Masterproef

Effect of extracellular matrix degradation products on macrophage phenotype and the discovery of a novel bio-component within the extracellular matrix

Promotor :
dr. Jeroen BOGIE

Promotor :
Prof. dr. STEPHEN BADYLAK

Copromotor :
dr. L. HULEIHEL

Theresa Rausch

Scriptie ingediend tot het behalen van de graad van master in de biomedische wetenschappen

De transnationale Universiteit Limburg is een uniek samenwerkingsverband van twee universiteiten in twee landen: de Universiteit Hasselt en Maastricht University.

universiteit hasselt
KNOWLEDGE IN ACTION

Universiteit Hasselt | Campus Hasselt | Martelarenlaan 42 | BE-3500 Hasselt
Universiteit Hasselt | Campus Diepenbeek | Agoralaan Gebouw D | BE-3590 Diepenbeek

universiteit hasselt | Maastricht University

2015•2016
FACULTEIT GENEESKUNDE EN LEVENSWETENSCHAPPEN
master in de biomedische wetenschappen

Masterproef

Effect of extracellular matrix degradation products on macrophage phenotype and the discovery of a novel bio-component within the extracellular matrix

Promotor :
dr. Jeroen BOGIE

Promotor :
Prof. dr. STEPHEN BADYLAK

Copromotor :
dr. L. HULEIHEL

Theresa Rausch

Scriptie ingediend tot het behalen van de graad van master in de biomedische wetenschappen

universiteit hasselt | Maastricht University

Acknowledgement

I would like to thank Prof. Dr. Stephen Badylak giving me the opportunity to perform my Senior Internship at the Dr. Badylak's Laboratory of the McGowan Institute for Regenerative Medicine in Pittsburgh, U.S.A.. I would like to thank Dr. Luai Huleihel for mentoring me during my internship. I also want to thank Dr. Jeroen Bogie (BIOMED) and all employees of the McGowan Institute who helped me with my research project. I really appreciate the time you invested helping me during laboratory work, preparing a variety of presentations and to proofread my Senior Internship thesis.

TABLE OF CONTENTS

Abbreviations

ACell® MatriStem	Commercial UBM extracellular matrix
APs	Apoptotic bodies
ARG-1	Arginase 1
BARD XenMatrix™	Commercial dermal extracellular matrix
β-GUS	β-glucuronidase
BMDM	Murine bone marrow-derived macrophages
CD206	Mannose receptor (MRC1)
Cook® Biotech	Commercial SIS extracellular matrix
ECM	Extracellular matrix
EVs	Extracellular vesicles
FBS	Fetal bovine serum
G6PC3	Glucose-6 phosphatase
GAPDH	Glyceraldehyde 3-phosphate dehydrogenase
GLUT1	Glucose transporter 1
HIF1a	Hypoxia-inducible factor 1-α
HK3	Hexokinase 3
IFNγ	Interferon gamma
IL1Ra	Interleukin-1 receptor antagonist
IL-4	Interleukin-4
ILV	Intraluminal vesicles
iNOS	Nictric oxide synthase
IRF	Interferon regulatory factor
KLF	Krüppel-like transcription factor (KLF4, KLF6)
LDHA	Lactate dehydrogenase A
LPS	Lipopolysaccharide
MBVs	Matrix-bound nanovesicles
MSCs	Mesenchymal stem cells
MVB	Multivesicular bodies
MVs	Microvesicles
Mφs	Macrophages
NTA	Nanoparticle Tracking Analysis
PCK	Phosphoenolpyruvate carboxykinase (PCK1, PCK2)
PDK4	Pyruvate dehydrogenase lipoamide kinase isozyme 4
PFKFB3	6-phosphofructo-2-kinase-fructose-2,6-biphosphatase 3
PGK1	Phosphoglycerate kinase 1
PPARg	Peroxisome proliferator-activated receptor gamma
RPIA	Ribose 5-phosphate isomerase A
SIS	Small intestinal submucosa
STAT	signal transducer and activator of transcription (STAT1, 2, 3, 5, 6)
TEM	Transmission electron microscopy
TGM2	Transglutaminase 2
THP-1	THP-1 differentiated macrophages
TNF-α	Tumor necrosis factor-alpha
UBM	Urinary bladder mucosa

Abstract *(English)*

Introduction: Acute injuries and chronic wounds are associated with diminished complex wound healing processes. Therefore, decelluarized extracellular matrix (ECM) bioscaffolds of dermis, small intestinal submucosa (SIS), and urinary bladder (UBM) tissue source are currently applied to improve wound healing of damaged soft and weak tissue. ECM scaffolds are known to induce a variety *in vivo* biologic effects, including angiogenesis, macrophage polarization, and stem/progenitor cell mobilization, among others. These responses are associated with ECM biocomponents such as ligands, growth factors/cytokines, the release of cryptic peptides from ECM parent molecules, and surface physical/mechanical properties of the matrix itself. Extracellular vesicles (EVs) are nano-size vesicles created by mammalian and non-mammalian cells, which mediate cell-to-cell communication and affect cell behavior by carrying signaling and effector molecules, including microRNAs, mRNAs, and proteins. In our first project we hypothesize that EVs withstand the tissue decellularization process and are present within ECM bioscaffolds as matrix-bound nanovesicles (MBVs), thus having the potential to affect cell behavior. Furthermore, our group has previously been shown that tissue remodeling induced by ECM-bioscaffolds are associated with an enhance in M2-macrophage polarization in *in vivo*, which needs to be further analyzed in in-depth studies. Therefore, we hypothesize in our research second project that ECM degradation products stimulate macrophage polarization towards an anti-inflammatory M2 phenotype.

Material & methods: Porcine UBM, SIS, and dermis were digested with collagenase or proteinase K for 24 hours. Transmission electron microscopy, Western Blots and RNA sequencing techniques were used to identify EVs and their contents. In addition, macrophages were exposed to ECM degradation products and their phenotype was evaluated via qPCR and Western Blots for M1 and M2 markers.

Results: Results show clear evidence of MBVs within ECM bioscaffolds and the ability of these MBVs to affect cell morphology and behavior. MBVs were shown to stimulate neuritic extension growth and the proliferation of perivascular stem cells, both are known to be important regulatory pathways during tissue remodeling. Furthermore, microRNAs that may influence tissue regenerative mechanisms were identified as MBVs cargo. Additionally, ECM degradation products have been shown to change the macrophage phenotype to an "M_{ECM}" phenotype.

Discussion & conclusion: In summary, the described work identifies the presence of MBVs within naturally occurring bioscaffolds composed of ECM and as well as that ECM degradation products have the ability to modify macrophage phenotype. These results are important for the understanding of the molecular mechanism by which ECM contributes to the constructive remodeling *in vivo*.

Abstract *(Dutch)*

Introductie: Acute en chronische wonden zijn vaak verbonden met gereduceerde complexe genezingsprocessen. Daarom wordt gedecellulariseerd extracellulaire matrix (ECM) bioscaffold afkomstig van dermis, dunne darm submucosa (SIS) en urine blaas (UBM), in mensen getransplanteerd om wond genezing van gewonde zachte weefsel te induceren/te verbeteren. ECM oefent verschillende biologische effecten *in vivo* uit zoals angiogenese, macrofaag polarisatie en stimulatie van stamcel mobilisatie. Deze reacties zijn te weten aan de effecten van biocomponenten, die in de ECM aanwezig zijn, zoals liganden, groei factoren en cytokines, de vrijlating van crypte-peptiden uit parentale ECM moleculen en fysische/mechanische eigenschappen van de matrix zelf. Nanoscopische extracellular vesicles (EVs) van zoogdier en niet-zoogdier cellen bevatten signalisatie en effector moleculen, zoals microRNAs, mRNAs en proteinen, die de cel-cel communicatie en het cel gedrag kunnen beinvloeden. De hypothese van onze eerste research project is dat EVs deel van ECM bioscaffolds zijn, de decellularisatie proces tegenhouden en bovendien als eigenschap hebben cel gedrag te veranderen. EVs ingebed in ECM producten worden hierin matrix-bound nanovesicles (MBVs) genoemd. Bovendien werd een versterkte M2-macrofaag polarisatie gecombineerd met weefsel remodeling waargenomen post-ECM transplantatie in in-vivo models. In onze tweede research project gaan we deze uitvindingen verder analyseren. Hiervoor is onze hypothese dat ECM afbraak producten de anti-inflammatoire M2 phenotype polarisatie stimuleren.

Materiaal & methoden: Om varkens UBM, SIS en dermal weefsel te verwerken, werd een incubatietijd van 24h in collagenase of proteinase K gebruikt. Transmissie electron microscopie, Western Blots en RNA sequencing werden gebruikt, om MBVs zelf en het cargo van MBVs te identificeren. Macrofagen werden met ECM afbraak producten gestimuleerd, om hun phenotype met behulp van M1 en M2 markers door qPCR en Western Blots te analyseren.

Resultaten: De bevindingen illustreren duidelijk de aanwezigheid MBVs in ECM bioscaffolds en hun eigenschap om het cellulair gedrag en morfolgie te kunnen veranderen, zoals de stimulatie van neuritic extension of van stem cel proliefreatie. Bovendien werden microRNA, die tegelijkertijd een invloed kunnen hebben op regeneratieve processen, als MBVs cargo geidentificeerd. Daarenboven kunnen ECM afbraakproducten de polarisatie van macrofagen naar een "M_{ECM}" phenotype beïnvloeden.

Discussie & Conclusie: Deze studie toont de aanwezigheid van MBVs in biologische ECM scaffolds aan, alsook de eigenschap van ECM afbraak producten om het phenotype van macrofagen te kunnen veranderen. Deze resultaten zijn belangrijk om onderliggende mechanismen, waarin ECM gebruikt wordt als contructieve remodeling *in vivo* te stimuleren, te onderzoeken.

1. Introduction

Regenerative medicine is defined by the renewal of damaged tissue into functional tissue. Regenerative medicine strategies are important to help patients with various diseases and to improve patient's quality of life (1). Transplantation of decellularized extracellular matrix (ECM, Figure 1A) bioscaffolds of mammalian tissues source is a currently approved method to induce wound healing and tissue remodeling after chronic non-healing and acute diseases. These include: diabetic foot ulcer, diaphragmatic hernia (Figure 1B), and acute injuries (Figure 1C), such as military wounds (2-4). In order to produce highly preserved ECM scaffolds structure, physical and chemical methods are used to remove all matrix cellular components from isolated tissues, followed by washes to discard cellular debris. The whole process is referred as decellularization (5). Decellularization allows the bioscaffold to integrate within the body without rejection, minimal inflammation and no foreign body response, while the structure, the composition and the beneficial regenerative effects of the ECM are maintained (6).

ECM bioscaffolds are known to induce a variety of biologic remodeling effects *in vivo,* including angiogenesis, modulation of macrophage phenotype, proliferation and mobilization of stem/progenitor cells, among others (7). ECM cellular mechanisms are associated with specific ECM ligands, the release of ECM embedded growth factors/cytokines, chemokines, and cryptic peptides that are released and produced from ECM parent molecules, such as collagen, laminin (7) and fibronectin (8) due to enzymatic cleavage. To date, underlying mechanisms of wound healing induced by ECM transplantation are largely unknown. Despite the beneficial effects of ECM bioscaffolds, there are still some disadvantages associated with ECM application, including invasive surgery methods, several surgery-associated risk factors (e.g., seroma or hematoma) and scar tissue formation. Therefore, there is a need to identify the mechanism of action by which ECM promotes its regenerative effect and the physical/mechanical properties of the matrix itself to improve current ECM therapy/delivery.

1.1 Extracellular Matrix in Regenerative Medicine

ECM is a complex inter-cellular three-dimensional ultrastructure that was earlier thought to only support cell and tissue organization (9, 10). To date, ECM is known to consist also of bioactive components such as collagen, glycoproteins, laminin, fibronectin, cytokines, glycosaminoglycans (i.e. hyaluronan, heparan sulfate, heparin and dermatan sulfate) and growth factors (e.g. platelet derived growth factor PDGF and the transforming growth factor-beta TGF-β) (11, 12). These unique components can induce part of the remodeling processes, which makes ECM scaffolds a highly important therapeutic method in regenerative medicine (10). To date, ECM bioscaffolds have been isolated from a variety of mammalian tissues, including porcine urinary bladder, small intestine submucosa and dermis, and have been applied in multiple reconstructive surgeries, such as breast, facial, skeletal muscle, and ventral hernia reconstruction, among others (13).

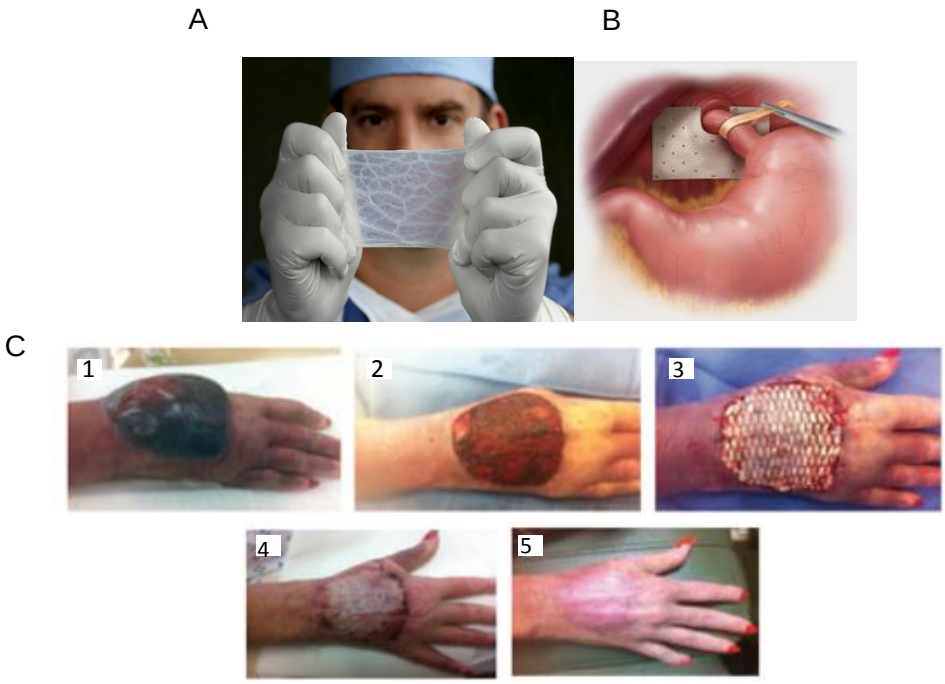

Fig. 1: **Decellularized extracellular matrix scaffold in regenerative medicine.** (**A**) Transplantation of ECM bioscaffolds are used to induce regeneration of weak or damaged soft tissues. For instance, to repair hernia, including diaphragmatic (**B**) and umbilical hernia, and to manage wound healing in diabetic foot and venous leg ulcer (2-4). ECM is a complex three-dimensional ultrastructure that supports cellular stability and that contains bioactive components (glycoproteins, glycosaminoglycans, and growth factors) which regulate cellular pro-regenerative mechanisms, including angiogenesis, proliferation, and cell migration (9, 10). (**C**) A 66-year old female developed a traumatic hematoma in her right hand. After debridement of the hematoma, an ECM bioscaffold from porcine small intestinal submucosa was performed. (**C4**) and (**C5**) show the beneficial regenerative effects induced by ECM bioscaffold application. A complete healing and the development of native functional tissue has been achieved after 4 weeks (14).

1.1.1 ECM scaffolds as clinical application

Clinical applied ECM scaffolds for regenerative medicine methods are produced and distributed by 20-30 companies, such as: BARD XenMatrix™ (2), ACell® MatriStem (3) and Cook® Biotech (4). Furthermore, there are over 100 different ECM products in the market (15). Examples for the different ECM bioscaffolds include the following: XenMatrix™ Graft is an acellular collagen scaffold originated from porcine dermis that consists of open collagen fibers for effective cellular infiltration and revascularization. Transplantation of XenMatrix™ scaffolds is done to reinforce weak and to repair damaged soft tissue, including reconstructive surgery of the abdomen, strengthening of a muscle flap and reparation of various hernia (e.g. abdominal, diaphragmatic, umbilical) (2). ACell® MatriStem is made of porcine urinary bladder matrix (UBM) and has been successfully used in more than 75,000 patients to induce wound healing after second degree burns and in ulcers, such as diabetic foot ulcer or venous leg ulcer (3). Cook® Biotech scaffolds are porcine small intestine submucosa (SIS) ECM products that has been used in more than 1.5 million patients as treatment for fistula, for different hernia or after prolapse of a pelvic organ (4).

1.1.2 Risks and deficiencies of ECM bioscaffold transplantation

Despite promising results in regenerative medicine, a number of obstacles remain in ECM-based application and ECM-induced wound healing. Detrimental clinical outcomes are: invasive surgery methods, and developing seroma and/or hematoma, among others (16).

Abnormal accumulation of serous fluid in dead spaces generated from ECM-based surgery could develop. Such seromas result in significant complications and do have life-threatening effects if not appropriately treated. Studies describing clinical implications occurring with seroma are: E.g. infection, prolonged wound healing, reoperation, extended hospital stay, and increasing health costs. Seroma can develop in 9.1% to 92% cases of post-surgery (17).

Beside seroma, surgery can have other detrimental consequences, including the development of hematoma. Hematomas are described as abnormal accumulations of blood outside the blood vessels. There are minor and major hematomas: Whereas minor hematomas can be removed by needle aspiration, with major hematomas surgery sutures or staples have to be reopened to reveal the bleeding for artificial coagulation. Hematoma can develop at all sites of the body and can be very harmful if not appropriately treated. Life threatening consequences are inflammation of surrounding tissues and additionally blood coagulation in and outside the blood vessels leading to necrosis of the overlying skin and of the adjacent subcutaneous fat (18, 19).

In order to address these disadvantages and therefore, to improve current ECM-based therapy, there is a need to understand the mechanisms by which ECM bioscaffolds affect wound healing mechanisms.

1.2 ECM scaffolds in immuno-modulatory processes

1.2.1 Wound healing

In general, wound healing is a complex dynamic process that is induced during acute, chronic and non-healing chronic diseases and is characterized by four different immuno-modulatory events: Hemostasis, inflammation, proliferation, and remodeling (20). The hemostasis consists of clot formation, vascular constriction and the release of cytokines and growth factors, such as transforming growth factor (TGF)-β, and epidermal growth factor (EGF) which induce inflammation and the infiltration of neutrophils, macrophages (Mφs), and lymphocytes (21). Whereas, neutrophils and Mφs release cytokines and reactive oxygen species (ROS) to enhance inflammatory mechanisms by known mechanisms, the function of lymphocytes, i.e. T- and B-lymphocytes, need to be further analyzed (22, 23). Additionally, to promote inflammation during early wound, another subtype of Mφs induce apoptotic cell clearance for inflammatory resolution. Hence, Mφs are responsible for inflammatory mechanisms and the transition to the proliferative phase (24, 25). The proliferative phase is characterized by scar tissue deposition and the generation of ECM products, including glycosaminoglycans and proteoglycans. After proliferation, wound healing process enters the remodeling phase in which remodeling to native tissue is induced. This phase can last for years and is an important process of wound healing (26).

1.2.2 Macrophage polarization

Mφs are associated with pro- and anti-inflammatory mechanisms, including inflammatory promotion, as well as apoptotic cell clearance and the resolution of inflammatory processes (26). The variety in Mφs behaviour during wound healing mechanisms is based on their plasticity, which allows Mφs to change in phenotype (25). The best known Mφs subtypes are unstimulated Mφs, pro-inflammatory Mφs, and anti-inflammatory Mφs. Non-activated Mφs are quiescent until they get pushed by a "classical" (M1) or an "alternatively" (M2) pathway, respectively. The classical pathway describes the activation of quiescent Mφs to an M1 Mφs phenotype due to pathogen-associated stimuli (i.e. lipopolysaccharide, LPS) and T-cell released cytokines (e.g. interferon gamma, IFNγ). The alternative pathway on the other hand is responsible for the activation of quiescent Mφs to an M2 Mφs phenotype, performed by interleukin (IL)-4 and IL-13 stimulation. Classical activated Mφs are characterized by an enhanced production of pro-inflammatory cytokines and are therefore associated with the inflammatory stimulation during early wound healing, whereas alternative activated Mφs act on fibroblasts to induce tissue repair post-injury and to resolve inflammation in later wound healing processes (27).

1.2.3 ECM degradation products affect macrophage polarization

Previously, our group has investigated that ECM transplantation to rat models with bilateral partial thickness abdominal wall injury is associated with improved wound healing when compared to the untreated control group (28). Furthermore, that tissue remodeling was associated with an enhance in pro-regenerative M2-"like" Mφs, while scar tissue formation was accompanied by an increase in pro-inflammatory M1-"like" Mφs. Furthermore, a third population of Mφs has been investigated with this study, the "M_{ECM}" phenotype. M_{ECM} Mφs were characterized by the expression of both, M1- and M2-associated Mφs surface markers and transcription factors. It has been suggested that M_{ECM} Mφs development was induced by the ECM bioscaffold (29). Therefore, we concluded that ECM bioscaffolds may drive Mφs polarization towards an M2-"like" phenotype to stimulate tissue remodeling by a yet unknown mechanism. Furthermore, that a different population of Mφs, the M_{ECM} Mφs, may play a role in ECM-induced regenerative mechanisms. Hence, the aim of the current study is to investigate the in-depth effects of ECM degradation products on Mφs polarization.

1.2.4 In-depth Macrophage study

In the present study, murine bone marrow-derived Mφs (BMDM) and human THP-1-cell differentiated Mφs were treated with ECM degradation products or with M1- or M2-Mφs associated cytokines to derive a M1-"like"- or a M2-"like-Mφs phenotype state, respectively. Both cell lines have been reported as valid *in vitro* models for monocyte and Mφs studies (30, 31). The gene and the protein expression level of M1 and M2 Mφ markers (M1 and M2-associated surface markers, transcriptional factors and metabolic Mφ markers) were analyzed by qPCR and Western Blot. Used previously indicated M1 and M2 marker include the following (Supplemental Material and Methods, Table 1): Tumor necrosis factor alpha (TNF-α) (32), nictric oxide synthase (iNOS) (33), interferon regulatory factor 3 (IRF3), IRF5 (34), krüppel-like transcription factor 6 (KLF6) (35), signal transducer and activator of transcription 1 (STAT1), STAT2 , and STAT5 (36) were detected as M1-

associated surface markers and transcrition factors, the glycolytic metabolics (Supplemental Data, Figure S1A) glucose transporter 1 (GLUT1), hypoxia-inducible factor 1-α (HIF1a), hexokinase 3 (HK3), lactate dehydrogenase A (LDHA), 6-phosphofructo-2-kinase-fructose-2,6-biphosphatase 3 (PFKFB3), phosphoglycerate kinase 1 (PGK1), pyruvate dehydrogenase lipoamide kinase isozyme 4 (PDK4), and ribose 5-phosphate isomerase A (RPIA) (37) as metabolic markers of M1-"like" Mφs (Supplemental Material and Methods, Table 1.a). Furthermore, M2 Mφs transcrition factors and surface markers that were detected were arginase-1 (ARG-1) (33), mannose receptor (CD206) (38), interleukin-1 receptor antagonist (IL1Ra) (39), IRF4 (40), KLF4 (41), STAT3, STAT6 (36), peroxisome proliferator-activated receptor gamma (PPARg) (42), transglutaminase 2 (TGM2) (39), FIZZ1 (43), and detected M2 Mφ metabolic markers associated with oxidative and gluconeogenetic pathways (Supplemental Data, Figure S1B and S1C) were phosphoenolpyruvate carboxykinase 1 (PCK1), PCK2, glucose-6 phosphatase (G6PC3), and PPARd (37) (Supplemental Material and Methods, Table 1.b).

Herein, in our first project we hypothesize that ECM degradation products drive Mφs towards an anti-inflammatory M2-phenotype.

1.3 ECM bioscaffolds contain matrix-bound nanovesicles (MBVs)

As indicated, ECM bioscaffolds contain a variety of biological active components that can regulate part of the regenerative mechanisms induced by ECM bioscaffolds, such as laminin, growth factors, and fibronectin. In order to address additional working mechanisms of ECM bioscaffolds, the regulatory functions of its biocomponents and the biocomponents itself, need to be further analyzed. Interestingly, it has never been shown before, that RNA is present in ECM bioscaffolds.

Therefore, the presence of small RNA molecules in various ECM bioscaffolds has been investigated in our group by nucleic acid extraction. Herein, it has been shown that nucleic acids of the size of small RNA molecules were integrated in various in-house and commercial produced extracellular matrix materials (Supplemental Data, Figure S2) (Huleihel et all. (Science advances – "in press")). Furthermore, treatment of ECM bioscaffolds with DNase I or RNase A prior to nucleic acid extraction showed an incomplete degradation of these mirco RNA molecules (miRNA), indicating that ECM miRNA may be protected from degradation processes (Supplemental Data, Figure S3) (Huleihel et all. (Science advances – "in press")). From this, we suggested that these miRNA molecules may be packed in extracellular vesicles embedded in a variety of ECM materials.

1.3.1 Extracellular vesicles

EVs are nano-sized vesicles created by mammalian and non-mammalian cells by different mechanisms (44). EVs can be divided by size and their different release pattern into various subtypes, i.e. exosomes, microvesicles, apoptotic bodies and. Exosomes are defined by a size of 30 to 100 nm in diameter (45), microvesicles (MVs) by 100 to 1000 nm, and apoptotic bodies (APs) by 1 to 5 µm (46). Furthermore, while MVs and APs, are both vesicles created from the plasma membrane by budding from cells (living cells for MVs and apoptotic cells for APs), exosomes are developed by a more complex mechanism (Figure 2) (46, 47).

For exosomal biogenesis, cell surface molecules, extracellular fluids and molecules are internalized by clathrin coated endocytosis to form vesicles which are called early endosomes (48, 49). Early endosomes mature then to its later stage, the late endosomes. At final maturation, late endosomes perform inward invagination of their own membrane to form intraluminal vesicles (ILV). Hereby, ILV encloses randomly intracellular particles. Late endosomes surrounding ILV are additionally referred to as multivesicular bodies (MVB) (49). MVB can undergo two different pathways. First, MVB may fuse with lysosomes leading to degradation of ILV and the residual MVB content. An alternative pathway to lysosomal fusion is the integration of MBV with the plasma membrane. Hereby, MVB release their content such as ILV which are then referred to as exosomes (48, 49). Exosomes are stimulated to interact with adjacent cells by unknown mechanisms. Hereby, exosomes can cause an activation of intracellular signaling cascades, can transfer genetic material and/or induce a change in cellular phenotype (50).

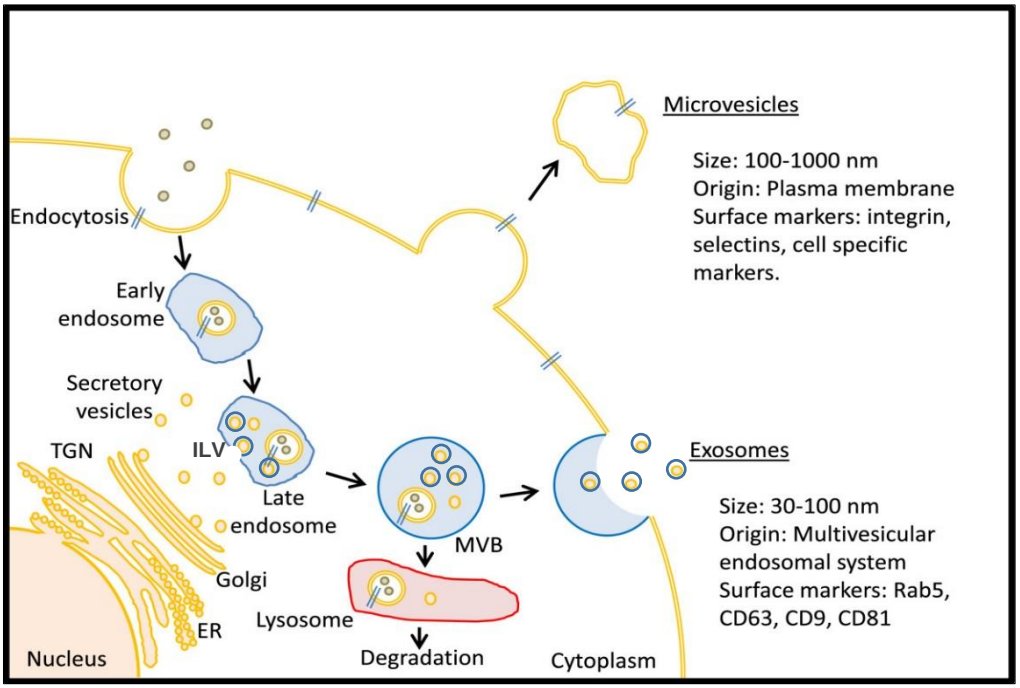

Fig. 2: **Biogenesis of exosomes and microvesicles.** While microvesicles are shed from the membrane as blebs, exosomes develop from a more complex way. Exosomes originate from molecules that are internalized into eukaryotic cells by endocytosis to form early endosomes. Early endosome mature to late endosomes. Late endosomes perform inward invagination of their own membrane during their latest maturation step to ILV. Late endosomes carrying ILV are also referred as MVB which can undergo two different ways. MVB can either fuse with lysosomes to induce ILV degradation or they fuse with the plasma membrane to release their content. Released ILV are then referred to as exosomes which are 30-100nm in diameter (Anthony et al., 2013, adapted). *ILV - intraluminal vesicles, MVB - multivesicular bodies.*

The definition of EVs has changed in distinct ways since 1973. Firstly, the function of EVs was underestimated; however, they were described by N. C. Mishra and E. L. Tatum in 1973 as DNA fragments that carry and transfer genetic material. Not being aware of the definition of EVs, it was thought that these DNA fragments could be eliminated during meiosis by several mechanisms causing loss of genetically information (51). However, Trams et al. (52) redefined EVs to be vesicles shed from the plasma membrane of healthy and neoplastic cell lines. They detected two different vesicles populations which were distinguished by their size in diameter (500 to 1000 nm and 40 nm diameter) (52). Later, EVs were characterized as vesicles with a size of 50nm (53) which develop during reticulocytes to erythrocytes maturation (54, 55).

In subsequent years, EVs were redefined with a size of 30 – 1000 nm in diameter (45, 56). Beside this, they were found to be released from different cell types, such as immune cells (B cells, T cells (56), and dendritic cells (57)), skeletal muscle cells (58), neural cells, epithelial cells, and mesenchymal stem cells (59). Furthermore, EVs were detected to be located in different body fluids including blood (56), serum, saliva (60), urine (61, 62), amniotic fluid (62) and semen (61). Another aspect which turned EVs to an interesting research field is that they can carry different cargos from cell-to-cell to regulate an uncharacterized range of various physiological mechanisms,

including lipids, growth factors, mRNA, microRNA (44), nucleic acids and transmembrane as well as soluble proteins (47). Among these are immuno-regulatory processes, such as adaptive and innate immune responses (63, 64), cell maturation (65), gene regulation (64), and nutrient transfer to cells (66). Reaching their target cells, EVs have different possibilities to interact with them. First, their transmembrane proteins can bind to membrane receptors to initiate cellular signaling cascades. Or as an alternative, EVs fuse with their target membrane and their cargo will be subsequently released into the cell to interact with different intracellular mechanisms (47).

1.3.2 EVs in Regenerative Medicine

Beside the pivotal role of EVs in healthy organisms, there is evidence that EVs play an important role during disease onset and progression. Moreover, EVs are characterized by a different release-patterns and cargo in pathological conditions when compared to healthy normal cells (67). Unhealthy cells release an increased amount of EVs to activate and to stimulate cell-to-cell communication during pathological conditions (68). This phenomena has already been shown in clinical and animal studies of different disease models. These are: E.g. cancer (68-70), neurodegeneration in Alzheimer and Parkinson disease (38, 68), fibrosis (71), and hypoxia induced pathologies, including stroke and myocardial infarction (72).

While EVs under pathological conditions are known to stimulate pathogenesis by affecting immune responses, angiogenesis, and cell growth (68-70, 73, 74), among others, making use of these characteristics sparked the possibilities of EVs as therapeutically application in regenerative medicine. Currently studied methods to enhance tissue remodeling are based on progenitor/stem-cells, such as mesenchymal stem cells (MSCs). Both are recruited to the site of injury to induce wound healing mechanisms and therefore attracted a lot of attention in different studies (75). Earlier, MSCs were reported to exert regenerative functions by itself (76), but now it is suggested that soluble factors and/or factors packed in EVs secreted by MSCs can stimulate regenerative processes (75, 76). To date, multiple cell lines show beneficial regenerative effects post-injury by their release of molecules and/or EVs, such as epithelial cells, and chondrocytes (77). Making use of these properties, AMS Biotechnology provides EVs derived from human placental and adipose stem cells for regenerative medical research (78).

While EVs seem to have a high impact on regenerative processes, lack of standardized EVs isolation protocols and its labor intensity makes EVs research a complicated and protracted process. Moreover, the variability in isolation protocols among various research groups (e.g. ultracentrifugation, precipitation using chemicals or other filtration methods) leads to a high variety in obtained EVs which makes it challenging to compare scientific results and to use EVs for diagnostics and therapeutically application methods. To date, optimization and standardization of isolation protocols is an important step in EV research to increase purity and specificity of the samples for further research purposes (79, 80).

1.3.3 MiRNA

MicroRNA (miRNA) are small, noncoding RNAs consisting of 19-25 nucleotides which downregulate gene expression by binding target mRNA to its 3'-untranslated regions to cause mRNA degradation. Hence, miRNA has a regulatory function on gene expression (81). To date, miRNAs are known to affect a variety of pathophysiological conditions, including multiple sclerosis (82), osteogenesis (83), carcinogenesis (84), but also regenerative mechanisms, such as fibrosis (85), among others. Therefore, miRNAs may play a major role as key regulator of diseases, tissue homeostasis and repair mechanisms (86), suggesting that targeting miRNA could be used as potential therapeutically treatment in tissue remodeling and regenerative medicine methods (81).

The aim of the second research project was to identify ECM embedded EVs, to analyze their miRNA cargo and the cell regulatory mechanisms that these miRNAs are associated with. Furthermore, we wanted to investigate if EVs can mimic the effects ECM bioscaffolds on cellular behavior. These EVs have been indicated as matrix-bound vesicles (MBVs).

1.4 Study hypothesis and objectives

Hypothesis

We hypothesize that ECM degradation products mimic the *in-vivo* effect and drive macrophage to a more anti-inflammatory M2-"like"- phenotype. Furthermore, the presence of protected small RNA molecules in body fluids has been indicated in previous studies. We hypothesize that these small RNA molecules may be also packed in the matrix by "MBVs" and may play a key role in various molecular and cellular functions associated with regenerative mechanisms.

Objective

The objectives of the present studies were to identify the in vitro effects of ECM degradation products on macrophage phenotype polarization. This study will involve analyzing gene and protein expression of M1- and M2- associated surface markers, transcription factors and metabolic markers in two different cell types. Additionally, to examine the presence, cargo (RNA molecules) and function EVs embedded in naturally occurring ECM scaffolds.

2. Material and methods

2.1 Preparation of ECM Bioscaffolds

Dermal ECM, urinary bladder matrix (UBM) and small intestine submucosa (SIS) has been used. All of them originate from porcine tissue and were prepared by a similar process, consisting of mechanical delamination and a following decellularization process. Pigs underwent strict controls previously to and after euthanasia.

Dermal Extracellular matrix. ECM of porcine dermis has been produced as previously described (87). Namely, immediately after sacrificing, full thickness dermis has been harvested from the dorsolateral side of freshly slaughtered market weight (ca. 110kg) pigs (Tissue source, Lafayette - Indiana, U.S.A.). Upon arrival, all skin tissues have been cut into 35 x 50 cm pieces and afterwards mechanical handled to remove subcutaneous fat. Dermal sheets were then placed into distilled water for 60 to 180 minutes and afterwards the residual subcutaneous fat, the epidermis and residual collagen were mechanically removed. All dermal tissue has immediately been frozen at -80°C for storage. For decellularization, thawed porcine skin samples were chemically treated by agitation at room temperature using 300 RPM. Hereby, following solutions were used (Supplemental Material and Methods, Table 2.a): The samples were first incubated into 0.25% trypsin (Thermo Fisher Scientific, Waltham - Massachusetts, U.S.A.) for 6 hours, three times washed with deionized H_2O, each for 15 minutes, then exposed to 70% ethanol for 10 hours, treated with 3% hydrogen peroxide for 15 minutes, twice washed with deionized H2O for respectively 15 minutes, treated with 1% Triton X-100 (Sigma-Aldrich, St. Louis - Missouri, U.S.A.) in 0.26% EDTA/0.69% Tris for 6 hours, which was followed by an incubation period in renewed solution of 16 hours, and subsequently three times washed with deionized water. Additionally, tissues were then exposed to 0.1% peracetic acid (PAA) with 4% ethanol (Rochester Midland, Rochester - New York, U.S.A.) for 2 hours, twice washed with 1x Phosphate-buffered saline (PBS, pH7.4), each for 15 minutes, and twice with deionized water for 15 minutes. All dermal samples were then lyophilized and powdered using a Wiley Mill and a #40 mesh screen.

Urinary Bladder Matrix. UBM was isolated from porcine urinary bladder as previously described (88). In brief, urinary bladders were collected from freshly slaughtered market weight pigs (Tissue source). Adipose tissue and collagen of the bladder were cleared using scissors. Residual urine has been cleaned with water. Afterwards, the urinary bladder was cut in half and the muscular tunic was removed by scraping. Residual layers are the submucosal and the serous tunic which were then removed by physical delamination to receive an intact basal lamina and lamina propria of the mucosal tunic. The obtained UBM layers were then washed with deionized water and afterwards treated with 0.1% PAA/4% ethanol for decellularization (Supplemental Material and Methods, Table 2.b) and disinfection using a vortex shaker at 300 RPM for 2 hours. Decellularization was followed by four times 15 minutes washing steps: Twice with 1x PBS (pH7.4), followed by two times rinsing with deionized water. All UBM samples were then lyophilized and reduced to small particles using a Wiley Mill with a #60 mesh screen.

Small Intestinal Submucosa Matrix. Small intestinal submucosa (SIS) has been prepared from jejunum as previously described (89). In brief, small intestines (SI) have been isolated from freshly slaughtered market weight pigs (108 - 117 kg). Jejunum was harvested by cutting the SI close to its Peyer`s Patch using scissors. Afterwards, the SI has been rinsed with deionized water 4 to 5 times. The clean SI tissue has been longitudinally opened with a razor blade. The method of mechanical delamination and decellularization to obtain SIS tissue was similar to the process for UBM preparation. First, the overlying layers of the tunica mucosa, the serous tunic and the external muscular tunic, have been mechanically removed, maintaining the basement membrane and the submucosa tunic, as referred to be SIS. All SIS samples were then decellularized (Supplemental Material and Methods, Table 2.b) by an incubation period of 2 hours into 0.1% PAA/4% ethanol using a vortex shaker at 300 RPM at room temperature. SIS sheets were then washed with 1x PBS (pH7.4), with deionized H2O and then lyophilized. Afterwards they were reduced into particulate form by making use of Wiley Mill with a #60 mesh screen.

Commercial ECM bioscaffolds were obtained from various companies: MatriSTEM™ UBM from ACell® (Columbia - Maryland, U.S.A.), XenMatrix™ dermis from C.R. BARD, Inc. (Providence - Rhode Island, U.S.A.) and Biodesign™ SIS from Cook® Biotech (West Lafayette - Indiana, U.S.A.). All products are non-crosslinked ECM scaffolds to allow revascularization and cellular infiltration. ECM scaffolds are used in patients nowadays to reinforce weak and to repair damaged soft tissue (2-4).

2.2 Derivation of ECM Degradation Products

UBM and SIS were enzymatically degraded as previously described (90) with pepsin from Porcine Stomach Mucosa (MP Biomedicals, Santa Ana - California, U.S.A.) by mixing lyophilized, powdered UBM (10 mg/mL) and pepsin (1 mg/mL) in 0.01 M HCl (pH 2.0). This solution was stirred at room temperature for 48 hours. After stirring, the UBM slurry was neutralized to a pH of 7.4 in 1× PBS (137 mM NaCl, 2.7 mM KCl, 12 mM Phosphate, Thermo Fisher Scientific) to inactivate the pepsin.

2.3 Cell culture

THP-1 human monocytes. Human monocytic THP-1 cells (American Type Culture Collection, Manassas - Virginia, U.S.A.) were cultured as previous described (91). Briefly, THP-1 human monocytes were obtained from the American Tissue Culture Collection (ATCC, Manassas – Virginia, U.S.A. and maintained in RPMI, 10% FBS (Invitrogen, Carlsbad - California, U.S.A.), 1% penicillin/streptomycin (Sigma Aldrich), and 50 µM of 2-Mercaptoethanol in a humidified atmosphere at 37 °C with 5% CO_2. Two million THP-1 cells were plated with 320 nM phorbol 12-myristate 13-acetate (PMA, Sigma Aldrich) for 24 hours to induce differentiation into macrophages. Adherent macrophages were washed in PBS and placed in fresh media, followed by 72 hours incubation in fresh media to acquiesce. THP-1 monocytes were differentiated towards macrophages with PMA and rested. This protocol has been shown to result in a phenotype that is nearly indistinguishable activity from human peripheral blood macrophages (92).

Bone marrow-derived macrophages. Murine bone marrow-derived macrophages (BMDM) were isolated as previously described (80). Briefly, tibia and femur were isolated from the proximal hind limb of adult, female 6–8-week old C57bl/6 mice obtained from Jackson Laboratories (Bar Harbor - Maine, U.S.A.). Mice were euthanized with CO_2 and by additional cervical rupture. Bones were kept on ice and rinsed in a sterile dish containing macrophage complete medium consisting of DMEM high glucose (Gibco, Grand Island - New York, U.S.A.), 10% FBS (Invitrogen), 10% L929 supernatant, 0.1% 2-mercaptoethanol (Gibco), 100 U/ml penicillin, 100 µg/ml streptomycin, 10 mM non-essential amino acids (Gibco), 1% penicillin/streptomycin (Sigma Aldrich) and 10 mM hepes buffer. In a sterile environment, the ends of each bone were transected and the marrow cavity flushed with complete medium using a 30-gauge needle. Harvested cells were washed and plated at 10^6 cells/ml, and allowed to differentiate into macrophages for 7 days at 37 °C, 5% CO2 with complete media changes every 48 h for seven days resulting in naïve macrophages.

C2C12 muscle myoblasts. C2C12 mouse muscle myoblast cells from the American Type Culture Collection (ATCC) were cultured in media containing DMEM high glucose media (Invitrogen), 10% FBS and 1% penicillin/streptomycin (Sigma Aldrich) 5% CO2, 37°C.

N1E-115 mouse neuroblastoma cells. Murine neuroblastoma cells from ATCC were cultured in DMEM high glucose media (Invitrogen), completed with 5% FBS, 1% L-glutamine of 2mM and 1% penicillin/streptomycin (Sigma Aldrich) at 37°C, 5% CO2. 10^6 cells/ well were plated on 6-wells plates and then exposed to MVBs (5µg/ml) of UBM source.

Perivascular stem cells. 20,000 cells/cm² of perivascular cells were (company) were cultured as previously described (93). Briefly, confluent cells were seeded in endothelial growth media 2 (Cambrex BioSciences, Charles City - Iowa, U.S.A.) on 0.2% gelatin coated plates (Calbiochem, Billerica- Massachusetts, U.S.A.) at 37°C for 2 weeks. Cells were then detached using trypsin-EDTA (Gibco) at an incubation period of 10 min at 37°C and then 1:3 plated on uncoated plates in grow media (DMEM high glucose, 20% FCS, and 1% penicillin/streptomycin, Gibco) until the 5th passage was reached. Cells were then split 1:6 under similar conditions. To measure the cell proliferation of perivascular cells, the bromodeoxyuridine (BrdU proliferation assay (Millipore, Billerica - Massachusetts, U.S.A.) was performed as previously described (94). In brief, BrdU was applied for 4 hours and the cells were then isolated by a centrifugation step. BrdU was then detected with appropriate anti-BrDU antibodies. Using a microplate reader (Infinite M200, Tecan), the plate was read with an emission of 325nm and emission of 420 nm.

2.4 Macrophage polarization and treatment

THP-1 differentiated macrophages and BMDM macrophages were treated with **(1)** 20 ng/ml Interferon gamma (IFNγ, Sigma Aldrich) and 100 ng/ml Lipopolysaccharide (LPS, Sigma Aldrich) to derive M1 macrophages, or **(2)** 20 ng/ml Interleukin-4 (IL-4, Sigma Aldrich), and **(3)** 250 ug/ml of UBM and SIS ECM degradation products to derive M2 macrophages. 250 ug/ml of pepsin was used as control buffer. All incubation periods were 24 hours at 37 °C, 5% CO_2. Additionally, both cell lines were treated with 20 ng/ml IFNγ and 100 ng/ml LPS or 20 ng/ml IL-4 for 6 hours at 37 °C, 5% CO_2, followed with 250 ug/ml UBM and SIS ECM degradation products for 24 hours at 37 °C,

5% CO_2. The reverse experiment was also performed: First, 250 ug/ml UBM and SIS ECM degradation products treatment for 24 hours and then 20 ng/ml IFNγ and 100 ng/ml LPS or 20 ng/ml IL-4 treatment for 6 hours. Cells were washed with sterile 1x PBS after incubation and in between each treatment cells and fixed with 2% paraformaldehyde for immunolabeling or harvested with TRIZOL/RIPA buffer (Thermo Fisher Scientific) for RNA/Protein assessment, respectively.

2.5 RNA isolation and cDNA synthesis.

Cellular RNA was isolated using the miRNeasy Mini kit (Qiagen, Valencia – California, U.S.A.) according to the manufacturer's instructions (Supplemental Material and Methods, Protocol 1). RNA concentration was analyzed by the Nanodrop spectrophotometer (NanoDrop, Wilmington – Delaware, U.S.A.). Reverse transcriptase from RNA to cDNA was preformed via high capacity RT kit (ABI, Foster City - California, U.S.A.) according to the manufacturer's instructions (Supplemental Material and Methods, Protocol 2).

2.6 qPCR

SYBR Green gene expression assays (ABI, Foster City – California, U.S.A.) were used to determine the relative gene expression of M1- and M2-associated macrophage transcription factors, surface markers and metabolic markers: M1-associated surface markers and transcription factors were TNF-α, iNOS, IRF3, IRF5 KLF6, STAT1, STAT2, STAT5, STAT5A, and STAT5B, and metabolic M1-markers accodring to glycolytic metabolics were GLUT1, HIF1A, HK3, LDHA, PFKFB3, PGK1, PDK4, and RPIA (Supplemental Material and Methods, Table 3). M2-associated surface markers and triscrition factors that were detected were Arg-1, CD206, IL1Ra, IRF4, KLF4, STAT3, STAT6, PPARγ, TGM2, and FIZZ-1, and as metabolic M2-associated markers were PCK1, PCK2, G6PC3, and PPARδ detected (Supplemental Material and Methods, Table 3). Results were analyzed by the ΔΔCt method using β-glucuronidase (β-GUS) control for treated THP-1 cell differentiated macrophages and Glyceraldehyde 3-phosphate dehydrogenase (GAPDH) for treated BMDM to normalize the results. Fold change was calculated taking untreated as the baseline.

2.7 SDS Page and Western blot

Prior to Western Blot, protein concentration of each sample was analyzed using bicinchoninic acid (BCA) protein assay kit of Pierce Chemical (Thermo Fisher Scientific; Supplemental Material and Methods, Protocol 3). Samples were diluted 1:1 in Laemmli buffer (Bio-Rad, Minneapolis, Minnesota - U.S.A.). To a proper protein separation by size, disulfide bonds in and between molecules were reduced by adding 5% (v/v) 2-mercaptoethanol (Gibco). Protein samples were denaturized for 5 minutes at 95°C and then loaded on 5% to 15% gradient acrylamide gels (Bio-Rad, Hercules - California, U.S.A.). Specifically, 20 µg of protein was loaded into each well. Polypeptides of ~2 to 400 kD were separated from each other by running the gel at 120 mV for ~90 minutes (Supplemental Material and Methods, Protocol 4). For gel running, the Mini-Protean® Electophoresis System (Bio-Rad, Hercules - California, U.S.A.) and 1x running buffer (25 mM Tris base, 192 mM glycine, 0.1% (v/v) SDS, pH8.3) was used. Proteins present in gels were then

transferred to polyvinylidene difluoride transfer membranes (Millipore) by semi dry transfer for 45 minutes at 20mV using transfer buffer (25mM Tris base, 192 mM glycine, 20% (v/v) methanol, 0.025% (v/v) SDS, pH8.3). Polyvinylidene difluoride membranes were 3x washed for 15 minutes using 1x TBST washing buffer (1X TBS/0.1% Tween-20) and then blocked in Pierce™ Protein-Free (PBS) Blocking Buffer (Thermo Fisher Scientific), to avoid nonspecific bindings. This was followed by an incubation period with these primary antibodies overnight: STAT1 (1:1000, Cell Signaling Technology, #9172S, Danvers – Massachusetts, U.S.A.) CD206 (1:500, Abcam, #ab64693), TGM2 (1:500, Abcam, #ab21258) and TNF-α (1:200, Abcam, #ab6671) (Supplemental Material and Methods, Table 4) to detect M1- and M2-macrophage phenotype protein expression levels in THP-1 samples that were prior treated with appropriate cytokines or ECM degradation products for 24 hours or with CD-63, CD-81, CD9 and Hsp70: rabbit anti-CD63, -CD81, -CD9, and – Hsp70 (1:800 dilution, #EXOEL-CD63A-1, #EXOEL-CD81A-1, #EXOEL-CD9A-1, #EXOEL-Hsp70A-1, SBI Mountain View – California, U.S.A) (Supplemental Material and Methods, Table 4) to detect the extracellular vesicle surface marker. β-actin was used as endogenous control (1:1000, sc-4778, Santa Cruz Biotechnology, Dallas – Texas, U.S.A.). After incubation, membranes were 3x washed for 15 minutes and then incubated with appropriate secondary antibody (Supplemental Material and Methods, Table 4). Afterwards, the membranes underwent a last 3x washing step and were then exposed to the chemiluminescent Clarity™ Western ECL Blotting Substrate (Bio-Rad, Hercules - California, U.S.A) which induces the oxidation of luminol by HRP to produce light and therefore visualizes the surface proteins. For visualization, the ChemiDoc Touch Imaging Instrument of Bio-Rad (Hercules - California, U.S.A) was used.

2.8 ECM digestion for MBVs release

As previously described, all ECM bioscaffolds were isolated from porcine tissue, which was followed by mechanical delamination, decellularization, lyophilization and milling to receive ECM powder. For MBVs isolation from ECM particles, all powdered samples were digested by using one of the following enzymatic digestion solutions for 24 hours at room temperature: 0.1 mg/ml proteinase K diluted in buffer containing 50mM Tris-HCl of pH8 and 200mM NaCl, 1mg/ml pepsin in buffer consisting of 0.01M HCl, or 0.1mg/ml collagenase in buffer containing 50mM Tris of pH8, 5mM CaCl2 and 200mM NaCl. All enzymatic buffers were filtered through a 0.22µm filter united (Millipore) previously to ECM addition.

For digestion methods, commercial pepsin isolated from the porcine gastric mucosa of MP Biomedical (Solon - Ohio, U.S.A.), collagenase isolated from the culture filtrate of Clostridium histolyticum (Sigma Aldrich), and the broad-range endolytic protease Proteinase K (Thermo Fisher Scientific) were used. While pepsin was required to digest ECM powder into ECM hydrogels for cellular treatment, Collagenase and Proteinase K were used to isolate extracellular vesicles from ECM powder.

2.9 MBVs isolation

Previously digested ECM samples underwent following centrifuge steps to obtain a collagen free supernatant: 3x 500g for 10 minutes, 3x 2,500g for 20 minutes and 3x 10,000g for 30 minutes. In between each step, all pure supernatans were transferred to a clean 15 ml tube. After the last 10,000g centrifugation, the supernatants were filtered through a 0.22µm filter united (Millipore) and transferred to ultracentrifuge tubes. The supernatant underwent then an additional spinning using the ultracentrifuge at 100,000g for 70 minutes at 4°C (Optima L-90K - Beckman Coulter, Inc.) to pellet MBVs. Pellets were resuspend in 500 µl of 1x PBS and stored on -80°C. To ensure that no MBVs were present in the digestive solutions, the plain preparations underwent the same centrifugation steps. Herein, these samples were referred to as negative controls.

2.10 MBVs imaging

MBVs resuspended in 500 µl PBS were imaged using the transmission electron microscope (TEM) (Supplemental Material and Methods, Protocol 5). MBVs were loaded on copper grids and for their visualization negative stained with 1% uranyl acetate. Residual liquid on the grid was afterwards discarded with cellulose filter paper (Whatman, Pittsburgh - Pennsylvania, U.S.A.). Imaging of MBVs was performed at 80kV by using the JEOL 1210 TEM containing a digital high-resolution ATM camera and the JEOL TEM software.

2.11 Determination of MBVs size

The size and the concentration of MBVs diluted in 500 µl of particle free PBS have been determined by the Nanoparticle Tracking Analysis (NTA) as previously described (95). NTA is a feasible method that was used to analyze each particle in solution simultaneously and to distinguish the different particles from each other by fluorescent methods (96). NTA was accomplished using the NanoSight NS500 instrument and the 2.3 Analytical Software (Release Version Build 0025, NanoSight Ltd., Wiltshire, UK). LM10 system was used to determine MBVs size by analyzing the Brownian motion rate. The setup for the camera was as follows: The ambient temperature was ranging from 24°C to 27°C, camera shutter speed was 30.01 ms, camera gain was 500, the threshold of camera sensitivity was adjust to its maximum (15 or 16) and of camera detection to its minimum (3 or 4) for small-sized MBVs detection. Diluted MBVs were administered into a NanoSight cubicle using a syringe pump. Of each sample, 30 to 60 sec of flow was recorded under controlled conditions resulting in a histogram. The area under the curve measured by the Prism-4 software (Version 4.03, Graph Pad, San Diego, California, U.S.A.) indicated the amount of all particles per sample.

2.12 Silver staining

SDS-PAGE gel was performed as previously described. Protein cargo of loaded MBVs samples were stained using the Silver Stain Plus Kit (Bio-Rad, Hercules - California, U.S.A) according to manufacture instruction and visualized by a Chemidoc Touch instrument (Bio-Rad, Hercules - California, U.S.A).

2.13 RNA sequencing

Non-coding miRNA libraries were obtained by using Ion Total RNA Seq Kit v2 (Thermo Fisher). RNA was selected by its bead size ranging from 10 to 200 nucleotides (nts) and then hybridization, ligation of sequencing adapters and reverse transcription was performed to create cDNA, followed by PCR. To analyze library size distribution, bead size selected small RNA libraries were run on a bioanalyzer. Emulsion PCR was performed by Ion One Touch 2 System. For miRNA sequencing, Ion Proton and a P1 sequencing chip was used and data was analyzed (CLC Genomics Workbench 8, Quiagen). Reads with 2 ambiguously nts, a Phred score <30, or with less than 15 or more than 100 nts were eliminated. Residual reads were standardized to the Human genome (Hg38), extracted and counted by the miRNA database miRBase 21. A mismatch of 2 nts/sample was allowed. MiRNA signaling pathways were then determined using Ingenuity Pathway Analysis (IPA) of identified miRNA samples.

2.14 Fluorescent labeling of MBVs nucleic acid cargo

For MBVs tracking, their cargo was fluorescent labeled using SBI Exo-Glow kit (Mountain View – California, U.S.A.). In brief, in 500 µl 1x PBS resuspended MBVs were exposed to Exo-Glow labeling for RNA (red) and protein (green) detection and then incubated for 10 minutes at 37°C. To stop the reaction, 100 µl of ExoQick-TC were added and labeled solution was then placed on ice for 30 minutes. To separate MBVs from the solution, samples were centrifuged at 14,000 x g for 10 minutes using a microfuge and the supernatant was removed. The pellet was then resuspended in 500 µl 1x PBS of which 50 µl was transferred to cultured C2C12 cells. After an incubation period of 4 hours, tracking of MBVs cargo has been analyzed by using an Axio Observer Z1 microscope.

2.15 Macrophage Immunolabeling

To determine macrophage surface marker expression profiles, treated BMDM were fixed with 2% paraformaldehyde. Primary antibodies used for immunofluorescent staining on BMDM were: (1) monoclonal anti-F4/80 (Abcam, Cambridge – Massachusetts, U.S.A.) at 1:200 dilution for a pan-macrophage marker, (2) polyclonal anti-iNOS (Abcam) at 1:100 dilution for an M1 marker, and (3) polyclonal anti-Fizz1 (Peprotech, Rocky Hill – New Jersey, U.S.A.) for an M2 marker. Cells were incubated in blocking solution consisting of PBS, 0.1% Triton-X, 0.1% Tween-20, 4% goat serum, and 2% bovine serum albumin to prevent non-specific binding for 1 h at room temperature. Blocking solution was removed and cells were incubated in primary antibodies for 16 h at 4 °C. After washing in PBS, cells were incubated in fluorophore-conjugated secondary antibodies (Alexa Fluor donkey anti-rat 488 or donkey anti-rabbit 488, Invitrogen) for 1 h at room temperature. After washing again with PBS, nuclei were counterstained with 4’6-diamidino-2-phenylindole (DAPI) prior to imaging. Images of three 20× fields were taken for each well using a live-cell microscope. Light exposure times for ECM-treated macrophages were standardized based upon those set for cytokine-treated macrophages, which served as a control. Images were quantified using a CellProfiler pipeline for positive F4/80, iNOS, and Fizz1 percentages.

3. Results

ECM can effect macrophage polarization

Real-time PCR of isolated RNA from murine bone-marrow derived macrophages (BMDM) and human THP-1 differentiated macrophages (THP-1) that underwent prior each three different treatment methods was performed to detect M1- and M2-associated Mφs markers. These treatments include the following (Supplemental Material and Methods, Protocol 6): (1) 24 hours incubation period of LPS and IFNγ to derive an "M1-like" macrophage phenotype (M1-treatment), of IL-4 to derive an "M2-like" macrophage phenotype (M2-treatment), or of pepsin digested UBM and SIS ECM degradation products to derive "M_{ECM}-like" macrophages (ECM treatment). Herein, cells that were treated with pepsin or with appropriate culture media were used as control groups. (2) The second treatment group underwent M1- or M2-treatment for 6 hours, followed by a change in media and 24 hours ECM-treatment or (3) the reverse experiment, which is 24 hours ECM-treatment followed by 6hours M1- or M2-treatment. The last two treatments are referred as "challenge experiments". A scoring system was used to determine the gene expression level of M1- and M2-markers. Scoring was based on cells treated with media instead of ECM degradation products (Supplemental Data, "Tables and Figures Gene Expression M1- and M2- macrophage marker", Table S1).

Identified M1- and M2-associated transcription factors and surface markers were TNF-α, iNOS, IRF3, IRF5 KLF6, STAT1, STAT2, STAT5, STAT5A, and STAT5B or Arg-1, CD206, IL1Ra, IRF4, KLF4, STAT3, STAT6, PPARγ, TGM2, and FIZZ-1, respectively (Fig. 3A and B). Identified glycolytic metabolics (GLUT1, HIF1a, RPIA, HK3, PGK1, PDK4, PFKBF3, and LDHA) were referred as M1 metabolic marker, whereas gluconeogenetic or oxidative substrates (PCK1, PCK2, G6PC3, FBP2, PPARδ, and PPARγ) were identified as M2 Mφs marker (Fig 3C and D) (Supplemental Data, "Tables and Figures Gene Expression M1- and M2- macrophage marker", Table S1, Fig. S4 and S5).

Real-time PCR results indicate a difference in gene expression of M1- and M2-marker post-ECM-treatment, depending on the source of ECM tissue as well as the cell type that interact with ECM degradation products. Whereas 24 hours ECM-treatment to BMDM enhanced M1-associated surface markers and transcription factors as well as decreased M2-Mφs markers (Fig. 3A, panel 1), there was overall no change seen in THP-1 differentiated cells after 24 hours ECM-treatment (Fig. 3B, panel 1). The results in BMDM were similar to M1- and M2-treated control groups, indicating reliable results. This enhance in M1-Mφs marker in BMDM was attenuated with M1- (Fig. 3A, panel 2 and 3) or hold with M2-treatment (Fig. 3A, panel 4 and 5) prior or after ECM-treatment. A clear difference between UBM and SIS degradation product is apparent in the challenge experiments using BMDM. Furthermore, gene expression of M2-associated surface markers and transcription factors were decreased after exposure ECM-treatment for 24 hours or after the challenge experiments. Furthermore, THP-1 differentiated Mφs that underwent the challenge experiments showed no change in M1- but an enhance in M2-Mφs markers when cells were additionally prior or after to ECM exposure treated with IL-4 (Fig. 3B, panel 4 and 5).

Overall, the gene expression of metabolic M1- and M2-Mφs markers showed similar results in expression of transcription factors and surface markers. Whereas a treatment with 24 hours UBM degradation products enhances the expression of M1-Mφs marker in BMDM, a decrease was seen in M2 markers (Fig. 3C, panel 1). Furthermore, compared to UBM-treatment, SIS exposure to BMDM affected M1 macrophage marker in a different way, indicating that various ECM products may have distinct effects on macrophage polarization. BMDM that underwent the challenge experiments showed in metabolic Mφs markers almost similar results to the surface markers and transcription factors: Whereas M1-treatment prior or after ECM treatments decreases M1-associated macrophage markers (Fig. 3C, panel 2 and 3) M2-treatment prior to ECM-exposure enhanced M1 macrophage polarization (Fig. 3C, panel 4 and 5). The effect of all treatments to M2-associated metabolic markers was consistently decreased in BMDM. Also, there was overall no change in gene expression of metabolic macrophage markers seen in THP-1 differentiated macrophages (Fig. 3D).

Protein expression of M1- and M2-macrophage markers was determined in THP-1 differentiated macrophages that were prior to protein isolation exposed to the different 24 hour treatments by Western Blot (Figure 1E). Two markers of each phenotype have been identified, STAT1 (STAT1α and STAT1β) or TNF-α as M1 marker and Mannose receptor 1 and 2 (CD206) or Transglutaminase (TGM2) as M2 marker. Similar to the qPCR results, there was overall no change in protein expression of M1- and M2-macrophage markers seen after 24 hour treatments. Interestingly, SIS-treatment enhanced the protein expression of TNF-α protein.

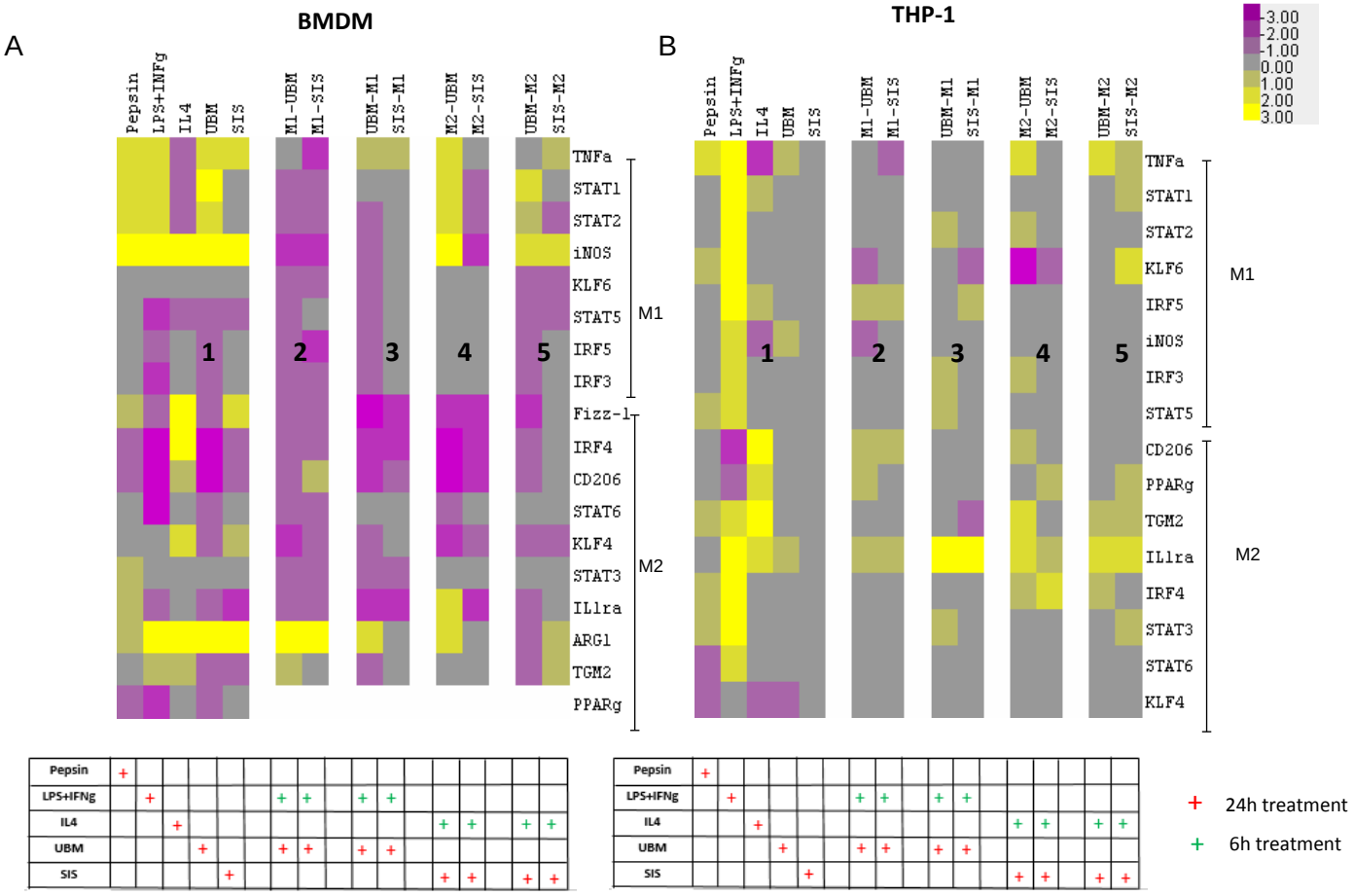

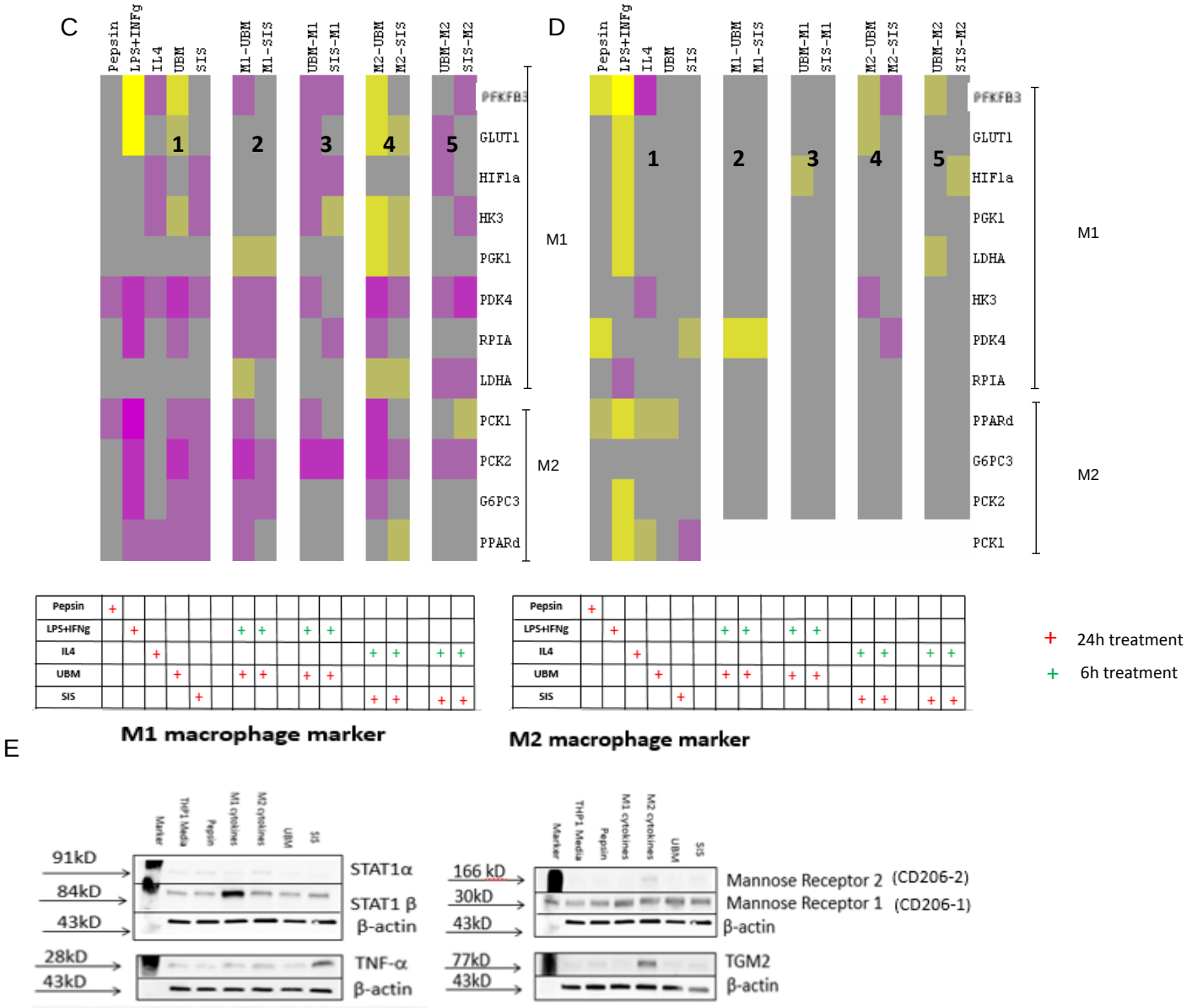

Fig. 1: ECM degradation products can affect M1- and M2 macrophage polarization. Gene expression levels of various M1- and M2-macrophage marker in BMDM and THP-1 cell differentiated macrophages were identified by qPCR following to exposure of the cells to one of these three treatments: Exposure to pepsin digested ECM-degradation products, M1- (LPS and IFNγ) or M2-cytokines (IL-4) for 24 hours respectively (n=5) wherein treatment with pepsin was used as control; 24 hours treatment of ECM-products followed by 6 hours M1- or M2-cytokines (n=5 for THP-1 and n=3 for BMDM); or the reverse experiment (6 hours cytokine and 24 hours degraded ECM, n=5 for THP-1 and n=3 for BMDM). Surface markers, transcription factors and metabolic markers were identified as M1- or M2-macrophage marker. M1- and M2-associated transcription factors and surface markers were TNF-α, iNOS, IRF3, IRF5 KLF6, STAT1, STAT2, STAT5, STAT5A, and STAT5B or Arg-1, CD206, IL1Ra, IRF4, KLF4, STAT3, STAT6, PPARγ, TGM2, and FIZZ-1, respectively (**A+B**), whereas the glycolytic metabolics (GLUT1, HIF1a, RPIA, HK3, PGK1, PDK4, PFKBF3, and LDHA) were referred as M1 metabolic marker, and the gluconeogenetic or oxidative substrates (PCK1, PCK2, G6PC3, FBP2, PPARδ, and PPARγ) as M2 marker (**C+D**). A difference in macrophage polarization, depending on the ECM source of tissue cells were exposed to and the cell type itself was identified. A push with M1- (LPS and IFNγ) or M2-cytokines (IL-4) prior or after ECM-treatment to the cells, was indicated as additional effector, to enhance or to decrease the expression of M1- or M2-macophages, mainly in BMDM. Overall, THP-1 differentiated macrophages were identified with a less change in gene expression post-treatments than BMDM. (**E**) Two M1- (STAT1α, STAT1β, and TNF-α) and M2 (Mannose receptor 1 and 2, and TGM2) and their subtypes respectively were identified in THP-1 differentiated macrophages post-24 hour treatments by Western Blot. Similar results compared to gene expression levels were indicated. *M1- M1-associated macrophage marker; M2- M2-associated macrophage marker; TGM2 – Transglutaminase 2; LPS – Lipopolysaccharide; IL-4 – Interleukin-4; Mannose receptor – CD206*

MBVs are embedded in ECM bioscaffolds

Porcine urinary bladder matrix (UBM) was post fixed with osmium tetroxide to identify matrix-bound nanovesicles (MBVs) using transmission electron microscope (TEM). Lipid membranes stained positive for osmium were determined, indicating the presence of round vesicle-shaped structures (Figure 4A, *left panel*). Pepsin exerted only a partial enzymatic digestion of the ECM-scaffold (Figure 4A, *middle panel*), but showed clearly MBVs embedded within the collagen fibers of the ECM.

More Intense enzymatic digestion with Proteinase K (Figure 4A, *right panel*) releases MBVs from the collagen network (Figure 4A, *right panel*). Ultracentrifugation combined with Proteinase K digestion purifies MBVs from dermis, small intestinal submucosa (SIS), and UBM ECM-products, including commercially available matrix products (Figure 4B). The particle size was determined by Nanoparticle Tracking Analysis (97), indicating a size range of 10 – 1000 nm in diameter size similar as attributed to microvesicles (98).

MBVs surface markers according to exosomes (CD63, CD81, CD9 and Hsp70) were analyzed by Western blot analysis (99). Whereas commercial isolated exosomes derived from porcine serum, human serum or human mesenchymal stem cells (hMSCs) were positive for these markers, bioscaffold-derived MBVs did not express CD63, CD81, CD9 and Hsp70 (Figure 4D).

A

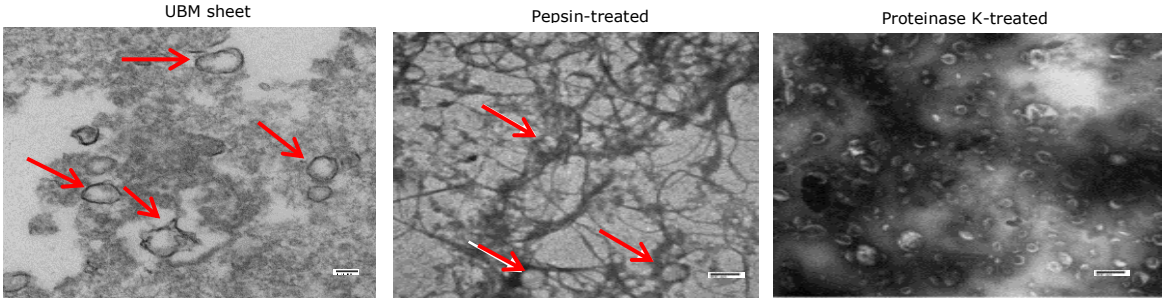

B

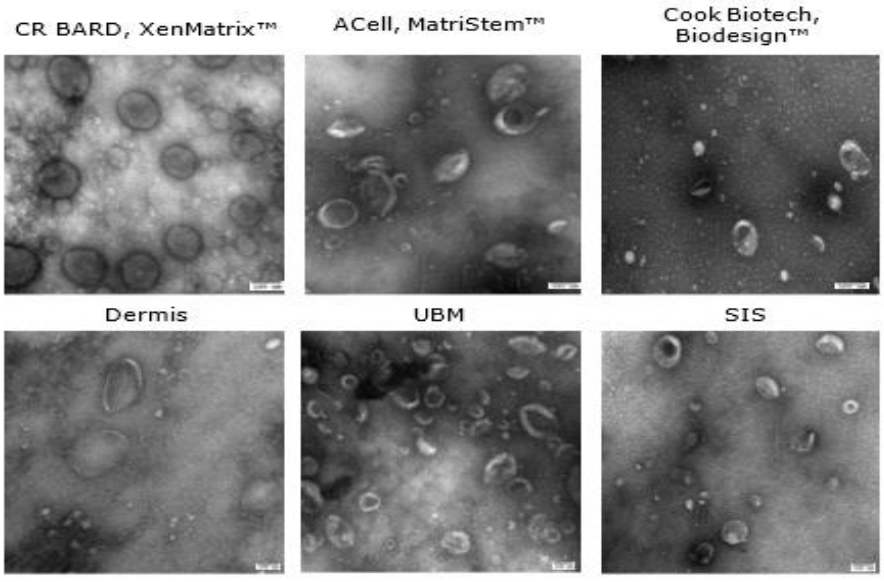

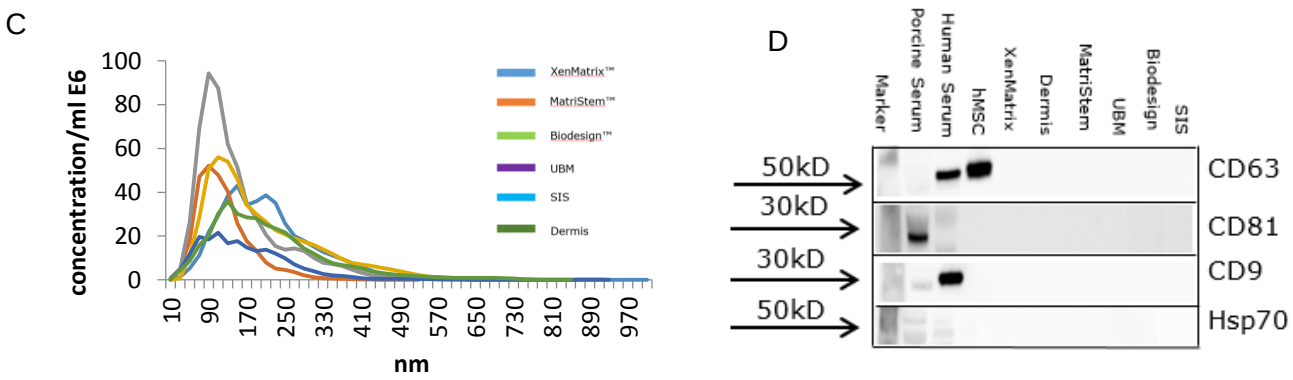

Fig. 4: MBVs are embedded in ECM bioscaffolds. (**A**) UBM-derived MBVs were identified in UBM sheets as stained positive for osmium (left panel), in Pepsin digested UBM (middle panel), or Proteinase K digested UBM (right panel) by TEM imaging. (**B**) TEM imaging identified MBVs that were isolated from Proteinase K digested ECM from three commercial and in-house produced bioscaffolds. Scale bar size is equal to 100nm. (**C**) With Nanosight, MBVs size was analyzed. (**D**) Four exosomal surface markers CD63, CD81, CD9, and Hsp70 were identified by immunoblot analysis. Whereas porcine serum exosomes (Porcine serum), human serum exosomes (Human serum) or hMSCs-derived exosomes (hMSCs) were positive for these markers, expression levels were not detectable in bioscaffold-derived MBVs.

Identification of miRNA as MBVs cargo

To determine if MBVs contain protein cargo, SDS PAGE and Silver stain have been performed (Figure 5A). Moreover, MBVs of all ECM-products were characterized by a different protein signature when compared to hMSCs-derived exosomes. MiRNA of MBVs isolated from laboratory produced and equivalent commercial products were identified by RNA sequencing. Prior to RNA isolation, MBVs were treated with RNase A for 30 min to catalyze the degradation of RNA outside of MBVs and to perform RNA sequencing only on RNA within MBVs (100). Previously, it has been reported that microvesicles and exosomes protect nucleic acids by their plasma membrane (101). Similar results have been observed in previous experiments of our group (Supplemental Data, Fig. S2 and S3). Herein, nucleic acid extraction has been performed in in-house and commercial produced ECM bioscaffolds, which indicated the presence of nucleic acids in ECM bioscaffolds. Additionally, a nuclease treatment prior to nucleic acid extraction has been performed. Results showed that not all nucleic acids were degraded, suggesting that residual nucleic acids were protected from the degradation process. Furthermore, the size of these nucleic acids was analyzed by gel electrophoresis, indicating a size of ~25-200bp consistent to small RNA molecules. Furthermore, these micro RNAs could be degraded by RNAse treatment. From this it was suggested that miRNAs may be packed in EVs in ECM bioscaffolds which are now identified as MBVs. In the present study, non-coding miRNA molecules were extracted to construct miRNA cDNA libraries from RNAs less than 200 nucleotides. To read the cDNA libraries, Ion Proton Platform was used. 33 to 240 miRNAs were described per sample, of which more than the half were found to be common in laboratory produced and the equivalent commercial products (Figure 5A). Furthermore, 22 miRNAs were mutual in all ECM-products (Figure 5B). To reveal cellular pathways that are

associated with miRNAs identified in ECM bioscaffolds, ingenuity pathway analysis (IPA) has been performed. Interestingly, miRNAs have been correlated with a variety of regulatory cell pathways that are indispensable for cellular functions, including cellular vitality, cellular motility, cell proliferation, cell growth, and regulation of the cell cycle (Figure 5C). Similarly, identified miRNAs were shown to be involved in the development and function of connective tissue, organism, and organ (Figure 5D).

A

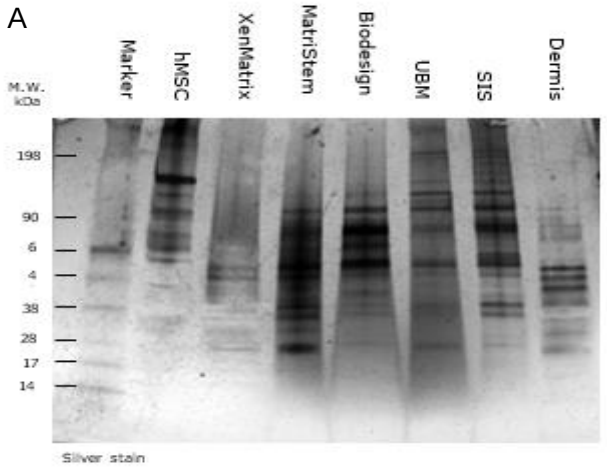

B

Product / Description	CR BARD, XenMatrix™	Dermis	ACell, MatriStem™	UBM	Cook Biotech, Biodesign™	SIS
miRNA count	46	33	223	240	62	53
Mutual miRNAs	25		185		35	

C

D

Product / Molecular and Cellular Functions	CR BARD XenMatrix ™	Dermis	ACell, MatriStem™	UBM	Cook Biotech, Biodesign™	SIS
Cellular Development	26	18	50	74	30	30
Cellular Growth and Proliferation	27	19	48	73	30	29
Cell Death and Survival	21	14	36	64	22	23
Cellular Movement	17	12	32	58	22	20
Cell Cycle	10	7	19	37	11	10

E

Product / Physiological System Development and Function	CR BARD XenMatrix ™	Dermis	ACell, MatriStem™	UBM	Cook Biotech, Biodesign™	SIS
Connective Tissue Development and Function	7	6	12	0	7	4
Organismal Development	12	0	17	33	0	14
Organ Development	0	9	13	32	11	11

Fig. 5: Identification of miRNA as MBVs cargo. (**A**) MBVs were loaded on SDS-Page and Silver stain have been performed to analyze the different protein cargo of MBVs. hMSCs-derived exosomes (hMSCs) were indicated by a different protein cargo signature compared to MBVs of all ECM products. (**B**) Small RNA sequencing has been performed to analyze the specific miRNA signature of commercial and laboratory produced ECM-products (n=1 per ECM product). (**C**) Venn diagram shows the number of miRNA present in specific ECM tissues sources and miRNAs that are mutual to all ECM-products. IPA indicates the numbers of miRNAs that are associated with molecular and cellular function pathways (**D**) and pathways of the physiological system development and function (**E**).

MBVs influence cell behaviour

Exo-Glow was used to label UBM isolated MBVs fluorescent for tracking. RNA and DNA were successfully labeled by Exo-Red stain based on Acridine Orange, and Exo-Green stain based on Carboxyfluorescein succinimidyl diacetate ester respectively. To avoid phagocytotic absorption of MBVs into the cells, non-phagocytotic C2C12 cells were exposed to MBVs. Successful invagination in fibroblast C2C12 cells has been shown following co-culturing with MBVs (Figure 6A). Furthermore, as previously indicated, our group has shown that ECM-bioscaffolds enhances the constructive M2 macrophage polarization. To investigate if MBVs exert similar effects, murine bone marrow-derived macrophages (BMDM) were stimulated with MBVs (Figure 6B). To induce M1-like and M2-like macrophage phenotype, BMDM were treated with IFNɣ and LPS or IL-4 respectively. Furthermore, cells were stimulated with a pepsin control, pepsin degraded UBM, collagenase control, or MBVs isolated UBM following to collagenase digestion of UBM. Similar to IL-4 treated BMDM, MBVs were found to be positive for the pro-regenerative M2-phenotype macrophage marker Fizz1. BMDM treated with MBVs stained negative for the M1-marker iNOS. Further pro-regenerative effects have been associated in our group with ECM bioscaffolds previously, including the development of neurite extension in 1E-115 neuroblastoma cells and the increased proliferation of perivascular stem cells post-ECM treatment. To see if MBVs mimic these effects, these experiments have been repeated but with MBVs treatment. 1E-115 neuroblastoma cells successfully developed neurite extensions after exposure to ECM substrate (UBM) and MBVs compared to no change in the control group after 5 or 3 days stimulation respectively (Figure 6C). Additionally, a significant increase of the thymidine analog 5-bromo-2'-deoxyuridine (BrdU) incorporation into newly synthesized DNA was associated with MBVs treated cells (Figure 6D), indicating a proliferative effect.

A

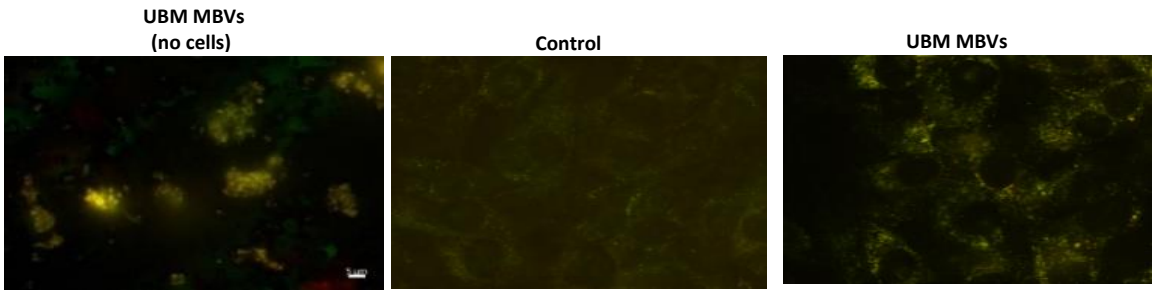

B

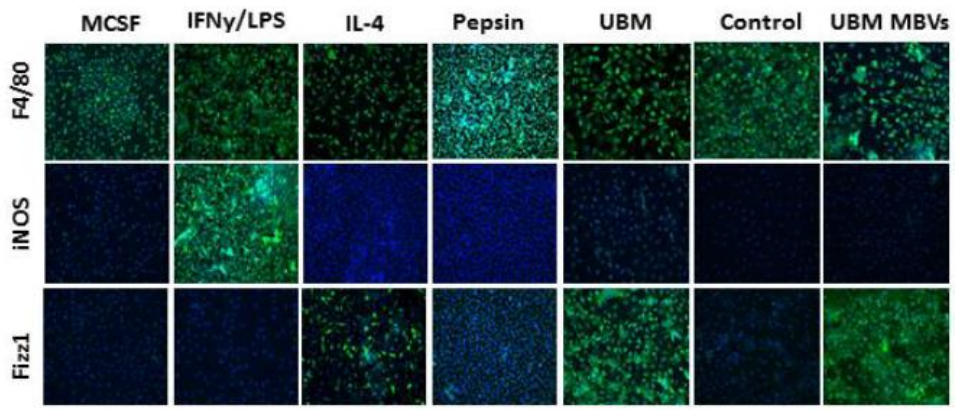

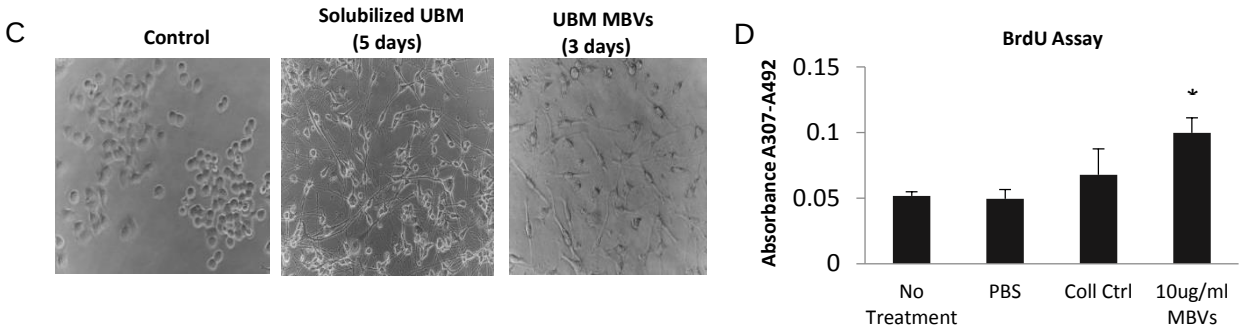

Fig. 6: MBVs exert biological effects. (**A**) Fluorescent labeling by Exo-Glow was used for UBM-derived MBVs tracking. RNA (red) and DNA (green) cargo of MBVs were sucessfully labeled prior to cell culture exposure (left panel). Exo-Glow labeling indicates that MBVs were incorporated in C2C12 cells after 4 hours of exposure (right panel) compared to control (middle panel). (**B**) Bone marrow-derived monocytes were isolated from C57lb/6 mice and cultured in maturation media with macrophage-colony-stimulating factor (M-CSF) for macrophage (Mφs) differentiation. Mφs were polarized into an M1-like phenotype by 20 ng/ml IFNγ and 100 ng/ml LPS or into an M2-like phenotype by 20 ng/ml IL-4 treatment, each for 6 hours. Additionally, Mφs were treated with 5 ug/ml of UBM-derivd MBVs. After stimulation, Mφs were fixed and immunolabaled for F4/80, a pan-macrophage marker, and for markers that are reported to be associated with M1 (iNOS) or M2 (Fizz1) macrophage phenotype. An increase in Fizz1 expression after MBVs exposure indicates an enhanced M2-like state. The experiment (n=2) has been performed with a technical replicate of 4. (**C**) 1E-115 neuroblastoma cells were stimulated with ECM of UBM source and UBM-derived MBVs. Compared to control, neurite extensions in treated cells got present post exposure. Exposure time was five days for UBM and three days for MBVs. (**D**) BrdU assay on perivascuar cells was performed to analyze the proliferative effect of MBVs on cells. A significant increase of BrdU incorporation into newly synthesized DNA was associated with MBVs treated cells. *Coll Ctrl – Collagenase control group; MBVs – matrix-bound nanovesicles* * $p<0.05$

4. Discussion

The present study shows that ECM products, produced from a variety of decellularized ECM bioscaffolds, i.e. urinary bladder mucosa, small intestinal submucosa, and dermis, can affect the polarization of BMDM or human differentiated THP-1 macrophages to an "M_{ECM}" macrophage state depending on the source of ECM tissue and the cell type itself; furthermore, ECM bioscaffolds were identified to contain embedded matrix-bound nanovesicles ranging in diameter size from 10 to 1000 nm and carrying miRNA materials that play a role in controlling cellular activity such as cell motility, cell proliferation, and regulatory functions of the cell cycle, and in the development and function of connective tissue, organism, and organ. Moreover, MBVs have an impact on the macrophage phenotype and the development of dendritic processes in neural progenitor cells.

Wound healing is a complex dynamic process in which macrophages are known to play distinguished roles (25). Whereas classical activated M1 macrophages are known to stimulate pro-inflammatory mechanisms, alternatively activation of M2 macrophages induces pro-regenerative processes (27). Therefore, the activation of M2 macrophages may play a key role during tissue remodeling, homeostasis and wound healing. Furthermore, our group has previously been shown that ECM application to injured rats was accompanied by an enhance in "M2-like" macrophage polarization, whereas untreated rats were associated with scar tissue formation, fibrosis and an increase in "M1-like" macrophage phenotype. These results indicate that ECM-bioscaffolds may drive macrophage polarization towards an M2 phenotype to stimulate tissue remodeling. The current study shows that 24 hours ECM treatment to bone-marrow derived macrophages enhances M1-, and decreases M2-macrophage polarization, suggesting that ECM biocomponents also interact with pro-inflammatory mechanisms. Interestingly, when recapitulating an injury, i.e. due to additional treatment of M1-cytokines to the cells prior or after ECM exposure, ECM decreases the functional effects of M1 cytokines, which is identical to previous findings, indicating the anti-inflammatory effects ECM products. An additional treatment with M2-cytokines diminished these pro-regenerative effects of the ECM-bioscaffolds, suggesting that anti-inflammatory molecules may interact with ECM regulatory pathways during cell and tissue homeostasis. To analyze the regulatory effect of ECM-biocomponents on macrophage polarization, underlying pathways need to be investigated in further studies.

Furthermore, our results show that the ECM-products have distinct effects on macrophage polarization, depending on the cell type they interact with. BMDM were overall characterized by a change in M1-phenotype macrophage polarization in all treatment groups compared to the control, THP-1 differentiated macrophages showed overall no change and an enhance in anti-inflammatory macrophage polarization when treated together with M2-cytokines. This difference could be due to their different origin and cell characteristics. Whereas BMDM derive from murine primary cells, THP-1 differentiated macrophages were obtained from a human cell line. Further studies need to be performed to investigate the effect of ECM-products on distinct cell types.

Additionally, SIS and UBM affected macrophage polarization in distinct ways. This was mainly shown in our challenge experiments of BMDM when additionally treated with M2-cytokines. Whereas cells treated with UBM were characterized by an enhance in M1-macrophage polarization,

cells treated with SIS pushed this polarization down, indicating that SIS may play a more effective role in decreasing pro-inflammatory mechanisms than UBM-bioscaffolds. These differences in ECM-bioscaffolds may be due to their distinct compositions. SIS is known to consist of basal layers of tunica mucosa, tunica muscularis mucosa, and tunica submucosa (102), UBM is composed of tunica lamina, tunica propria and basement membrane (103). Therefore, it may be suggested that various ECM-bioscaffolds consists of different biocomponents which affect regulatory pathways of macrophage polarization in distinct ways. This assumption need to be further investigated in following studies.

To analyze the protein expression level of M1- and M2- associated macrophage phenotype marker, Western Blot has been performed. Herein, similar results to the gene expressions have been shown. THP-1 differentiated macrophages showed overall no change in protein expression post-ECM treatment, indicating that our qPCR results are reliable. In further studies Western Blots of treated cells using the challenge experiment need to be performed to determine the protein expression of distinct M1- and M2-marker.

Furthermore, the function of EVs was earlier underestimated. During the last decades, EVs got an interesting research field in intercellular communication processes due to their ability to carry lipids, enzymes, proteins, and RNA to various cell types, thereby changing physiological and pathophysiological cellular functions. Previously, EVs have been reported to be attached to ECM components due to the function of adhesion molecules, e.g. ICAM-1, and/or different integrins, e.g. αM-integrin and β2-integrin (104, 105). For instance, exosomes released from B cells were found to contain integrins that mediate their attachement to collagen-1 and fibronectin (106). Additionally, chondrocyte-, osteoclast-, and odontoblast-released EVs (107) were shown to interact with the bone matrix and cartiladge (108, 109). Whereas MBVs cargo and size indicate similar charesteristics as EVs, they were shown to be present in ECM products and do not express exosomal surface markers, i.e. CD63, CD81, CD9, and Hsp70, suggesting that isolated MBVs may be part of a different signaling EVs population or that enzymatic digestion by proteinase-K may clip off specific markers. To analyze if MBVs are part of a different population group, further studies need to be performed. Moreover, MBVs were identified by a distinct protein signature compared to commercial hMSCs-derived exosomes using silver stain methods; additionally, signature is dependent on source of tissue. Whereas MBVs isolated from UBM or SIS are defined by a similar protein pattern, dermal MBVs are indicated by different protein cargo. ELISA or Western Blots are necessary in further studies to determine the unique protein signature of MBVs. Herein, specific markers for MBVs could be revealed.

Our present study indicates a distinct miRNA signature in MBVs which depends on their different source tissues. Interestingly, 22 miRNAs were common to all MBVs. This may reveal miRNA as potential MBV marker, but further studies are required. Furthermore, miRNA sequencing has been performed with an sample size of 1, therefore further studies are necessary to make definitive conclusions regarding consistent miRNA profiles. However, the present study shows that miRNA isolated from MBVs exert similar biologic effects as ECM bioscaffolds, i.e. cell migration, differentiation (5, 110), cell proliferation, cellular growth (111), and cell vitality (112). Therefore it may be suggested that MBVs could mimic regenerative effects of their parent ECM bioscaffolds.

In previous studies it has been indicated that miRNAs are evolutionarily conserved among distinct animal species (113, 114). Hence, porcine MBV-derived miRNA may have biologic effects on human cells, but further studies need to be performed to fully understand the function of MBV miRNA in cell regulatory mechanisms and their potential in regenerative medicine.

Furthermore, despite numerous studies have indicated the regulatory role of EVs during pathological conditions, including cancer (68-70), neurodegeneration (38, 68), and fibrosis (71), their function in wound healing, tissue hoemeostasis and remodeling is not well investigated. EVs have been shown to modulate cell survival (115, 116), inter-cellular miRNA transfer (117, 118), ECM development and rearrangement (71, 119), and immuno-modulatory mechanisms, including the stimulation of pro-regenerative cytokines and hence modulate M1/M2 macrophage polarization (44, 120), all are known to be relevant in tissue remodeling. In the present study, it has the potential of MBVs been indicated to drive the anti-inflammatory "M2-like" macrophage polarization. Similar effects were earlier investigated as ECM-mediated process, during *in vivo* studies (121, 122). Therefore, MBVs may stimulate tissue remodeling due to regulating cell homeostasis and ECM regeneration.

Additionally, previous studies indicated that the distinct EVs cargo is associated with their cellular origin and the pathological state of tissues they were secreted from (97). Therefore, MBVs cargo may be dependent on different states in immuno-modulatory and regenerative mechanisms, including inflammation, fibrosis, and tissue remodeling and could therefore serve as biomarker in regenerative medicine.

In summary, the present studies identified MBVs within ECM bioscaffolds and showed their ability to modify cell behaviour. Furthermore, that ECM degradation products have the ability to affect macrophage polarization. These findings offer new insights into regenerative mechanisms that are induced by ECM-bioscaffolds.

5. Conclusion and Synthesis

Our laboratory group has previously shown that ECM-bioscaffold induced regenerative outcomes which were associated with an enhanced anti-inflammatory "M2-like" macrophage. However, the underlying mechanisms are not known and need to be further analyzed. Our results indicate that ECM-products drive macrophage polarization towards an "mECM" macrophage phenotype, which depends on the source of ECM tissue and the cell type ECM products interact with. Additionally, ECM affect immuno-modulatory molecules, including cytokines. The hypothesis of enhancing M2-like macrophage polarization by ECM without additional stimulus could not be confirmed by analyzing the gene expression of M1- and M2-associated markers. In further studies, protein expression of associated markers need to be analyzed.

Furthermore, the role of EVs in pathological conditions, including cancer and neurodegeneration, has been well investigated during the last decade, while their functions in cellular and tissue regenerative mechanisms need to be further analyzed. However, EVs are known to affect biological pathways of the adaptive and innate immune system (63, 64), cell maturation (65), gene regulation (64), apoptosis (115), and ECM development (119), which play all a role during tissue remodeling. The results of the present study show that MBVs can drive macrophage polarization towards an anti-inflammatory "M2-like" state and additionally that they can influence stem cell differentiation, a known hallmark of ECM-induced remodeling processes (121). Furthermore, in different studies it has been shown that miRNAs and their variety in signature are involved in various regulatory cell functions during pathological conditions, suggesting that miRNAs may also affect cell and tissue homeostasis in fibrosis, neoplastic progression, and chronic inflammation and therefore, during remodeling induced by ECM bioscaffolds.

Results reported herein indicate the potential effect ECM-components do have on macrophage polarization. Furthermore, MBVs embedded in ECM bioscaffolds are a novel biocomponent which has not been previously described. Our results offer mechanistic insights of regenerative processes by which ECM-bioscaffolds modulate tissue homeostasis.

Further studies will include the analysis of regenerative mechanisms induced by MBVs in *in vivo* and their effect on macrophage polarization in *in vitro*. Therefore, a site specific administration of MBVs will be performed in rats that underwent partial thickness abdominal wall injury to investigate their effect on tissue remodeling processes. Furthermore, gene and protein expression of M1- and M2-associated macrophage markers will be analyzed of THP-1 cell differentiated macrophages and BMDM that were previously exposed to MBVs. Lastly, EVs are known to carry different cargo, such as miRNA, DNA, and lipids. Beside miRNA, the full EVs cargo signature and its potential to affect tissue remodeling need to be further investigated.

6. References

1. Christ GJ, Saul JM, Furth ME, Andersson KE. The pharmacology of regenerative medicine. Pharmacol Rev. 2013;65(3):1091-133.
2. Bard CR. XenMatrix™ Surgical Graft 2016.
3. facility AM. MATRISTEM DEVICES. 2015.
4. Cook Biotech I. Technology. 2016.
5. Crapo PM, Gilbert TW, Badylak SF. An overview of tissue and whole organ decellularization processes. Biomaterials. 2011;32(12):3233-43.
6. Choi YC, Choi JS, Kim BS, Kim JD, Yoon HI, Cho YW. Decellularized extracellular matrix derived from porcine adipose tissue as a xenogeneic biomaterial for tissue engineering. Tissue Eng Part C Methods. 2012;18(11):866-76.
7. Turner NJ, Badylak SF. The Use of Biologic Scaffolds in the Treatment of Chronic Nonhealing Wounds. Adv Wound Care (New Rochelle). 4. 140 Huguenot Street, 3rd FloorNew Rochelle, NY 10801USA2015. p. 490-500.
8. Brown BN, Badylak SF. Extracellular matrix as an inductive scaffold for functional tissue reconstruction. Transl Res. 2014;163(4):268-85.
9. Naba A, Clauser KR, Ding H, Whittaker CA, Carr SA, Hynes RO. The extracellular matrix: Tools and insights for the "omics" era. Matrix Biol. 2016;49:10-24.
10. Eweida AM, Marei MK. Naturally Occurring Extracellular Matrix Scaffolds for Dermal Regeneration: Do They Really Need Cells? Biomed Res Int. 2015;2015:839694.
11. Lindberg K, Badylak SF. Porcine small intestinal submucosa (SIS): a bioscaffold supporting in vitro primary human epidermal cell differentiation and synthesis of basement membrane proteins. Burns. 2001;27(3):254-66.
12. Badylak SF. The extracellular matrix as a scaffold for tissue reconstruction. Semin Cell Dev Biol. 2002;13(5):377-83.
13. Londono R, Gorantla VS, Badylak SF. Emerging Implications for Extracellular Matrix-Based Technologies in Vascularized Composite Allotransplantation2016.
14. AbouIssa A, Mari W, Simman R. Clinical Usage of an Extracellular, Collagen-rich Matrix: A Case Series 2015.
15. Santambrogio L. Biomaterials in Regenerative Medicine and the Immune System. Switzerland: Springer; 2015.
16. Kuroi K, Shimozuma K, Taguchi T, Imai H, Yamashiro H, Ohsumi S, et al. Effect of mechanical closure of dead space on seroma formation after breast surgery. Breast Cancer. 2006;13(3):260-5.
17. Zawaneh PN, Putnam D. Materials in surgery: a review of biomaterials in postsurgical tissue adhesion and seroma prevention. Tissue Eng Part B Rev. 2008;14(4):377-91.
18. Bell MSG, Doumit G. Evacuation of hematomas using liposuction technology: Technique and literature review. Can J Plast Surg. 142006. p. 51-2.
19. Niamtu J, 3rd. Expanding hematoma in face-lift surgery: literature review, case presentations, and caveats. Dermatol Surg. 2005;31(9 Pt 1):1134-44; discussion 44.
20. Gosain A, DiPietro LA. Aging and wound healing. World J Surg. 2004;28(3):321-6.
21. Broughton G, 2nd, Janis JE, Attinger CE. The basic science of wound healing. Plast Reconstr Surg. 2006;117(7 Suppl):12s-34s.
22. Swift ME, Burns AL, Gray KL, DiPietro LA. Age-related alterations in the inflammatory response to dermal injury. J Invest Dermatol. 2001;117(5):1027-35.
23. Park JE, Barbul A. Understanding the role of immune regulation in wound healing. Am J Surg. 2004;187(5a):11s-6s.
24. Mosser DM, Edwards JP. Exploring the full spectrum of macrophage activation. Nat Rev Immunol. 2008;8(12):958-69.

25. Meszaros AJ, Reichner JS, Albina JE. Macrophage-induced neutrophil apoptosis. J Immunol. 2000;165(1):435-41.
26. Guo S, Dipietro LA. Factors affecting wound healing. J Dent Res. 2010;89(3):219-29.
27. Ferrante CJ, Leibovich SJ. Regulation of Macrophage Polarization and Wound Healing. Adv Wound Care (New Rochelle). 12012. p. 10-6.
28. Brown BN, Valentin JE, Stewart-Akers AM, McCabe GP, Badylak SF. Macrophage phenotype and remodeling outcomes in response to biologic scaffolds with and without a cellular component. Biomaterials. 2009;30(8):1482-91.
29. Brown BN. CONSTRUCTIVE TISSUE REMODELING OF BIOLOGIC SCAFFOLDS: A PHENOMENON ASSOCIATED WITH SCAFFOLD CHARACTERISTICS AND DISTINCTIVE MACROPHAGE PHENOTYPES2011.
30. Chanput W, Mes JJ, Wichers HJ. THP-1 cell line: an in vitro cell model for immune modulation approach. Int Immunopharmacol. 2014;23(1):37-45.
31. Cunnick J, Kaur P, Cho Y, Groffen J, Heisterkamp N. Use of bone marrow-derived macrophages to model murine innate immune responses. J Immunol Methods. 2006;311(1-2):96-105.
32. Ma AZ, Zhang Q, Song ZY. TNFa alter cholesterol metabolism in human macrophages via PKC-theta-dependent pathway. BMC Biochem. 2013;14:20.
33. Yu T, Zhao L, Huang X, Ma C, Wang Y, Zhang J, et al. Enhanced Activity of the Macrophage M1/M2 Phenotypes and Phenotypic Switch to M1 in Periodontal Infection. J Periodontol. 2016:1-21.
34. Beljaars L, Schippers M, Reker-Smit C, Martinez FO, Helming L, Poelstra K, et al. Hepatic Localization of Macrophage Phenotypes during Fibrogenesis and Resolution of Fibrosis in Mice and Humans. Front Immunol. 2014;5:430.
35. Date D, Das R, Narla G, Simon DI, Jain MK, Mahabeleshwar GH. Kruppel-like Transcription Factor 6 Regulates Inflammatory Macrophage Polarization. J Biol Chem. 289. 9650 Rockville Pike, Bethesda, MD 20814, U.S.A.2014. p. 10318-29.
36. Wang N, Liang H, Zen K. Molecular mechanisms that influence the macrophage m1-m2 polarization balance. Front Immunol. 2014;5:614.
37. Galván-Peña S, O'Neill LAJ. Metabolic Reprograming in Macrophage Polarization. Front Immunol. 2014;5.
38. Yang Y, Keene CD, Peskind ER, Galasko DR, Hu SC, Cudaback E, et al. Cerebrospinal Fluid Particles in Alzheimer Disease and Parkinson Disease. J Neuropathol Exp Neurol. 2015;74(7):672-87.
39. Rőszer T. Understanding the Mysterious M2 Macrophage through Activation Markers and Effector Mechanisms. 2015.
40. Satoh T, Takeuchi O, Vandenbon A, Yasuda K, Tanaka Y, Kumagai Y, et al. The Jmjd3-Irf4 axis regulates M2 macrophage polarization and host responses against helminth infection. Nat Immunol. 2010;11(10):936-44.
41. Liao X, Sharma N, Kapadia F, Zhou G, Lu Y, Hong H, et al. Kruppel-like factor 4 regulates macrophage polarization. J Clin Invest. 2011;121(7):2736-49.
42. Odegaard JI, Ricardo-Gonzalez RR, Goforth MH, Morel CR, Subramanian V, Mukundan L, et al. Macrophage-specific PPARgamma controls alternative activation and improves insulin resistance. Nature. 2007;447(7148):1116-20.
43. Raes G, Noel W, Beschin A, Brys L, de Baetselier P, Hassanzadeh GH. FIZZ1 and Ym as tools to discriminate between differentially activated macrophages. Dev Immunol. 2002;9(3):151-9.
44. Yin H, Jiang H. [Application Prospect of Stem Cell-derived Microvesicles in Regeneration of Injured Tissues]. Sheng Wu Yi Xue Gong Cheng Xue Za Zhi. 2015;32(3):688-92.
45. Anthony DF, Shiels PG. Exploiting paracrine mechanisms of tissue regeneration to repair damaged organs. Transplant Res. 2013;2(1):10.
46. György B, Szabó TG, Pásztói M, Pál Z, Misják P, Aradi B, et al.
47. Fuster-Matanzo A, Gessler F, Leonardi T, Iraci N, Pluchino S.

48. Ghossoub R, Lembo F, Rubio A, Gaillard CB, Bouchet J, Vitale N, et al. Syntenin-ALIX exosome biogenesis and budding into multivesicular bodies are controlled by ARF6 and PLD2. Nat Commun. 2014;5:3477.
49. Beach A, Zhang H-G, Ratajczak MZ, Kakar SS.
50. Corrado C, Raimondo S, Chiesi A, Ciccia F, De Leo G, Alessandro R.
51. Mishra NC, Tatum EL. Non-Mendelian inheritance of DNA-induced inositol independence in Neurospora. Proc Natl Acad Sci U S A. 1973;70(12):3875-9.
52. Trams EG, Lauter CJ, Salem N, Jr., Heine U. Exfoliation of membrane ecto-enzymes in the form of micro-vesicles. Biochim Biophys Acta. 1981;645(1):63-70.
53. Johnstone RM, Ahn J. A common mechanism may be involved in the selective loss of plasma membrane functions during reticulocyte maturation. Biomed Biochim Acta. 1990;49(2-3):S70-5.
54. Mathew A, Bell A, Johnstone RM. Hsp-70 is closely associated with the transferrin receptor in exosomes from maturing reticulocytes. Biochem J. 1995;308 (Pt 3):823-30.
55. Bette-Bobillo P, Vidal M. Characterization of phospholipase A2 activity in reticulocyte endocytic vesicles. Eur J Biochem. 1995;228(1):199-205.
56. Zech D, Rana S, Buchler MW, Zoller M. Tumor-exosomes and leukocyte activation: an ambivalent crosstalk. Cell Commun Signal. 2012;10(1):37.
57. Haibo L, Wei G, Jie Y, Chaoneng W, Kang Y, Li Z, et al. Exosomes derived from dendritic cells improve cardiac function via activation of CD4 T lymphocytes after myocardial infarction. J Mol Cell Cardiol. 2015.
58. Choi JS, Yoon HI, Lee KS, Choi YC, Yang SH, Kim IS, et al. Exosomes from differentiating human skeletal muscle cells trigger myogenesis of stem cells and provide biochemical cues for skeletal muscle regeneration. J Control Release. 2015;222:107-15.
59. Théry C. Exosomes: secreted vesicles and intercellular communications. F1000 Biology Reports. 2011;3:15.
60. Gallo A, Tandon M, Alevizos I, Illei GG. The majority of microRNAs detectable in serum and saliva is concentrated in exosomes. PLoS One. 2012;7(3):e30679.
61. Wojtowicz A, Baj-Krzyworzeka M, Baran J. [Characterization and biological role of extracellular vesicles]. Postepy Hig Med Dosw (Online). 2014;68:1421-32.
62. Keller S, Rupp C, Stoeck A, Runz S, Fogel M, Lugert S, et al. CD24 is a marker of exosomes secreted into urine and amniotic fluid. Kidney Int. 2007;72(9):1095-102.
63. L. U, A. M, S. B. Signaling Pathways in Exosomes Biogenesis, Secretion and Fate2013.
64. Blin J, Fitzgerald KA. Perspective: The RNA exosome, cytokine gene regulation and links to autoimmunity. Cytokine. 2015;74(2):175-80.
65. Takeda YS, Xu Q. Neuronal Differentiation of Human Mesenchymal Stem Cells Using Exosomes Derived from Differentiating Neuronal Cells. 2015.
66. Garcia NA, Moncayo-Arlandi J, Sepulveda P, Diez-Juan A. Cardiomyocyte exosomes regulate glycolytic flux in endothelium by direct transfer of GLUT transporters and glycolytic enzymes. Cardiovasc Res. 2016;109(3):397-408.
67. Zoller M. Exosomes in Cancer Disease. Methods Mol Biol. 2016;1381:111-49.
68. Pupyshev AB. [EXTRACELLULAR VESICLES: INTERCELLULAR INFORMATION FLOW AND MEDICAL APPLICATIONS]. Tsitologiia. 2015;57(8):551-62.
69. Hoshino A, Costa-Silva B, Shen TL, Rodrigues G, Hashimoto A, Tesic Mark M, et al. Tumour exosome integrins determine organotropic metastasis. Nature. 2015;527(7578):329-35.
70. Costa-Silva B, Aiello NM, Ocean AJ, Singh S, Zhang H, Thakur BK, et al. Pancreatic cancer exosomes initiate pre-metastatic niche formation in the liver. Nat Cell Biol. 2015;17(6):816-26.
71. Borges FT, Melo SA, Ozdemir BC, Kato N, Revuelta I, Miller CA, et al. TGF-beta1-containing exosomes from injured epithelial cells activate fibroblasts to initiate tissue regenerative responses and fibrosis. J Am Soc Nephrol. 2013;24(3):385-92.

72. Belting M, Christianson HC. Role of exosomes and microvesicles in hypoxia-associated tumour development and cardiovascular disease. J Intern Med. 2015;278(3):251-63.
73. Soung YH, Nguyen T, Cao H, Lee J, Chung J. Emerging roles of exosomes in cancer invasion and metastasis. BMB Rep. 49. Korea (South)2016. p. 18-25.
74. Rodriguez M, Silva J, Herrera A, Herrera M, Pena C, Martin P, et al. Exosomes enriched in stemness/metastatic-related mRNAS promote oncogenic potential in breast cancer. Oncotarget. 2015;6(38):40575-87.
75. Ludlow J, Buehrer B. Mesenchymal Stem Cell Exosomes - Potential Regenerative Medicine Application for Tendinopathy. 2015.
76. Tetta C, Consiglio AL, Bruno S, Tetta E, Gatti E, Dobreva M, et al. The role of microvesicles derived from mesenchymal stem cells in tissue regeneration; a dream for tendon repair? Muscles Ligaments Tendons J. 2012;2(3):212-21.
77. De Jong OG, Van Balkom BW, Schiffelers RM, Bouten CV, Verhaar MC. Extracellular vesicles: potential roles in regenerative medicine. Front Immunol. 2014;5:608.
78. Amsbio. Exosomes for Regenerative Medicine Research. 2015.
79. Mitchell MD, Peiris HN, Kobayashi M, Koh YQ, Duncombe G, Illanes SE, et al. Placental exosomes in normal and complicated pregnancy. Am J Obstet Gynecol. 2015;213(4 Suppl):S173-81.
80. Abramowicz A, Widlak P, Pietrowska M. Proteomic analysis of exosomal cargo: the challenge of high purity vesicle isolation. Mol Biosyst. 2016.
81. Peng B, Chen Y, Leong KW. MicroRNA delivery for regenerative medicine. Adv Drug Deliv Rev. 2015;88:108-22.
82. Ma X, Zhou J, Zhong Y, Jiang L, Mu P, Li Y, et al. Expression, regulation and function of microRNAs in multiple sclerosis. Int J Med Sci. 2014;11(8):810-8.
83. Ji X, Chen X, Yu X. MicroRNAs in Osteoclastogenesis and Function: Potential Therapeutic Targets for Osteoporosis. Int J Mol Sci. 2016;17(3).
84. Wang Y, Tian Y. miRNA for diagnosis and clinical implications of human hepatocellular carcinoma. Hepatol Res. 2016;46(1):89-99.
85. Oglesby IK, Agrawal R, Mall MA, McElvaney NG, Greene CM. miRNA-221 is elevated in cystic fibrosis airway epithelial cells and regulates expression of ATF6. Mol Cell Pediatr. 2015;2(1):1.
86. Beavers KR, Nelson CE, Duvall CL. MiRNA inhibition in tissue engineering and regenerative medicine. Adv Drug Deliv Rev. 2015;88:123-37.
87. Reing JE, Brown BN, Daly KA, Freund JM, Gilbert TW, Hsiong SX, et al. The effects of processing methods upon mechanical and biologic properties of porcine dermal extracellular matrix scaffolds. Biomaterials. 2010;31(33):8626-33.
88. Freytes DO, Badylak SF, Webster TJ, Geddes LA, Rundell AE. Biaxial strength of multilaminated extracellular matrix scaffolds. Biomaterials. 2004;25(12):2353-61.
89. Badylak SF, Lantz GC, Coffey A, Geddes LA. Small intestinal submucosa as a large diameter vascular graft in the dog. J Surg Res. 1989;47(1):74-80.
90. Brennan EP, Tang XH, Stewart-Akers AM, Gudas LJ, Badylak SF. Chemoattractant activity of degradation products of fetal and adult skin extracellular matrix for keratinocyte progenitor cells. J Tissue Eng Regen Med. 2008;2(8):491-8.
91. Slivka PF, Dearth CL, Keane TJ. 2014.
92. Daigneault M, Preston JA, Marriott HM, Whyte MK, Dockrell DH. The identification of markers of macrophage differentiation in PMA-stimulated THP-1 cells and monocyte-derived macrophages. PLoS One. 2010;5(1):e8668.
93. Crisan M, Yap S, Casteilla L, Chen CW, Corselli M, Park TS, et al. A perivascular origin for mesenchymal stem cells in multiple human organs. Cell Stem Cell. 2008;3(3):301-13.
94. Liang R, Fisher M, Yang G, Hall C, Woo SL. Alpha1,3-galactosyltransferase knockout does not alter the properties of porcine extracellular matrix bioscaffolds. Acta Biomater. 2011;7(4):1719-27.
95. Webber J, Clayton A. How pure are your vesicles? J Extracell Vesicles. 2013;2.

96. Malvern. NanoSight rangeCharacterizing Nanoparticles: Visualizing, Sizing and Concentration. 2016.
97. Yanez-Mo M, Siljander PR, Andreu Z, Zavec AB, Borras FE, Buzas EI, et al. Biological properties of extracellular vesicles and their physiological functions. J Extracell Vesicles. 2015;4:27066.
98. van Dommelen SM, Vader P, Lakhal S, Kooijmans SA, van Solinge WW, Wood MJ, et al. Microvesicles and exosomes: opportunities for cell-derived membrane vesicles in drug delivery. J Control Release. 2012;161(2):635-44.
99. Stickney Z, Losacco J, McDevitt S, Zhang Z, Lu B. Development of exosome surface display technology in living human cells. Biochem Biophys Res Commun. 2016;472(1):53-9.
100. Lunavat TR, Cheng L, Kim DK, Bhadury J, Jang SC, Lasser C, et al. Small RNA deep sequencing discriminates subsets of extracellular vesicles released by melanoma cells--Evidence of unique microRNA cargos. RNA Biol. 2015;12(8):810-23.
101. Jenjaroenpun P, Kremenska Y, Nair VM, Kremenskoy M, Joseph B, Kurochkin IV. Characterization of RNA in exosomes secreted by human breast cancer cell lines using next-generation sequencing. PeerJ. 2013;1:e201.
102. Hafez AT, El-Assmy A, El-Hamid MA. 4 layer versus 1 layer small intestinal submucosa for correction of penile chordee: experimental study in a rabbit model. J Urol. 2004;171(6 Pt 1):2489-91.
103. Lanteri Parcells A, Abernathie B, Datiashvili R. The use of urinary bladder matrix in the treatment of complicated open wounds. Wounds. 2014;26(7):189-96.
104. Escola JM, Kleijmeer MJ, Stoorvogel W, Griffith JM, Yoshie O, Geuze HJ. Selective enrichment of tetraspan proteins on the internal vesicles of multivesicular endosomes and on exosomes secreted by human B-lymphocytes. J Biol Chem. 1998;273(32):20121-7.
105. Thery C, Regnault A, Garin J, Wolfers J, Zitvogel L, Ricciardi-Castagnoli P, et al. Molecular characterization of dendritic cell-derived exosomes. Selective accumulation of the heat shock protein hsc73. J Cell Biol. 1999;147(3):599-610.
106. Clayton A, Turkes A, Dewitt S, Steadman R, Mason MD, Hallett MB. Adhesion and signaling by B cell-derived exosomes: the role of integrins. Faseb j. 2004;18(9):977-9.
107. Golub EE. Role of matrix vesicles in biomineralization. Biochim Biophys Acta. 2009;1790(12):1592-8.
108. Anderson HC. Matrix vesicles and calcification. Curr Rheumatol Rep. 2003;5(3):222-6.
109. Anderson HC. Vesicles associated with calcification in the matrix of epiphyseal cartilage. J Cell Biol. 1969;41(1):59-72.
110. Vorotnikova E, McIntosh D, Dewilde A, Zhang J, Reing JE, Zhang L, et al. Extracellular matrix-derived products modulate endothelial and progenitor cell migration and proliferation in vitro and stimulate regenerative healing in vivo. Matrix Biol. 2010;29(8):690-700.
111. Reing JE, Zhang L, Myers-Irvin J, Cordero KE, Freytes DO, Heber-Katz E, et al. Degradation products of extracellular matrix affect cell migration and proliferation. Tissue Eng Part A. 2009;15(3):605-14.
112. Teodori L, Costa A, Marzio R, Perniconi B, Coletti D, Adamo S, et al. Native extracellular matrix: a new scaffolding platform for repair of damaged muscle. Front Physiol. 2014;5:218.
113. Pasquinelli AE, Reinhart BJ, Slack F, Martindale MQ, Kuroda MI, Maller B, et al. Conservation of the sequence and temporal expression of let-7 heterochronic regulatory RNA. Nature. 2000;408(6808):86-9.
114. Weber MJ. New human and mouse microRNA genes found by homology search. Febs j. 2005;272(1):59-73.
115. Barile L, Lionetti V, Cervio E, Matteucci M, Gherghiceanu M, Popescu LM, et al. Extracellular vesicles from human cardiac progenitor cells inhibit cardiomyocyte apoptosis and improve cardiac function after myocardial infarction. Cardiovasc Res. 2014;103(4):530-41.
116. van Balkom BW, de Jong OG, Smits M, Brummelman J, den Ouden K, de Bree PM, et al. Endothelial cells require miR-214 to secrete exosomes that suppress senescence and induce angiogenesis in human and mouse endothelial cells. Blood. 2013;121(19):3997-4006, s1-15.

117. Cantaluppi V, Biancone L, Figliolini F, Beltramo S, Medica D, Deregibus MC, et al. Microvesicles derived from endothelial progenitor cells enhance neoangiogenesis of human pancreatic islets. Cell Transplant. 2012;21(6):1305-20.
118. Ekstrom EJ, Bergenfelz C, von Bulow V, Serifler F, Carlemalm E, Jonsson G, et al. WNT5A induces release of exosomes containing pro-angiogenic and immunosuppressive factors from malignant melanoma cells. Mol Cancer. 2014;13:88.
119. Distler JH, Jungel A, Huber LC, Seemayer CA, Reich CF, 3rd, Gay RE, et al. The induction of matrix metalloproteinase and cytokine expression in synovial fibroblasts stimulated with immune cell microparticles. Proc Natl Acad Sci U S A. 2005;102(8):2892-7.
120. Zhang B, Yin Y, Lai RC, Tan SS, Choo AB, Lim SK. Mesenchymal stem cells secrete immunologically active exosomes. Stem Cells Dev. 2014;23(11):1233-44.
121. Brown BN, Londono R, Tottey S, Zhang L, Kukla KA, Wolf MT, et al. Macrophage phenotype as a predictor of constructive remodeling following the implantation of biologically derived surgical mesh materials. Acta Biomater. 2012;8(3):978-87.
122. Sicari BM, Rubin JP, Dearth LC. An Acellular Biologic Scaffold Promotes Skeletal Muscle Formation in Mice and Humans with Volumetric Muscle Loss. 2014.
123. Scientific T. Pierce BCA Protein Assay Kit. 2016.
124. Quiagen. RNeasy® Mini Kit, Part 1. 2015.
125. Biosystems A. High Capacity cDNA Reverse Transcription Kits. 2011
126. Biotech P. Western Blotting
HYSICAL PROPERTIES OF PROTEINSWhat Do You Know about Your Protein? 2013.
127. Bio-Imaging. Negative Staining 2004.

7. Supplemental Data

7.1 Figures

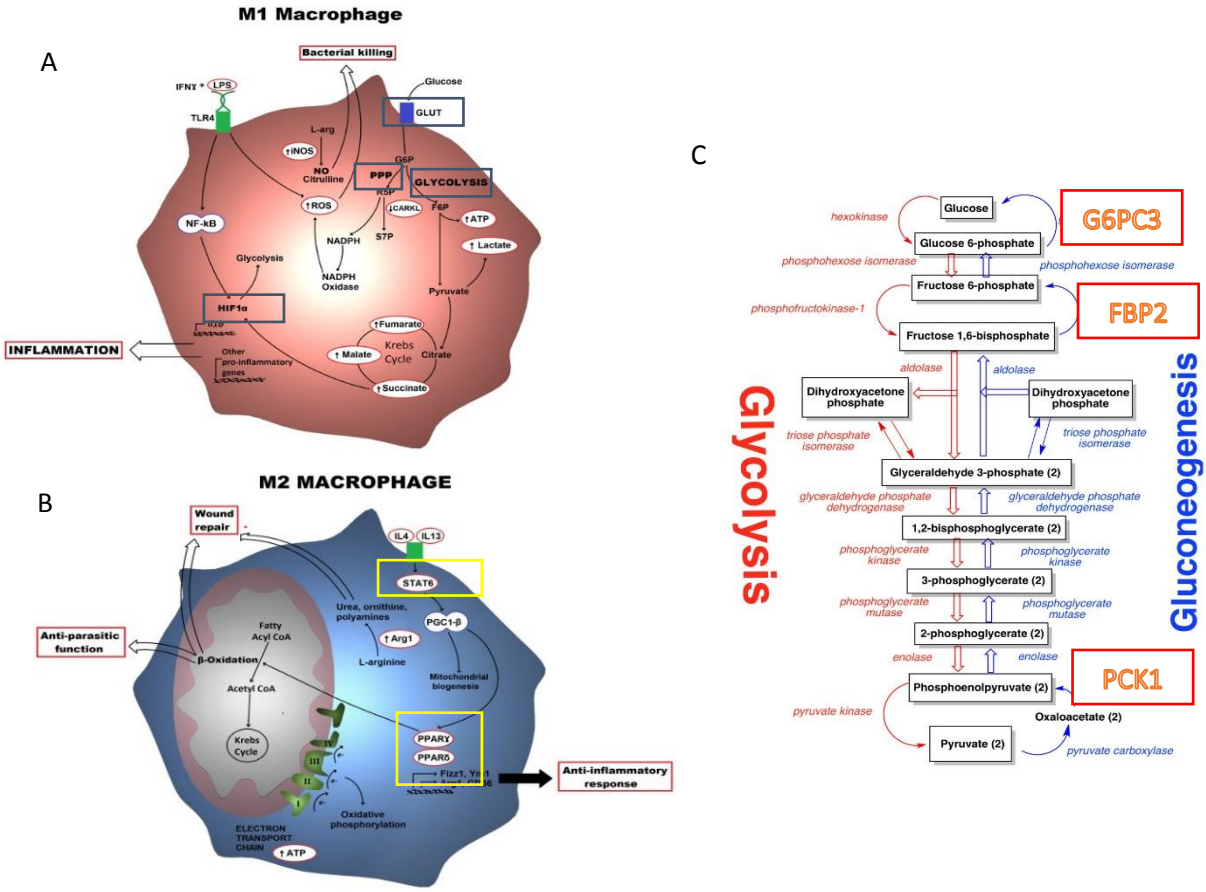

Fig. S1: Metabolic M1- and M2-macrophage phenotype pathways. Pro-inflammatory M1- and anti-inflammatory M2-macrophages are characterized by different metabolic pathways. (**A**) M1 macrophage phenotypes are part of the first defense of the innate immune system. Rapid energy is provided by its glycolytic pathways (**B**) M2 macrophages play a role in later immunological pathways and obtain their energy from oxidative metabolism and gluconeogenetic pathways (**C**), which sustains longer (36).

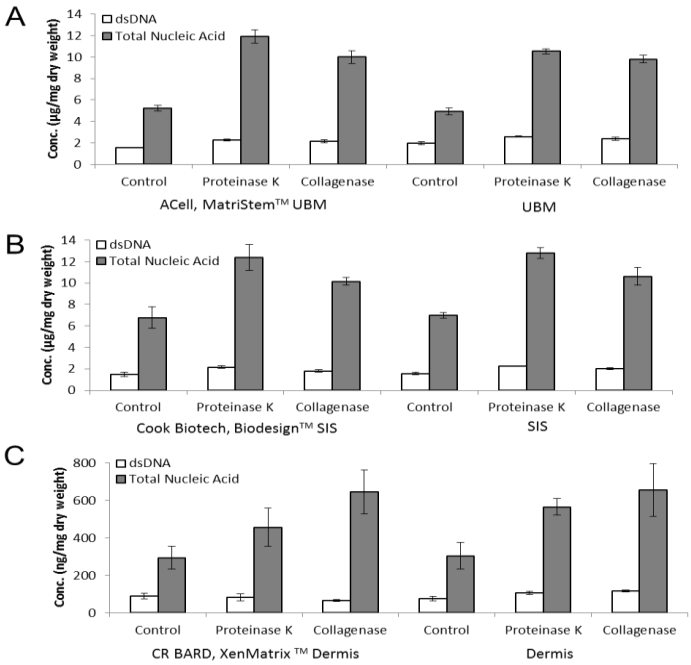

Fig. S2: Extracellular Matrix products contain nucleic acids that may be released by digestion.

In order to examine the presence of nucleic acids in acellular ECM materials, nucleic acid extraction has been performed in laboratory produced and commercial UBM (**A**), SIS (**B**), or dermis (**C**) products using a phenol:chloroform method. All ECM bioscaffolds were enzymatically digested with various proteases prior to extraction methods. Undigested scaffolds are referred to as "Control". Double strength DNA (dsDNA) was quantified using the PicoGreen assay and the total amount of nucleic acid was determined by UV absorbance at 260nm. Only approximately 25-40% of the total nucleic acid amount of each ECM product was present as dsDNA. Additionally, in all forms of digested ECM bioscaffold materials was the amount of extracted nucleic acids remarkable higher than in undigested controls. n=3 isolations/sample ((Huleihel et all. (Science advances – "in press")).

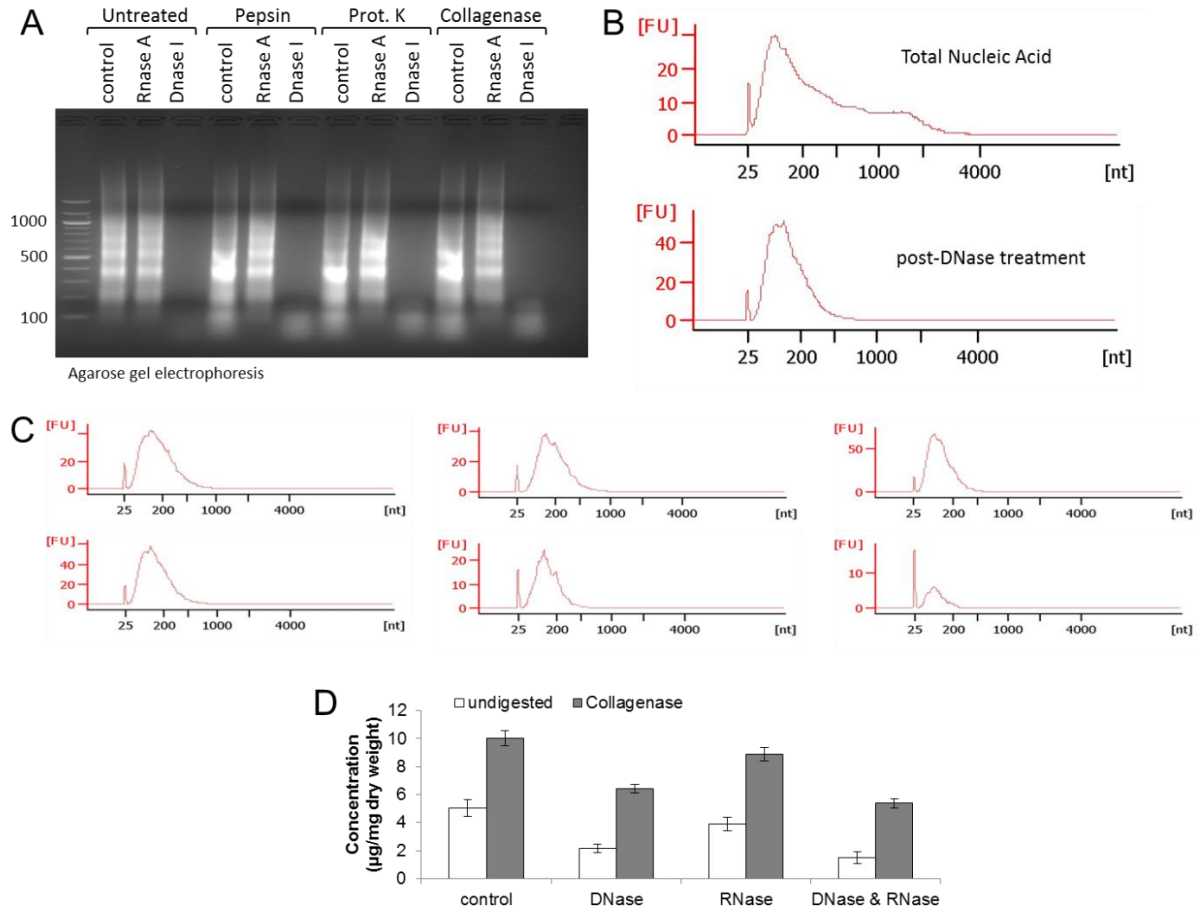

Fig. S3: Small RNA molecules present in ECM bioscaffolds could be protected by vesicles. (**A**) To examine if ECM bioscaffolds contain RNA, gel electrophoresis was performed on extracted nucleic acid samples that were prior treated with DNase I and RNase A nucleases. Whereas a small band of ~25-200bp remained after DNase I treatment, RNase A removed these nucleic acid material, indicating the presence of RNA molecules. These RNA particles were only present after digestion of ECM bioscaffolds when compared to undigested control ("Untreated"). (**B**) Agilent 2100 Bioanalyzer Electropherogram were used for further analysis of nucleic acid extracted samples. Compared to UBM samples not treated with DNase I (*upper panel*), results after nuclease treatment show that all nucleic acids beside the RNA molecules were removed (*lower panel*). (**C**) The same results were reported for all ECM materials. (D) Undigested and digested UBM materials were exposed to nuclease treatments, and nucleic acid concentration was measured. Nuclease treatments could not remove all nucleic acid molecules in both, digested and undigested bioscaffolds, indicating that nucleic acids could be incorporated in extracellular vesicles and protected from nuclease treatments (Huleihel et all. (Science advances – "in press")).

7.2 Tables and Figures Gene Expression M1- and M2- macrophage marker

7.2.1 Tables

Table S1: Scoring system of the gene expression level. All scores were compared as full change of the gene expression level of cells that were treated with culture media instead of ECM-degradation products. As baseline, media treated cells were indicated with a score of 1. (**A**) Scoring system legend. (**B+C**) Gene expression of M1- and M2- associated macrophage transcription factors and surface markers of Bone-marrow derived macrophages (**B**) and THP-1 differentiated (**C**) macrophages post-treatment with pepsin digested ECM degradation products or cytokines. (**D+E**) Gene expression of M1- and M2- associated metabolic markers of Bone-marrow derived macrophages (**D**) and THP-1 differentiated (**E**) macrophages post-treatment with pepsin digested ECM degradation products or cytokines.

A

Scoring system	Values	Scoring
≥5	3	+++
2 - 4.9	2	++
1.3 - 1.9	1	+
0.7 - 1.29	0	0
0.69 - 0.3	1	-
0.29 - 0.1	2	- -
<0.1	3	- - -

B

M1- and M2- associated transcription factors and surface markers

Bone-marrow derived macrophages

	Pepsin	LPS + IFNg (M1)	IL-4 (M2)	UBM	SIS	M1-UBM	M1-SIS	UBM-M1	SIS-M1	M2-UBM	M2-SIS	UBM-M2	SIS-M2
TNFa	++*	++	-*	++*	++*	0/-	--*	+*	+*	++*	0/+	0/-*	+
STAT1	++*	++*	-*	+++*	0/+	-	-	0/-	0	++*	-*	++*	0
STAT2	++*	++*	-*	++*	0/+	-	-	-*	0	++*	-*	+*	-*
KLF6	0	0	0	0	0/+	-*	-*	-	0	0	0	-*	-*
IRF5	0	_*	0/-*	-*	0/-	-	--	-*	0	0	0	-*	0/-
IRF3	0/-*	--*	0/-*	-*	0/-	-	-	-*	0/-	0/-	0/-	-*	0/-
STAT5	0/-	--*	-*	-*	-*	-*	0/-	-*	0/-	0/-*	0	-*	-
iNOS	+++*	+++*	+++*	+++*	+++*	--*	--*	-	0	+++*	--*	++	++
CD206	-*	---*	+*	---*	-*	-	+	--*	-*	---*	-*	-*	0
TGM2	0/-	+*	+*	-*	-*	+	0/+	-	0/-	0/-	0/+	-*	+*
IL1Ra	+	-*	0*	-*	--*	-	-*	--*	--*	++*	--*	-*	0/-
IRF4	-*	---*	+++*	---*	-*	-	-	--*	--*	---*	--*	-*	0/-*
STAT3	+	0/-	0/-	0	0/-*	-	-	-*	-*	0	0	0/-	0
STAT6	0	- - -*	0	- *	0/-	-*	-*	0/-	0/-	-*	0/-*	0/-*	0/-
KLF4	0	0	++*	-*	+	--*	-*	-*	0/-	--*	-*	-*	-*
Fizz-1	+*	-*	+++*	-*	++*	-	-	---*	--	--*	--*	--*	0
ARG1	+	+++*	+++*	+++*	+++*	+++*	+++*	++*	0/-	++*	0	-	+
PPARg	-	--*	0	-*	No results								

*p<0.05

C

THP1-differentiated macrophages

	Pepsin	LPS + IFNg (M1)	IL-4 (M2)	UBM	SIS	M1-UBM	M1-SIS	UBM-M1	SIS-M1	M2-UBM	M2-SIS	UBM-M2	SIS-M2
TNFa	++*	+++*	- -*	+*	0	0/-	-	0	0	++*	0/+	++*	+
STAT1	0	+++*	+*	0	0/-*	0	0	0/+	0	0/+	0/+	0	+*
STAT2	0*	+++*	0/-*	0	0	0	0	+*	0	+*	0/+	0	0
KLF6	+	+++*	0	0/-	0/-*	-	No results	0/+	-	- - -	-	0	++*
IRF5	0	+++*	+*	0	0	+*	+*	0/+*	+*	0/+	0/-	0	0/+
IRF3	0/+	++*	0	0/+	0/+*	0/-	0	+*	0/-*	+*	0/+*	0	0/-*
STAT5	+*	++*	0/+*	0	0/-	0	0	+*	0	0/+*	0/-	0/+	0/+
iNOS	0*	++*	-*	+	0*	-	0/-	0/-	0	0/-	0	0	0
CD206	0	- -*	+++*	0	0/-	+*	+*	0/+	0	+*	0/+	0/-	0/+
PPARg	0	-*	++*	0/-*	0	+	0	0/+	0/-	0/+*	+*	0/+	+
TGM2	+*	++*	+++*	0/+*	0	0	0/+	0/-	-*	++*	0	+*	+
IL1Ra	0/+	+++*	++*	+*	0/+	+*	+*	+++*	+++*	++*	+*	++*	++*
IRF4	+	+++*	0/-	0/+*	0/-	0/-	0/-	0/-	0	+	++*	+*	0/-
STAT3	+*	+++*	0	0	0	0	0	+*	0/+	0	0/-*	0/+*	+*
STAT6	-*	++*	0/-*	0	0*	07-	0	0/+*	0	0/+	0	0/+*	0
KLF4	-*	0/-*	-*	0/-*	0/-*	0	0	0/-	0/-	0	0	0/-*	0/+

*p<0.05

D

M1- and M2- metabolic markers

Bone-marrow derived macrophages

	Pepsin	LPS + IFNg (M1)	IL-4 (M2)	UBM	SIS	M1-UBM	M1-SIS	UBM-M1	SIS-M1	M2-UBM	M2-SIS	UBM-M2	SIS-M2
GLUT1	0	+++*	0	+*	0	0	0	-*	0/-*	++*	+*	-*	0/-
HIF1a	0	0/-	-*	0	-*	0	0/-	-*	-*	0	0/+	-*	0/-
HK3	0/-	0/+*	-*	+*	-*	0	0/-	-	+	++*	+	0	-*
PGK1	0	0/+	0	0	0	+	+	0	0/+	++*	+*	0/-	0/-
PDK4	-*	--*	-*	--*	-*	-*	-*	-*	0/-	- -*	-*	-*	- -
RPIA	0	--*	0/+	-*	0/-	-*	-*	0/-	-	-*	0/-*	0/-*	0/-*
PFKFB3	0/+	+++*	-*	++*	0/-	-	0/-	-*	-*	++*	0/+	0/-	-
LDHA	0	0	0/+*	0	0	+	0	0/-	0	+*	+	-*	-
PCK2	0	--*	0/-*	--*	-*	- -*	-*	- -*	- -*	- -*	-*	-*	0/-
G6PC3	0/-*	--*	0/-*	-*	-*	-*	-*	0	0	-*	0	0/-	0/-
PPARd	0/-	-	-	-*	-*	-*	0	0/-	0/-	0	+*	0/-*	0
PCK1	-*	---*	0/-	-*	-*	-	0/-	-	0/+	--*	0	0/-	+

*p<0.05

E

THP1-differentiated macrophages

	Pepsin	LPS + IFNg (M1)	IL-4 (M2)	UBM	SIS	M1-UBM	M1-SIS	UBM -M1	SIS-M1	M2-UBM	M2-SIS	UBM-M2	SIS-M2
GLUT1	0/+*	++*	+	0/+	0	0/-*	0/-*	0/+	0	+*	0/-	0/+	0
HIF1a	0*	++*	0	0	0/+	0	0	+*	0/+	0	0/-	0/+	+
HK3	0/-*	0	-*	0*	0	0/+	0	0	0/-	-*	0/-	0	0/-
PGK1	0	++*	0/-	0	0	0/-	0/-	0	0	0/+*	0	0*	0
PDK4	++*	0/-	0/-	0	+*	++*	++*	0	0/-	0/+	-	0	0/+
RPIA	0/+	-*	0	0/+	0/+*	0/+	0	0	0/+	0/+	0	0/+*	0
PFKFB3	++*	+++*	- -*	0	0	0/-	0/-	0/+	0/-	+	-*	+	0
LDHA	0/-*	++*	0	0	0/-*	0/-	0	0	0	0/+	0	+*	0
PCK2	0*	++*	0	0	0*	0	0/-	0/+	0	0/+	0	0/+*	0/+
G6PC3	0	0*	0*	0	0	0/+*	0/+	0/-	0	0/+	0/-*	0/-	0
PPARd	+*	++*	+*	+*	0	0/-	0	0	0/-	0/+	0/-	0	0/+
PCK1	0/+	++*	+*	0	-*	No results							

*p<0.05

7.2.2 Figures

M1- and M2 Macrophage associated Surface markers and Transcription Factors

THP-1 differentiated Macrophages

A

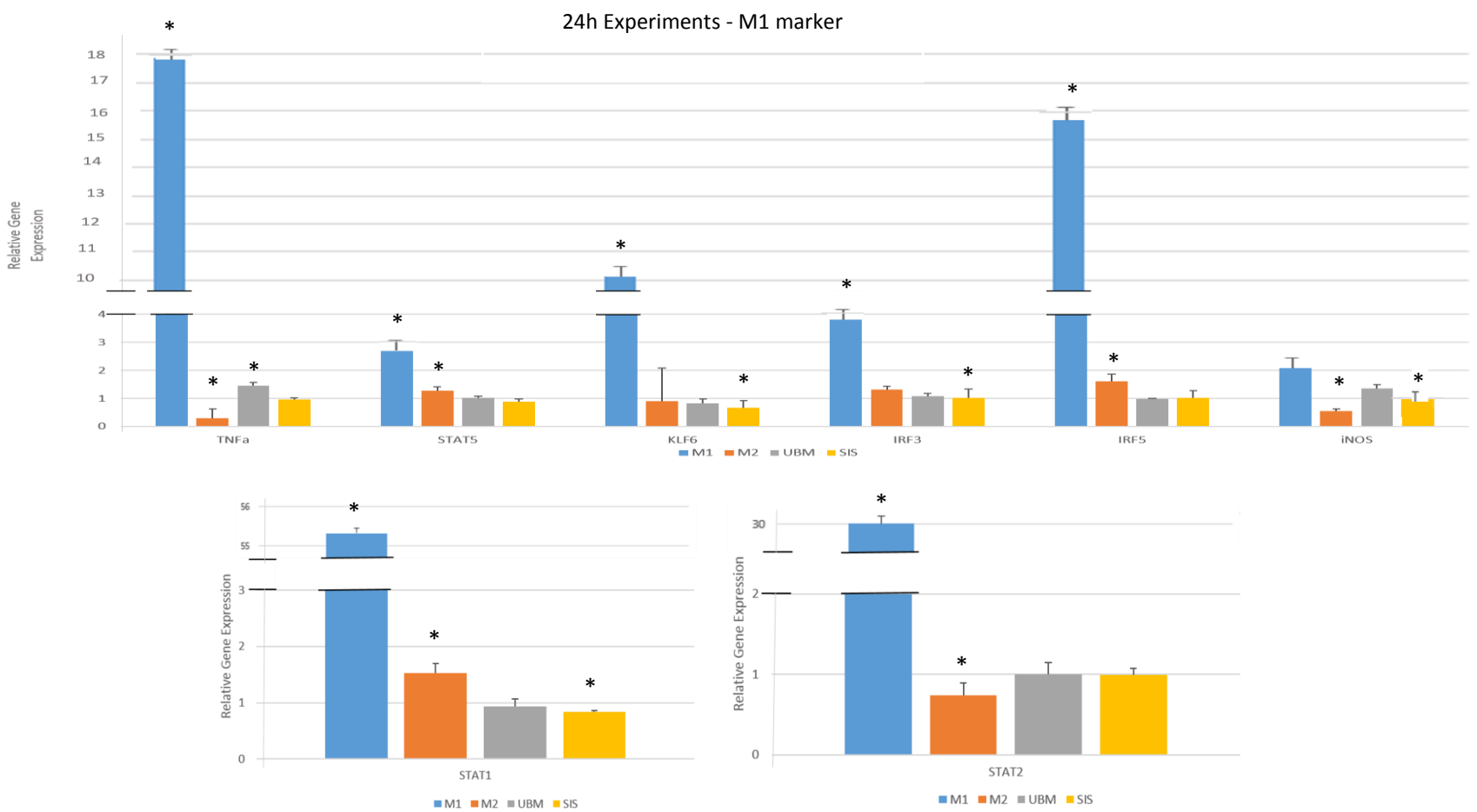

*p<0.05

B

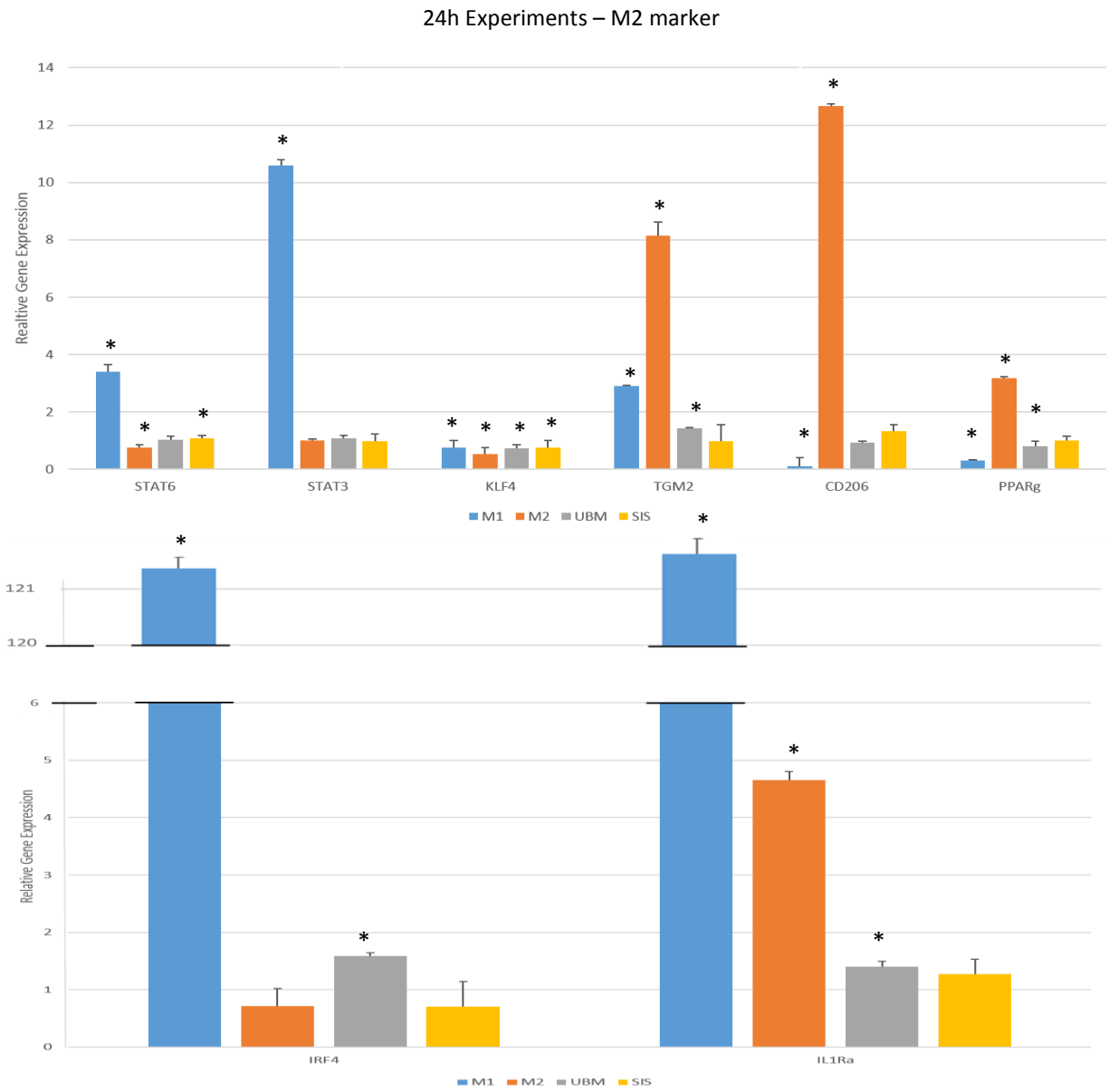
24h Experiments – M2 marker
Realtive Gene Expression
14
12
10
8
6
4
2
0
STAT6
STAT3
KLF4
TGM2
CD206
PPARg
M1 M2 UBM SIS
121
120
6
5
4
3
2
1
0
Relative Gene Expression
IRF4
IL1Ra
M1 M2 UBM SIS

*p<0.05

C

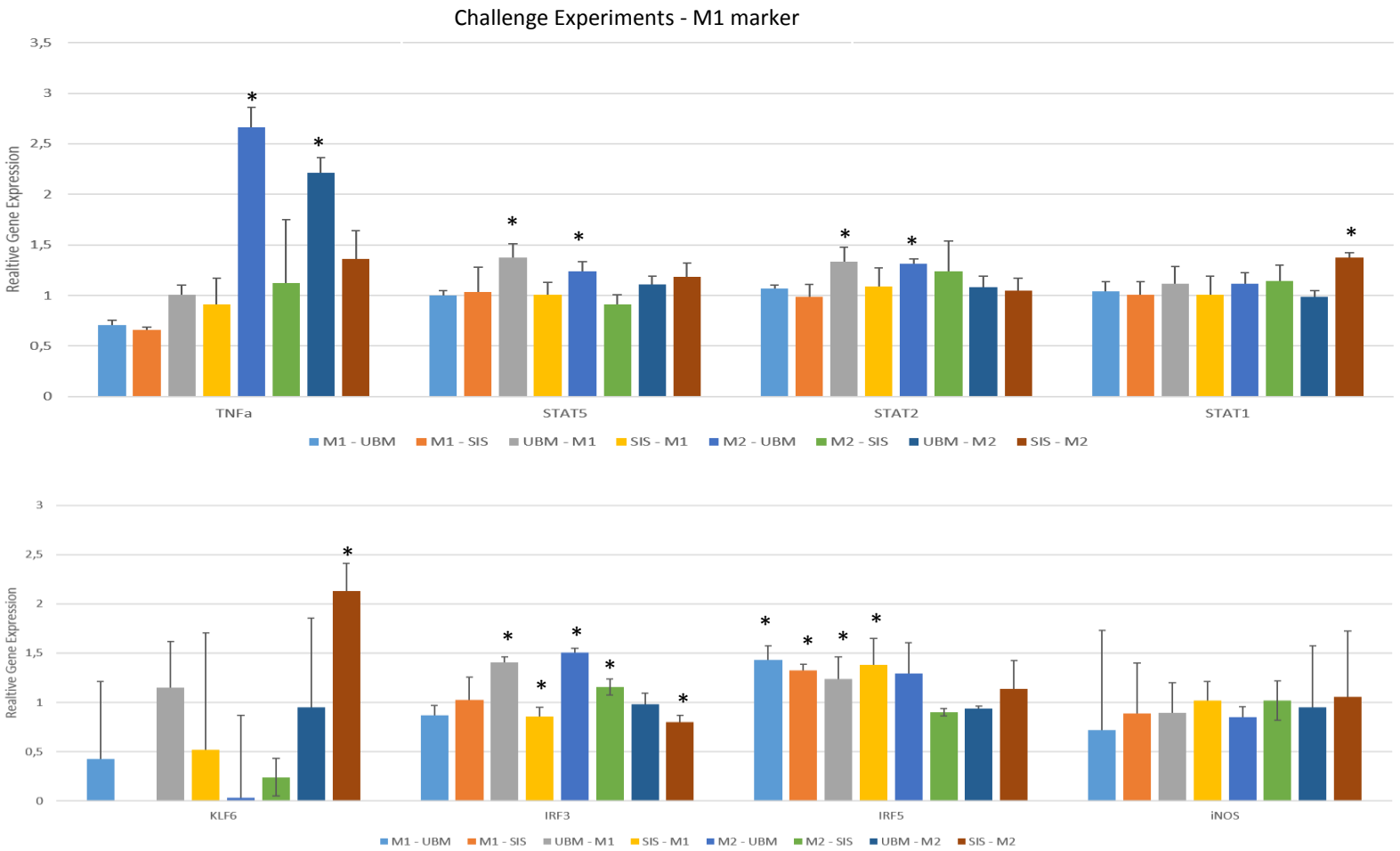
Challenge Experiments - M1 marker
Realtive Gene Expression
3,5
3
2,5
2
1,5
1
0,5
0
TNFa
STAT5
STAT2
STAT1
M1 - UBM
M1 - SIS
UBM - M1
SIS - M1
M2 - UBM
M2 - SIS
UBM - M2
SIS - M2
Realtive Gene Expression
KLF6
IRF3
IRF5
iNOS
M1 - UBM
M1 - SIS
UBM - M1
SIS - M1
M2 - UBM
M2 - SIS
UBM - M2
SIS - M2

*p<0.05

D

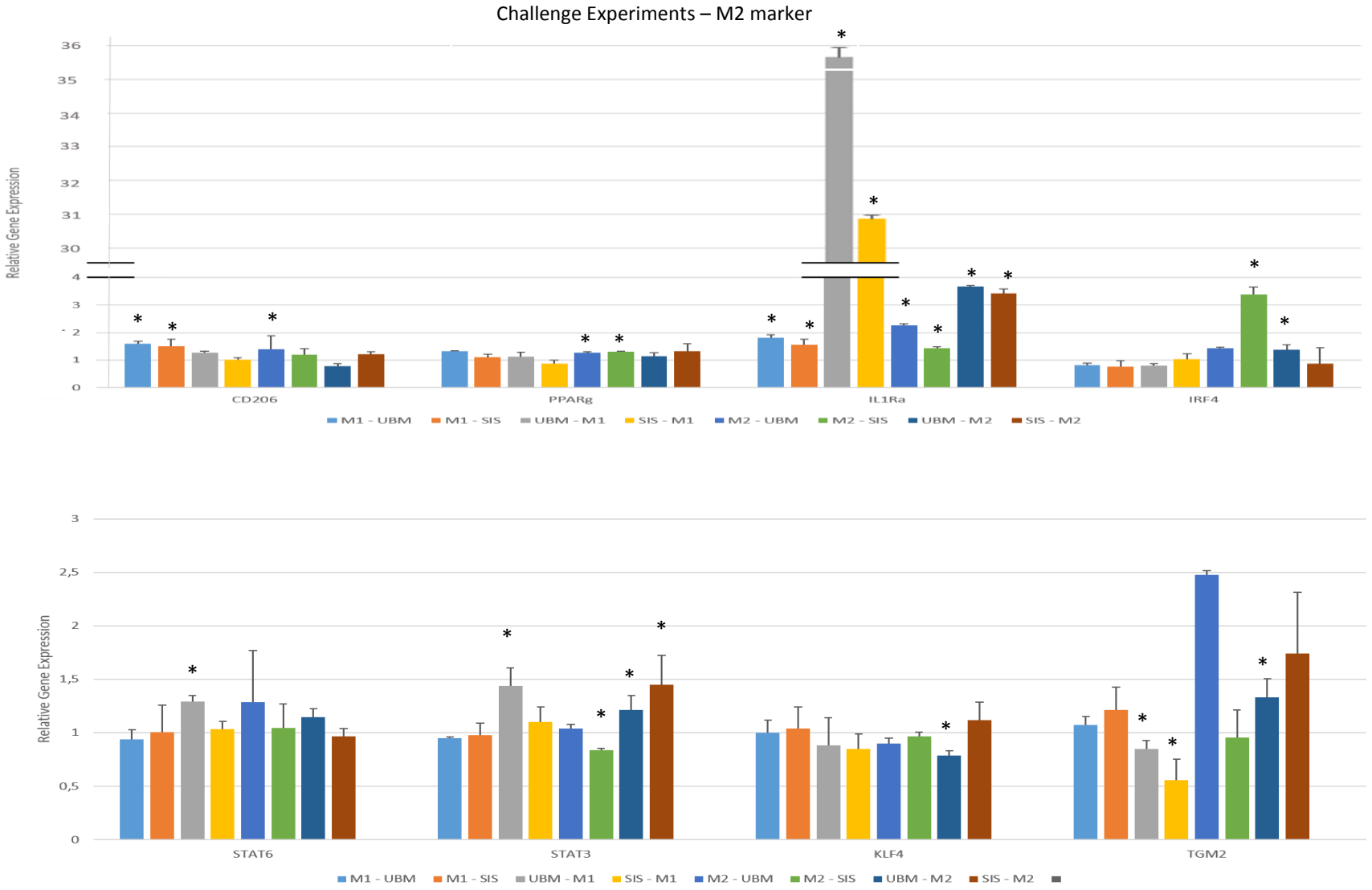
Challenge Experiments – M2 marker
Relative Gene Expression
CD206
PPARg
IL1Ra
IRF4
STAT6
STAT3
KLF4
TGM2
M1 - UBM
M1 - SIS
UBM - M1
SIS - M1
M2 - UBM
M2 - SIS
UBM - M2
SIS - M2

*p<0.05

M1- and M2 Macrophage associated Surface markers and Transcription Factors

Bone-marrow derived macrophages

E

24h Experiments – M1 marker

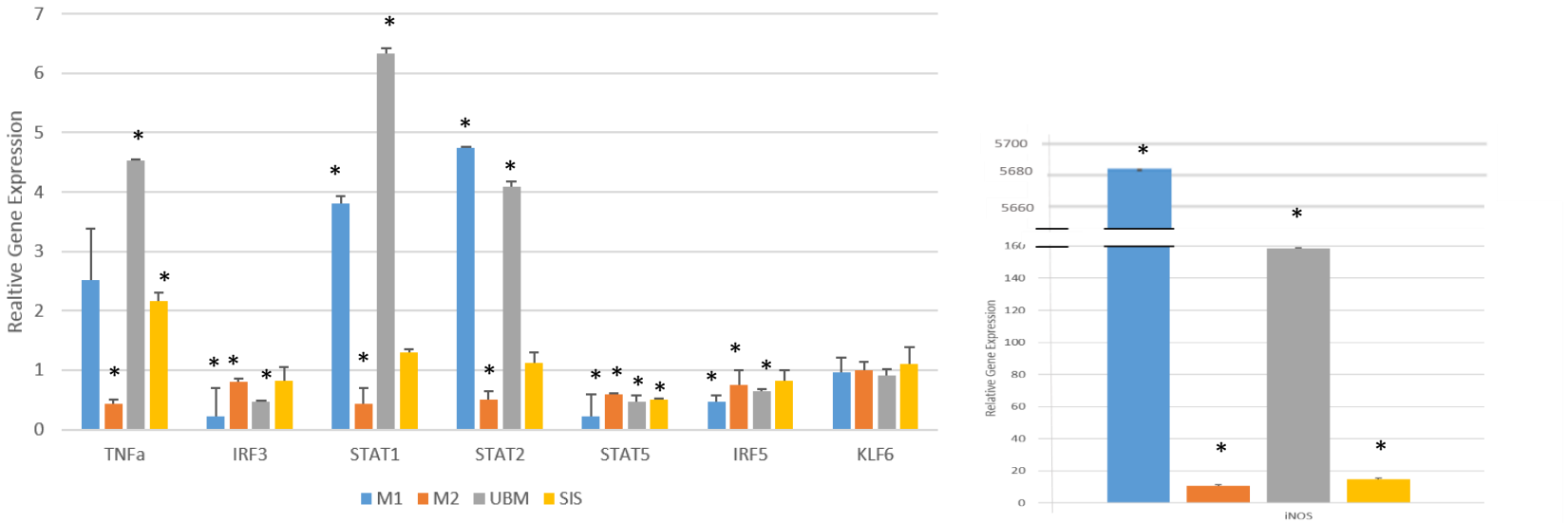

*p<0.05

24h Experiments – M2 marker

F

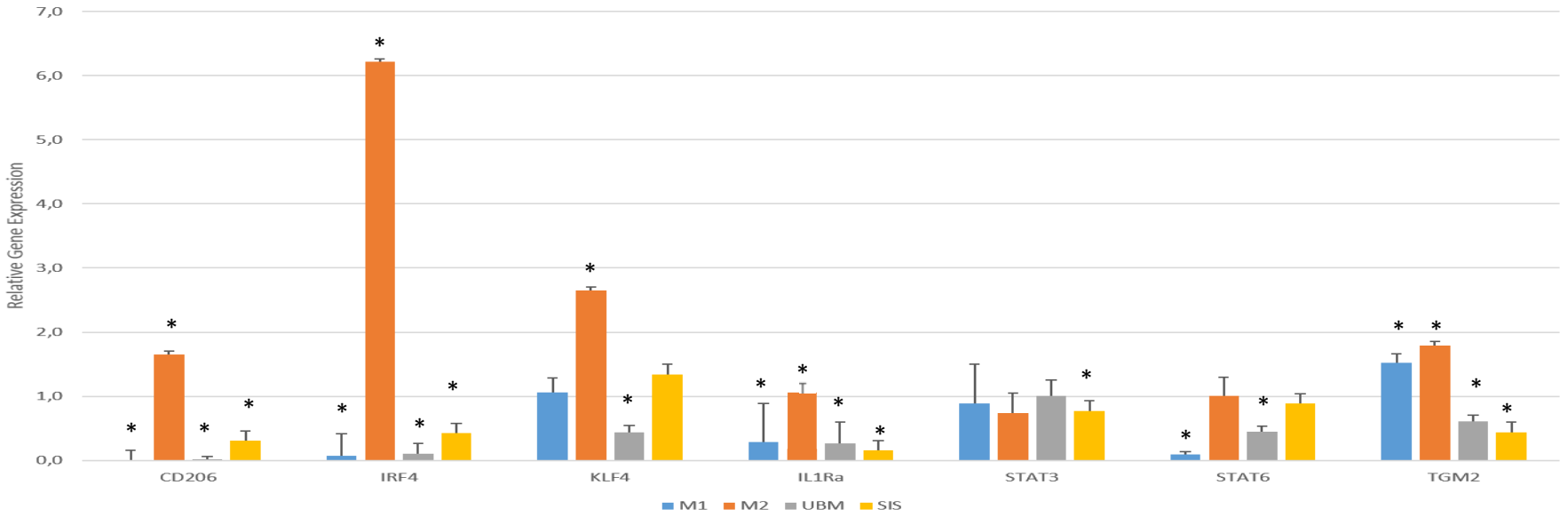

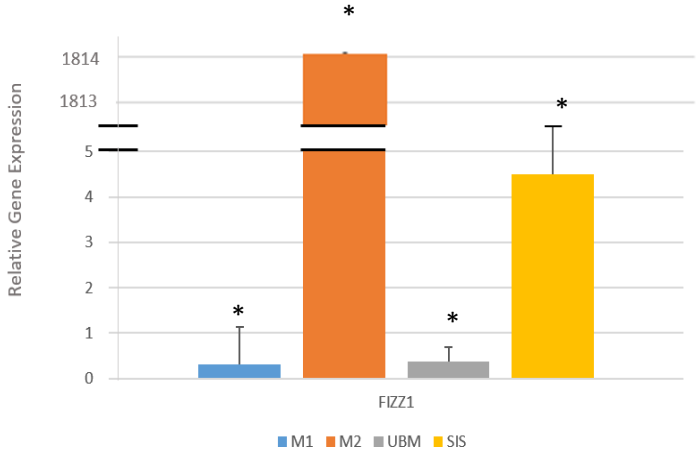

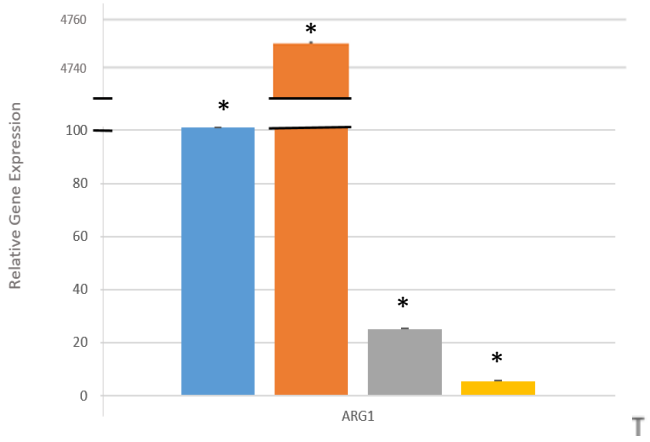

*p<0.05

G

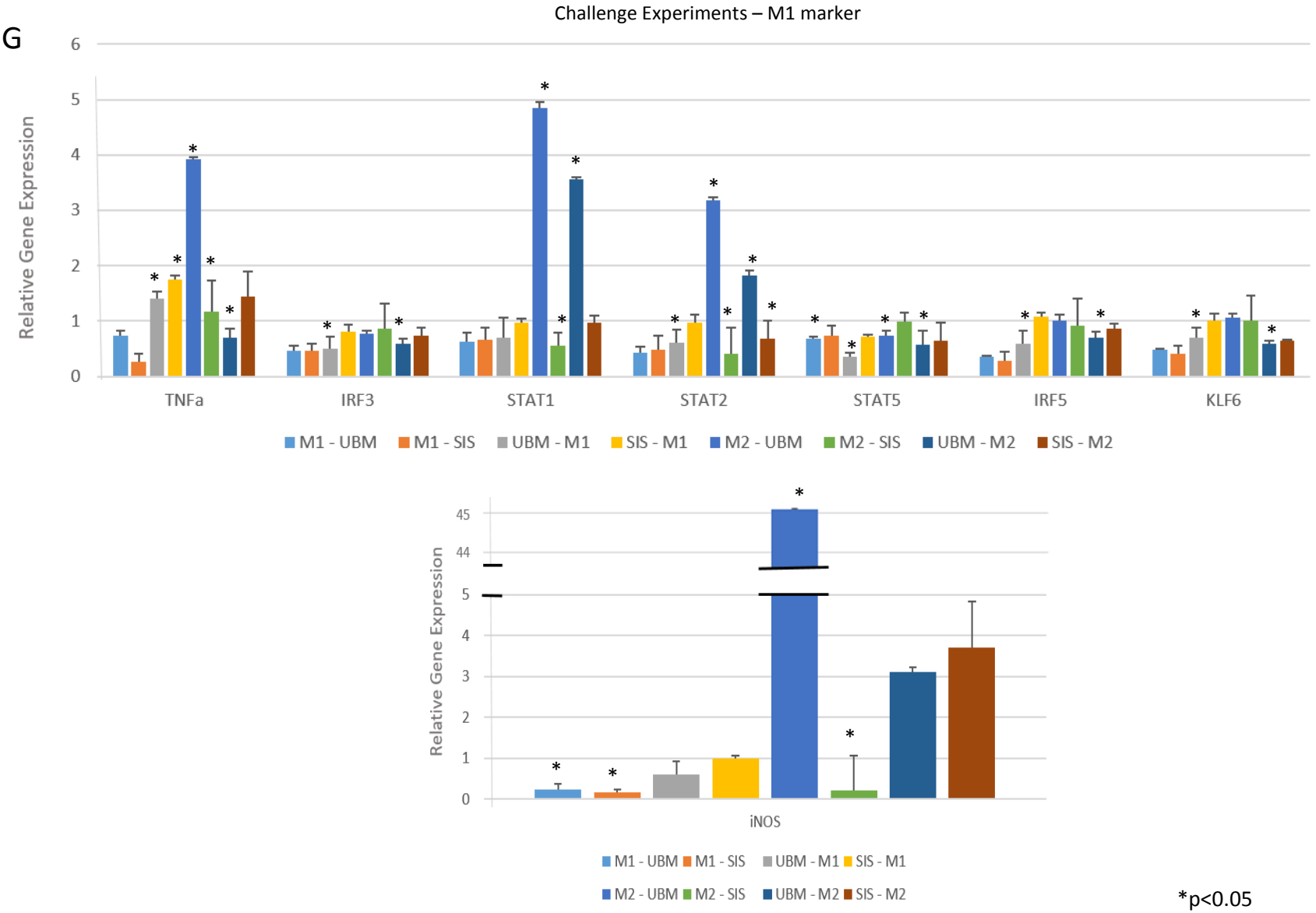
Challenge Experiments – M1 marker
Relative Gene Expression
TNFa
IRF3
STAT1
STAT2
STAT5
IRF5
KLF6
M1 - UBM
M1 - SIS
UBM - M1
SIS - M1
M2 - UBM
M2 - SIS
UBM - M2
SIS - M2
iNOS

*p<0.05

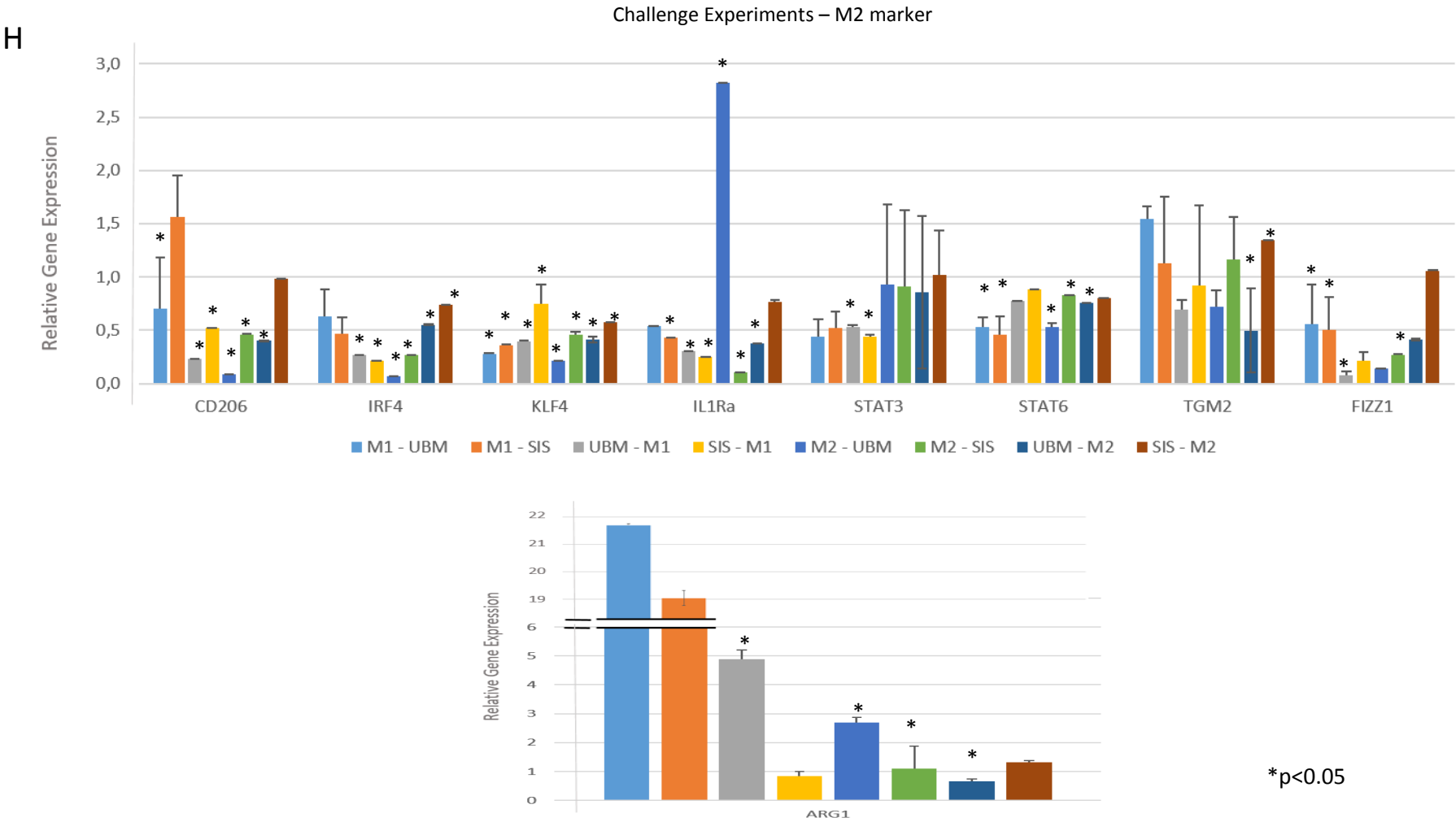

Fig. S4: Gene Expression of – M1- associated Transcription factors and Surface markers. THP-1 differentiated macrophages and BMDM macrophages were treated with 20 ng/ml Interferon gamma and 100 ng/ml Lipopolysaccharide to derive "M1-like" macrophages (M1), 20 ng/ml Interleukin-4 to derive "M2-like" macrophages (M2), or 250 ug/ml of UBM and SIS ECM degradation products to derive "M_{ECM} -like" macrophages. 250 ug/ml of pepsin was used as control buffer. (**A-D**) Relative gene expression in THP-1 differentiated macrophages post-treatment. (**E-H**) Relative gene expression in Bone-marrow derived macrophages post-treatment (For treatments see Supplemental Material and Methods, Protocol 6).

A

M1- and M2 Macrophage metabolic marker

THP-1 cell differentiated macrophages

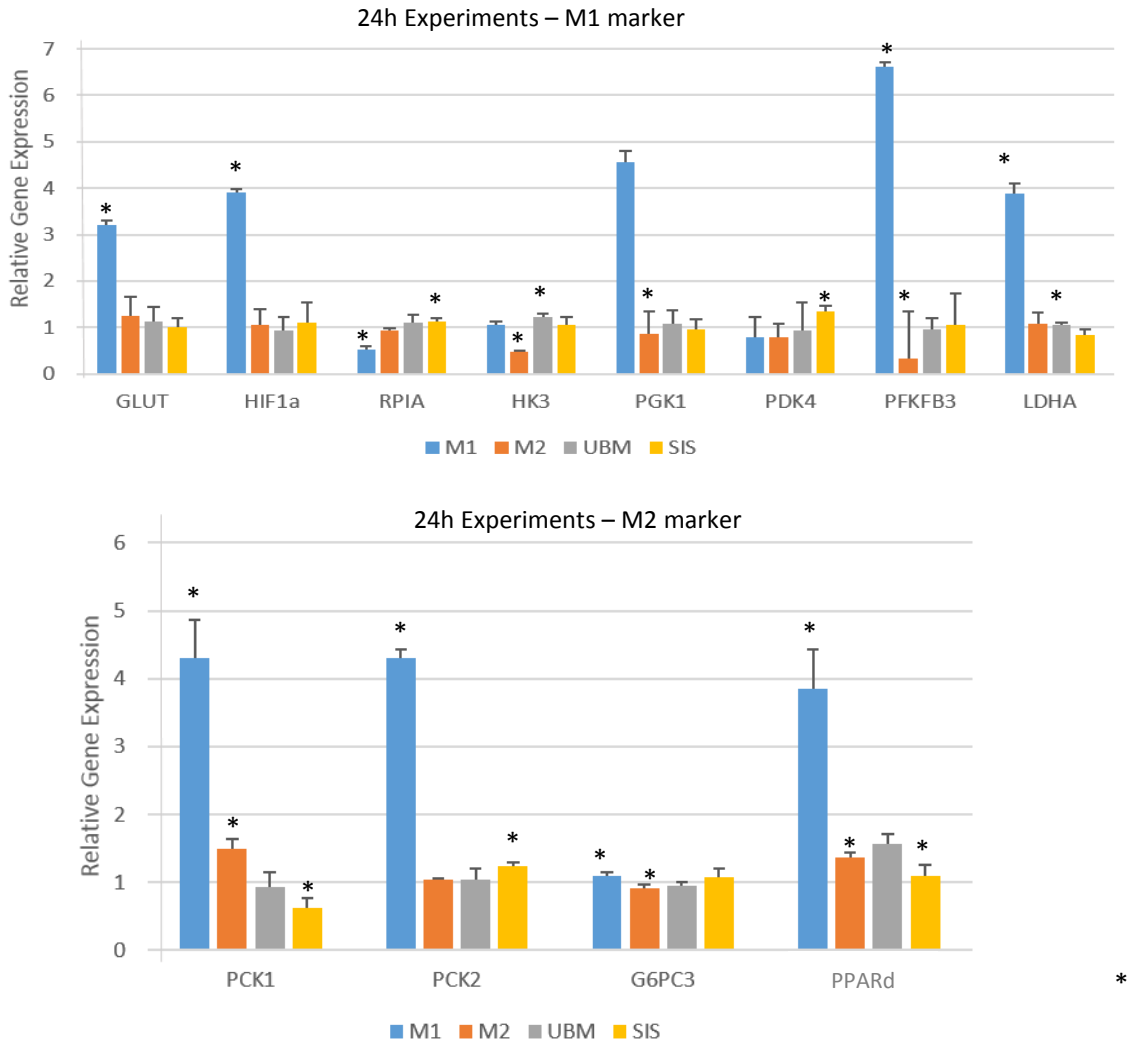

*p<0.05

B

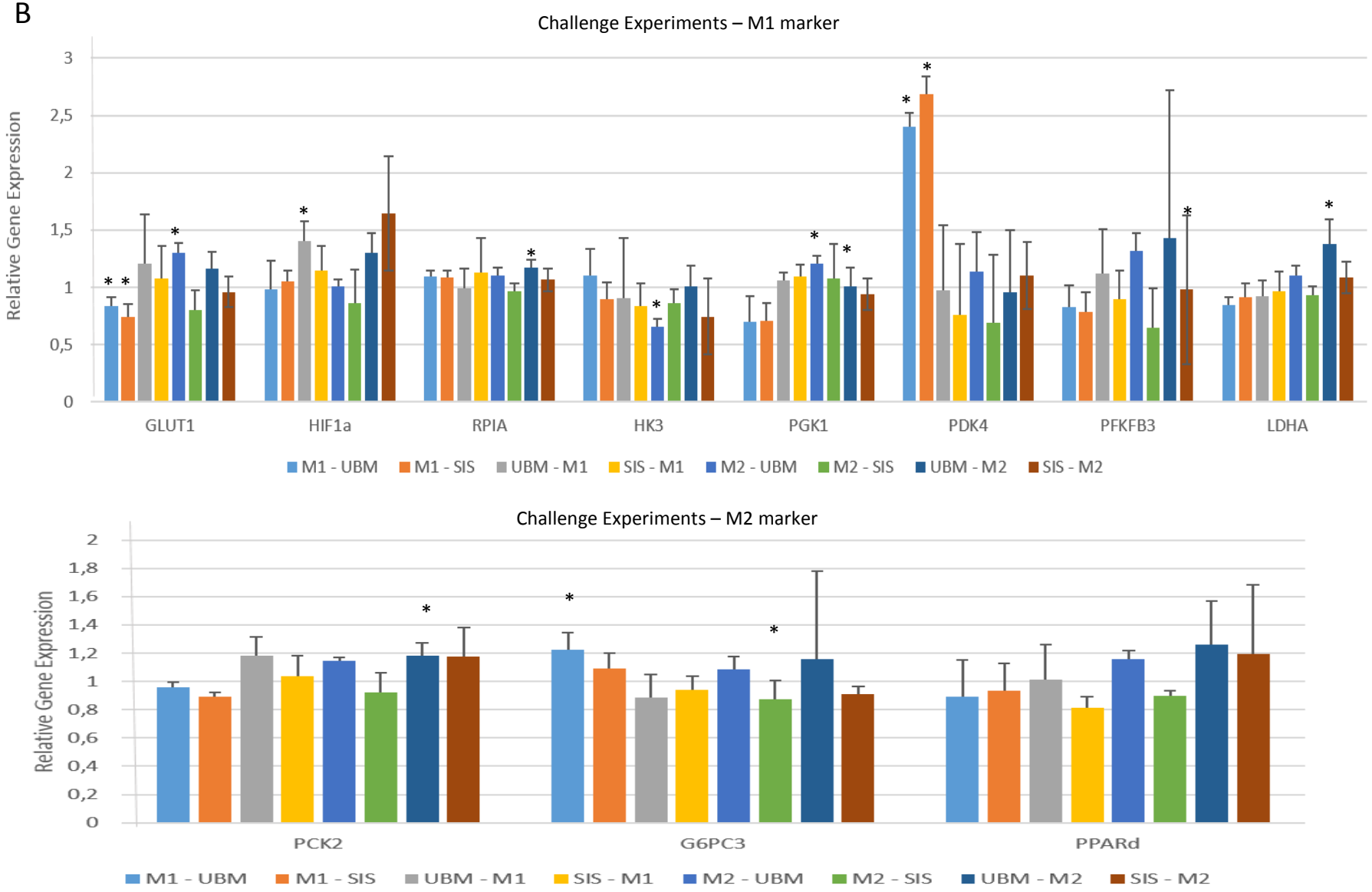
Challenge Experiments – M1 marker
Relative Gene Expression
3
2,5
2
1,5
1
0,5
0
GLUT1
HIF1a
RPIA
HK3
PGK1
PDK4
PFKFB3
LDHA
M1 - UBM
M1 - SIS
UBM - M1
SIS - M1
M2 - UBM
M2 - SIS
UBM - M2
SIS - M2
Challenge Experiments – M2 marker
Relative Gene Expression
2
1,8
1,6
1,4
1,2
1
0,8
0,6
0,4
0,2
0
PCK2
G6PC3
PPARd
M1 - UBM
M1 - SIS
UBM - M1
SIS - M1
M2 - UBM
M2 - SIS
UBM - M2
SIS - M2

*p<0.05

Bone-marrow derived macrophages

C

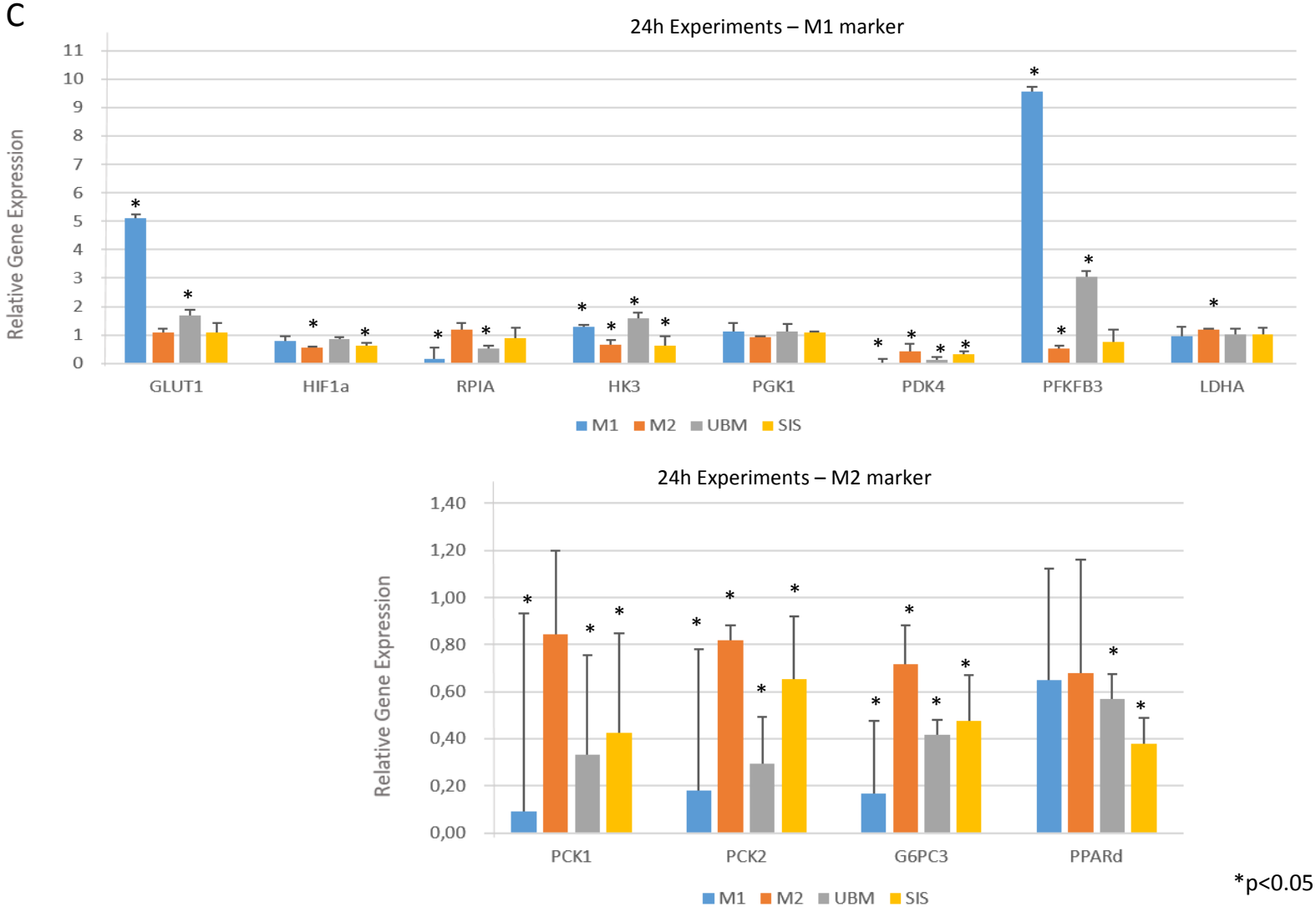

*p<0.05

D

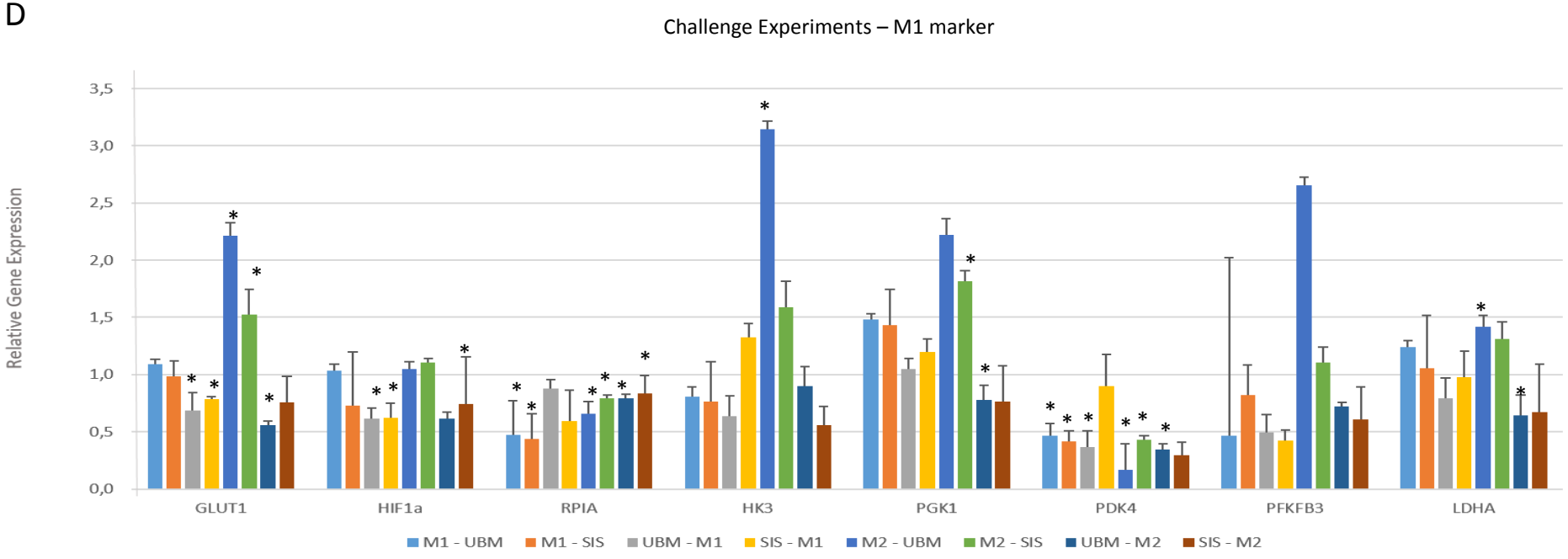

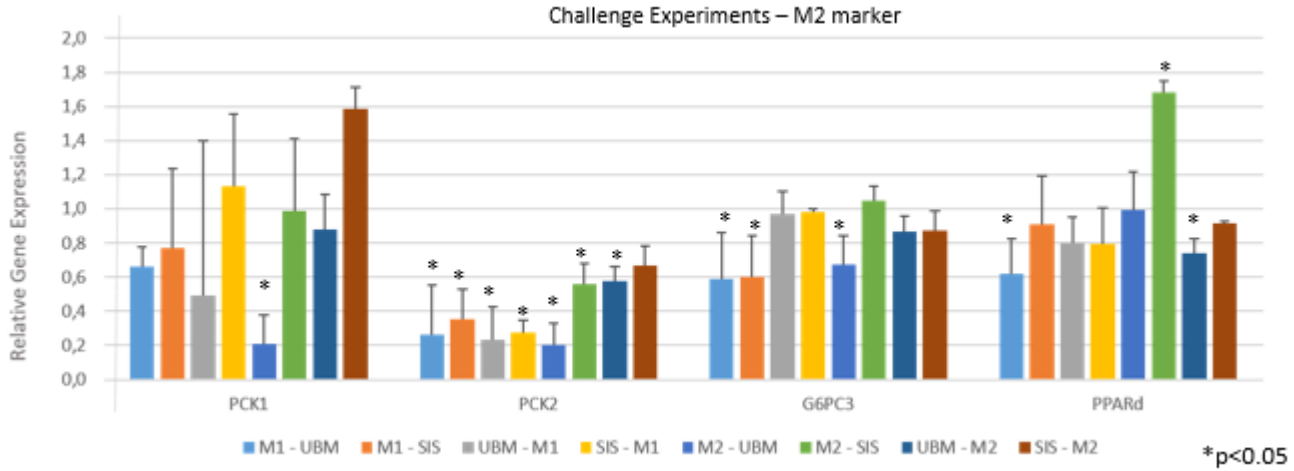

Fig. S5: Gene Expression of – M1- associated metabolic markers. THP-1 differentiated macrophages and BMDM macrophages were treated with 20 ng/ml Interferon gamma and 100 ng/ml Lipopolysaccharide to derive "M1-like" macrophages (M1), 20 ng/ml Interleukin-4 to derive "M2-like" macrophages (M2), or 250 ug/ml of UBM and SIS ECM degradation products to derive "M_{ECM} -like" macrophages. 250 ug/ml of pepsin was used as control buffer. (**A+B**) Relative gene expression in THP-1 differentiated macrophages post-treatment. (**C+D**) Relative gene expression in Bone-marrow derived macrophages post-treatment (For treatments see Supplemental Material and Methods, Protocol 6).

8. Supplemental Material and Methods

8.1 Tables

Table 1: Primers used to identify the gene expression of M1- and M2-assocaited macrophage markers.

1.a: M1- associated macrophage marker

M1-associated macrophage marker	Murine macrophage markers (BMDM)	Human macrophage markers (THP-1 differentiated macrophages)
M1 phenotype surface markers and transcription factors	TNF-α	TNF-α
	iNOS	iNOS
	IRF3	IRF3
	IRF5	IRF5
	KLF6	KLF6
	STAT1	STAT1
	STAT2	STAT2
	STAT5	STAT5
M1 phenotype metabolic markers	GLUT1	GLUT1
	HIF1α	HIF1α
	HK3	HK3
	LDHA	LDHA
	PFKFB3	PFKFB3
	PGK1	PGK1
	PDK4	PDK4
	RPIA	RPIA

1.b: M2-associated macrophage markers

M2-associated macrophage marker	Murine macrophage markers (BMDM)	Human macrophage markers (THP-1 differentiated macrophages)
M2 phenotype surface markers and transcription factors	CD206	CD206
	IL1Ra	IL1Ra
	IRF4	IRF4
	KLF4	KLF4
	STAT3	STAT3
	STAT6	STAT6
	TGM2	TGM2
	Arg1	PParg
	Fizz1	
M2 phenotype metabolic markers	PCK1	PCK1
	G6PC3	G6PC3
	PCK2	PCK2
	PPARd	PPARd

Table 2: Decellularization of Extracellular Matrix Bioscaffolds of various source tissue.

For all steps tissue was used that previously underwent mechanical delamination. All steps have been performed by an agitation at 300 RPM.

2.a: Porcine Dermal Extracellular Matrix

Solution	Incubation Period	Additional information
0.25% (v/v) trypsin	6 h	
Deionized H_2O	15 min	*This step was repeated 2x*
70% ethanol	10 h	
1% Triton X-100 in 0.26% EDTA/0.69% Tris	6 h and 16 h	*The solution was renewed in between the two incubation periods*
Deionized H_2O	15 min	*This step was repeated 2x*
0.1% PAA/4% ethanol	2 h	
1x PBS, pH7.4	15 min	*This step was repeated 1x*
Deionized H_2O	15 min	*This step was repeated 1x*

PAA – Peracetic Acid; PBS - Phosphate-buffered saline

2.b: Porcine Urinary Bladder Matrix and Small Intestinal Submucosal ECM

Solution	Incubation Period	Additional information
0.1% PAA/4% ethanol	2 h	
1x PBS, pH7.4	15 min	*This step was repeated 1x*
Deionized H_2O	15 min	*This step was repeated 1x*

PAA – Peracetic Acid; PBS - Phosphate-buffered saline

After decellularization, all tissues were lyophilized and milled into particles using a Wiley Mini Mill (123).

Table 3: Primers used for qPCR.

Gene	Mouse Primer			Human Primer		
	Primer Sequence 5′ - 3′	Annealing Temp. (°C)	Size (bp)	Primer Sequence 5′ - 3′	Annealing Temp. (°C)	Size (bp)
TNFa	For CCACCACGCTCTTCTGTCTAC Rev AGGGTCTGGGCCATAGAACT	63.3	102	For CTGCTGCACTTTGGAGTGAT Rev AGATGATCTGACTGCCTGGG	63.3	92
STAT1	For TCCCGTACAGATGTCCATGAT Rev CTGAATATTTCCCTCCTGGG	63.3	102	For AGGAAGACCCAATCCAGATGT Rev TGAATATTCCCCGACTGAGC	63.3	98
STAT2	For CGCTTGGAGAATTGGAAGTT Rev GCTGTCAAGGTTCTGCAACA	63.3	104	For GCTCATACTAGGGACGGGAAG Rev ATTCTGCAGCATTTCCCACT	63.3	104
iNOS	For GGCAGCCTGTGAGACCTTTG Rev GCATTGGAAGTGAAGCGTTTC	63.3	102	For GCAGAATGGACCATCATGG Rev ACAACCTTGGTGTTGAAGGC	63.3	98
KLF6	For CACGAAACGGGCTACTTCTC Rev ACACGTAGCAGGGCTCACTC	63.3	102	For GTAAGAAGCGGCATAGCACC Rev ATTTGATGCATTCAGGGAGG	55	94
STAT5	For GAAAGCATGAAAGGGTTGGAG Rev AGCAGCAACCAGAGGACTAC	63.3	100	For TTACTGAAGATCAAGCTGG GG Rev TCATTGTACAGAATGTGCCGG	65	102
IRF5	For ATGGGGACAACACCATCTTC Rev CAGGTTGGCCTTCCACTTG	63.3	97	For CAGAGCTCAGCTTGGTCCC Rev GATGGACTGGTTCATGGCAG	65	95
IRF3	For GATGGCTGACTTTGGCATCT Rev ACCGGAAATTCCTCTTCCAG	63.3	103	For ATGCACAGCAGGAGGATTTC Rev GTTGGCAGGTCTGGCTTATC	65	90
IL1Ra	For GTGAGACGTTGGAAGGCAGT Rev GCATCTTGCAGGGTCTTTTC	63.3	101	For CCTCAGAAGACCTCCTGTCCT Rev GCTTGCATCTTGCTGGATTT	63.3	90
IRF4	For TGCAAGCTCTTTGACACACA Rev CAAAGCACAGAGTCACCTGG	63.3	96	For CCTGCAAGCTCTTTGACACA Rev GAGTCACCTGGAATCTTGGC	65	89
CD206	For TTGGACGGATAGATGGAGGG Rev CCAGGCAGTTGAGGAGGTTC	63.3	98	For CAGGTGTGGGCTCAGGTAGT Rev TGTGGTGAGCTGAAAGGTGA	63.3	100
STAT6	For TGCCCGGTCTCACCTAACTA Rev CTGGGGTGGTTTCCTCTTG	63.3	93	For AGAAGACAGCAGAGGGGTTG Rev ACTTTTTCTGGGGGCATCTT	65	91
KLF4	For GCCACCCACACTTGTGACTA Rev CAGTGGTAAGGTTTCTCGCC	63.3	103	For AGAGTTCCCATCTCAAGGCA Rev GTCAGTTCATCTGAGCGGG	65	105
STAT3	For CTCAGCCCCGGAGACAGT Rev CTGCTCCAGGTAGCGTGTGT	63.3	90	For CCTCTGCCGGAGAAACAG Rev CTGCTCCAGGTACCGTGTGT	63.3	91
Fizz-1	For TCCCAGTGAATACTGATGAGA Rev CCACTCTGGATCTCCCAAGA	63.3	100			
ARG1	For AGAGATTATCGGAGCGCCTT Rev TTTTTCCAGCAGACCAGCTT	63.3	93			
TGM2	For GGCCACTTCATCCTGCTCTA Rev GGTAGATGAAGCCCTGTTGC	63.3	108	For CAACCTGGAGCCTTTCTCTG Rev GCACCTTGATGAGGTTGGAC	60	94

PPARg	For GATGCACTGCCTATGAGCAC Rev TCTTCCATCACGGAGAGGTC	65	109	For AGGCCATTTTGTCAAACGAG Rev GAGAGATCCACGGAGCTGAT	55	104
GLUT1	For GCTGTGCTTATGGGCTTCTC Rev CACATACATGGGCACAAAGC	63.3	98	For GCTAGAGAAGGCCGCGGAGGCTC Rev TAGCGACCGGCACGCTCGCTGTT	60	
HIF1a	For CGGCGAGAACGAGAAGAA Rev AACTTCAGACTCTTTGCTTCG	63.3	94	For GAAGACATCGCGGGGAC Rev TGGCTGCATCTCGAGACTTT	60	104
HK3	For GCGCCGTCTAGAACTAA Rev CTTTGTGACGGGCAAG	63.3	102	For CCCTGAGTTGCTCTGAGGAG Rev ATCTGCTGTAGCTGTGCCCT	60	105
PGK1	For CTGACTTTGGACAAGCTGGA Rev CAGCCTTGATCCTTTGGTTG	63.3	108	For CAAGCTGGACGTTAAAGGGA Rev CTTGGGACAGCAGCCTTAAT	60	107
PDK4	For AGTGAACACTCCTTCGGTGC Rev TGACAGGGCTTTCTGGTCTT	63.3	105	For TGCCTTTGAGTGTTCAAGGA Rev CACGATGTGAATTGGTTGGT	60	108
RPIA	For CCTCCACGATGTCCAAGG Rev CACTTCCAATTCCCAGCACT	63.3	98	For GCTGAAAGGGTGAAGCAAGA Rev CGATCCAGATCACTGAGGGT	60	106
LDHA	For AGGCTCCCCAGAACAAGATT Rev TCTCGCCCTTGAGTTTGTCT	63.3	102	For GGCCTGTGCCATCAGTATCT Rev GGAGATCCATCATCTCTCCC	60	97
PCK1	For CTGGATGAAGTTTGATGCCC Rev TGTCTTCACTGAGGTGCCAG	55	90	For GAGAAAGCGTTCAATGCCAG Rev ATGCCGATCTTTGACAGAGG	60	116
PCK2	For GTACTGGGAAGGCATTGACC Rev AGTTTGGATGTGCACAGGGT	63.3	106	For AGCCTCTTCCACCTGGTGTT Rev AATCGAGAGTTGGGATGTGC	60	93
G6PC3	For ATTGCTGAGTGGCTCAACCT Rev TGGAGTCTGGGTGGAGTACC	63.3	95	For CGAGTGGCTCAACCTCATCT Rev GCTGGAGCCTGGCTGTAGTA	60	92
PPARd	For ACTCAGAGGCTCCTGCTCAC Rev GGTCATAGCTCTGCCACCAT	63.3	93	For TCACACAGTGGCTTCTGCTC Rev TGAACGCAGATGGACCTCTA	60	89
GAPDH	For CGTCCCGTAGACAAAATGGT Rev TTGATGGCAACAATCTCCAC	55-65	109			
bGUS				For AAATCTGCAAAA TTCCA Rev TCATTATCCTTATGCAGAAGA	55-65	102

Table 4: Appropriate antibodies used for Western Blot for protein detection.

	Primary Antibody	Secondary Antibody
CD63, CD81, CD9, Hsp70	EXOAB-KIT-1 – Rabbit-anti human antibodies - #EXOEL-CD63A-1, #EXOEL-CD81A-1, #EXOEL-CD9A-1, #EXOEL-Hsp70A-1 SBI, Mountain View, California ***Dilution**: 1:800*	Goat-anti-Rabbit HRP secondary antibody – #EXOAB-HRP 141215-001 – SBI, Mountain View, California ***Dilution:** 1:5000*
CD206	Rabbit polyclonal to Mannose Receptor antibody - #ab64693 – Abcam, Cambridge, Massachusetts ***Dilution:** 1:500*	Goat-anti-Rabbit HRP secondary antibody – #EXOAB-HRP 141215-001 – SBI, Mountain View, California ***Dilution:** 1:5000*
TNFa	Rabbit polyclonal to TNF alpha antibody - #ab6671 - Abcam, Cambridge, Massachusetts ***Dilution:** 1:200*	Goat-anti-Rabbit HRP secondary antibody – #EXOAB-HRP 141215-001 – SBI, Mountain View, California ***Dilution:** 1:1000*
STAT1	Rabbit polyclonal to STAT1 antibody - #9172S, Cell signaling Technology, Danvers, Massachusetts ***Dilution**: 1:1000*	Goat-anti-Rabbit HRP secondary antibody – #EXOAB-HRP 141215-001 – SBI, Mountain View, California ***Dilution:** 1:5000*
TGM2	Mouse monoclonal to Transglutaminase 2 antibody – #ab21258 - Abcam, Cambridge, Massachusetts ***Dilution:** 1:500*	Polyclonal goat-anti mouse secondary antibody - #P0447 – Dako, Burloak, Canada ***Dilution:** 1:5000*
β-actin	Mouse monoclonal to β-actin - #sc-4778, Santa Cruz Biotechnology, Dallas – Texas ***Dilution:** 1:1000*	Polyclonal goat-anti mouse secondary antibody - #P0447 – Dako, Burloak, Canada ***Dilution:** 1:5000*

8.2 Protocols

Protocol 1: RNA extraction – Rneasy Mini Kit (Quiagen, Valencia – California, U.S.A., adapted)

1. Harvest cells using TRIZOL.
2. Add 1.5 volume of chloroform to lysed cells and shake roughly for 15 s.
3. Centrifuge 15 min at 12,000 x g.
4. Remove supernatant by pipetting, add 1 volume of 100% ethanol and mix well by pipetting. Transfer sample to an RNeasy Mini spin column and spin for 15 s at ≥8000 x g. Discard the flow-through.
5. Add 700 µl Buffer RW1 to the RNeasy spin column. Close the lid and centrifuge for 15 s at ≥8000 x g. Discard the flow-through.
6. Add 500 µl Buffer RPE to the RNeasy spin column. Close the lid and centrifuge for 15 s at ≥8000 x g. Discard the flow-through.
7. Add 500 µl Buffer RPE to the RNeasy spin column. Close the lid and centrifuge for 2 min at ≥8000 x g. Discard the flow-through.
8. Place the RNeasy spin column in a new 2 ml collection tube (supplied) and centrifuge at full speed (16,000 x g) for 1 min.
9. Place the RNeasy spin column in a new 1.5 ml collection tube (supplied), add 30-50 µl RNase-free water directly to the spin column membrane. Centrifuge for 1 min at ≥8000 x g to elute the RNA.

Overview:

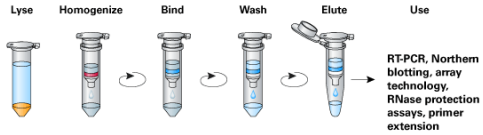

(124)

Protocol 2: cDNA synthesis - High capacity RT kit (ABI, Foster City - California, U.S.A., adapted)

1. Allow the kit components to thaw on ice.
2. Prepare 2X mastermix:

Component	**Volume/Reaction (µl)**
10X RT buffer	2.0
25X dNTP Mix (100 mM)	0.8
10X Random Primers	2.0
MultiScribe Reverse Transcriptase	1.0
RNAse-free H_2O	4.2
Total per reaction	**10**

3. Pipette 10 µl of 2X master mix into each individual tube.
4. Pipette 10 µl of RNA sample into each individual tube, pipetting up and down twice.
5. Seal the tubes and briefly spin down to eliminate any air bubbles.
6. Let the Reverse transcrition run using the thermos cycler:

	Step 1	**Step 2**	**Step 3**	**Step 4**
Temperature (°C)	25	37	85	4
Time	10 min	120 min	5 min	∞

(125)

Protocol 3: BCA Protein Assay kit (Thermo Scientific, 2016, adapted)

Note: Step 1 to 4 have to be performed on ice.

1. Prepare the BSA Standards as follows for the microplate procedure:

Concentration of BSA (µg/ml)	Volume of water (µl)	Volume and Source of BSA
2,000	0	100 µl of stock
1,500	25	75 µl of stock
1,000	70	70 µl of stock
500	70	70 µl of 1,000 µg/µl
250	70	70 µl of 500 µg/µl
125	70	70 µl of 250 µg/µl
25	80	20 µl of 125 µg/µl
0	100	0 µl

2. Prepare the Working Reagent (WR) using this formula:
   Volume WR = (# standards + # unknowns) × (# replicates) × (volume of WR per sample)
3. Add 25ul of each standard and sample into a well of a 96-well assay plate.
4. Add 200µL of WR to each standard or sample.
5. Incubate the assay plate for 30 minutes at 37°C.
6. Read the plate at 562 nm using the SpectraMax M2 Plate Reader and calculate the amount of protein of each sample using a standard curve.

Overview:

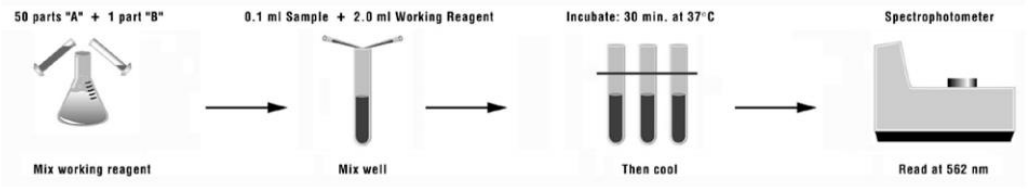

(123)

Protocol 4: Western Blot

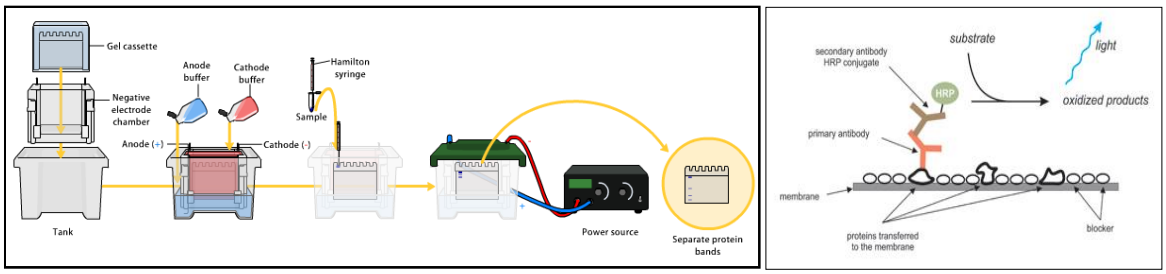

(126)

Western Blot is used to identify specific proteins of samples with protein-specific antibodies. The proteins are priory separated by gel electrophoresis and then transferred to polyvinylidene fluoride membranes for 45 minutes at 20 V. Proteins can now be visualized using appropriate primary and secondary antibodies and detection reagents (4).

Protocol 5: Negative Staining of Extracellular Vesicles using TEM (© Bio-Imaging, SWDSOP, 2004, adapted)

Method: Sequential two-droplet method

1. Place a drop (~5-10 µl) of EVs resuspended in 500 µl 1x PBS on to a copper grid.
2. Leave for ~20 sec until a part of the solution has dried. Then remove the residual solution with filter paper.
3. Apply a small drop of 1% uranyl acetate (~5-10 µl) to the grid and wait for 10 sec.
4. Remove excess stain with filter paper and let the grid dry at room temperature.

Note: 1% Uranyl acetate (UA) need to be dissolved in water with pH=4.2 to 4.5. Afterwards, the stain has to be filtered through a 0.22 µm filter and should be stored at 4°C in the dark. Fresh prepared 1% UA can be used for more than 1 year (127).

Protocol 6: Treatment methods for macrophage polarization

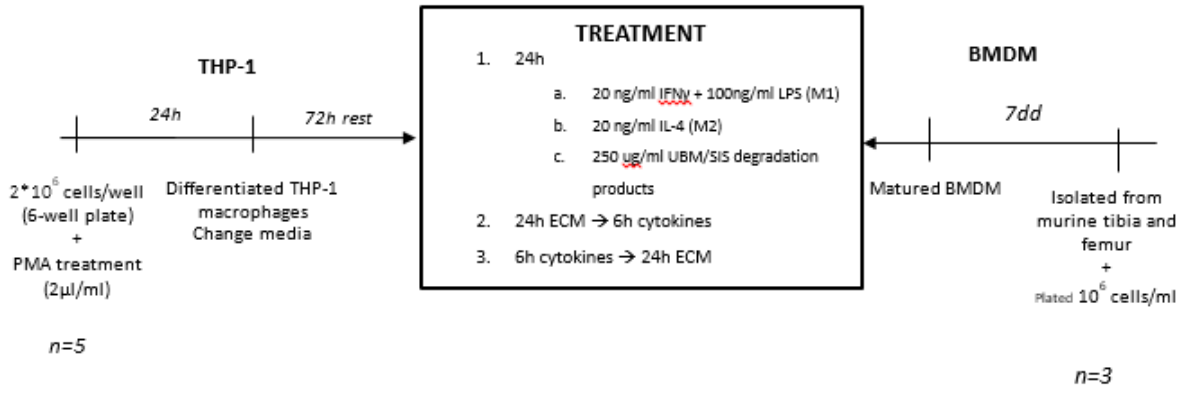

Auteursrechtelijke overeenkomst

Ik/wij verlenen het wereldwijde auteursrecht voor de ingediende eindverhandeling:
Effect of extracellular matrix degradation products on macrophage phenotype and the discovery of a novel bio-component within the extracellular matrix

Richting: **master in de biomedische wetenschappen-klinische moleculaire wetenschappen**
Jaar: **2016**

in alle mogelijke mediaformaten, - bestaande en in de toekomst te ontwikkelen - , aan de Universiteit Hasselt.

Niet tegenstaand deze toekenning van het auteursrecht aan de Universiteit Hasselt behoud ik als auteur het recht om de eindverhandeling, - in zijn geheel of gedeeltelijk -, vrij te reproduceren, (her)publiceren of distribueren zonder de toelating te moeten verkrijgen van de Universiteit Hasselt.

Ik bevestig dat de eindverhandeling mijn origineel werk is, en dat ik het recht heb om de rechten te verlenen die in deze overeenkomst worden beschreven. Ik verklaar tevens dat de eindverhandeling, naar mijn weten, het auteursrecht van anderen niet overtreedt.

Ik verklaar tevens dat ik voor het materiaal in de eindverhandeling dat beschermd wordt door het auteursrecht, de nodige toelatingen heb verkregen zodat ik deze ook aan de Universiteit Hasselt kan overdragen en dat dit duidelijk in de tekst en inhoud van de eindverhandeling werd genotificeerd.

Universiteit Hasselt zal mij als auteur(s) van de eindverhandeling identificeren en zal geen wijzigingen aanbrengen aan de eindverhandeling, uitgezonderd deze toegelaten door deze overeenkomst.

Voor akkoord,

Rausch, Theresa

Datum: **8/06/2016**